PERFORMANCE ANALYSIS OF A REVERSE ELECTRODIALYSIS STACK FOR ELECTRICITY GENERATION IN KZN, SA

by

Mfanelo Percival Mbokwana

This dissertation is submitted in the fulfilment of the requirements for the degree of Master of Engineering in Chemical Engineering to the Faculty of Engineering and the Built Environment at Durban University of Technology.

Supervisor: Dr. Peterson Thokozani Ngema

Co-Supervisors: Prof. Armel Tumba Kaniki

Dr. Nkululeko Nkosi

May 2024

Preface

In collaboration with co-supervisors (Prof. Armel T. Kaniki and Dr. Nkululeko Nkosi) from Mangosuthu University of Technology (MUT), Department of Chemical Engineering, this study was supervised by Dr. Peterson T. Ngema from Durban University of Technology (DUT), Department of Chemical Engineering. MUT's chemical engineering research laboratory was used for the experiments. The research was financially supported by NRF, **grant no.: 129314**.

Declaration

I, **Mfanelo Percival Mbokwana (21025503),** the undersigned student, declare that

(i) The research reported in this dissertation, except where otherwise indicated, is my original work.

(ii) This dissertation has not been submitted for any degree or examination at any other university.

(iii) This dissertation does not contain other persons' data, pictures, graphs, or other information, unless specifically acknowledged as being sourced from other persons.

(iv) This dissertation does not contain other persons' writing, unless specifically acknowledged as being sourced from other researchers. Where other written sources have been quoted, then:

(a) their words have been re-written, but the general information attributed to them has been referenced.

(b) where their exact words have been used, their writing has been placed inside quotation marks, and referenced.

(vi) This dissertation does not contain text, graphics or tables copied and pasted from the Internet, unless specifically acknowledged, and the source being detailed in the dissertation and in the References sections.

Signature of Candidate

…. 05/06/2024 ….
Day/Month/Year

As the candidates' supervisors, we have approved the submission of this dissertation.

Supervisor (Dr. Ngema) Co-supervisor (Prof. Kaniki) Co-supervisor (Dr. Nkosi)

Acknowledgments

Thanks to Dr. P.T. Ngema, my supervisor, and my co-supervisors, Prof. A.T. Kaniki and Dr. N. Nkosi, for their advice, support, guidance, and encouragement throughout my Master's project. The support I have received from my cousin Thando Njoko has been consistent throughout my darkest times. There is no one like her. The support and presence of Mr. S.F. Makhathini have been extremely valuable during challenging times. Mr. K. Shabangu gave me invaluable advice and contributed greatly to my work. Also, I am grateful to the TSC staff for allowing me to use their laboratories and offices without question. I extend my thanks to MUT for providing access to their labs. Lastly, I would like to thank NRF for their financial support.

Abstract

The Earth is now 1.1 ℃ warmer than in the 19th century, with a 50% surge in atmospheric CO_2 levels. Climate scientists stress the importance of limiting global warming to 1.5 ℃ by 2100, emphasizing the need for immediate action. However, without intervention, projections suggest a potential temperature rise exceeding 2 ℃ or even reaching 2.4 ℃ by the end of this century. Failure to address this issue could result in catastrophic consequences, including severe heatwaves, widespread displacement due to rising sea levels, and irreversible damage to plant and animal species. The urgency to curb greenhouse gas emissions and mitigate the impacts of climate change is paramount to safeguarding the future of the planet.

In 2015, leaders of different countries made a crucial global initiative in Paris, France—the Paris Agreement. This agreement addresses urgent climate challenges, recognizing that failure to tackle climate change could lead to catastrophic consequences, from severe heatwaves to the irreversible loss of biodiversity. By committing to curb greenhouse gas emissions, the Paris Agreement provides a vital framework for safeguarding the planet's future and fostering international collaboration in the face of climate adversity.

South Africa faces a critical energy challenge marked by frequent load shedding and heavy reliance on coal-based electricity generation. The energy sector plays a pivotal role in the nation's socio-economic development, and the persistent power shortages have significant repercussions on industrial output, livelihoods, and environmental sustainability. This precarious situation necessitates a shift towards sustainable and renewable energy sources. In February 2020, South Africa released its Low Emission Development Strategy, with the goal of achieving a net-zero carbon economy by 2050. This dynamic strategy provides flexibility for South Africa to adapt its approach, considering emerging innovations and alternative energy options. One promising avenue is the utilization of Reverse Electrodialysis (RED) technology, which harnesses the salinity gradient between concentrated solutions usually seawater and less concentrated solution usually river water to generate electricity. Despite its potential, the integration of RED technology into South Africa's energy landscape remains underexplored and underutilized.

This research aims to investigate the parameters that affects power generation in a RED stack using local waters. The impact of electrode rinse solution on the stack remains a scarcely explored area. Despite the significant advancements in RED technology, there is a notable gap in understanding the effect of electrode rinse solutions on RED stack performance. The study

was divided into three parts. The first part of the study involved comparing the effects of different electrode rinse solutions (ERS) on open-circuit voltage (OCV), power density, and internal resistance. The solutions tested included Potassium Chloride (KCl), Sodium Chloride (NaCl), Sodium Sulphate (Na_2SO_4), and a mixture of Potassium Ferricyanide anhydride, Potassium Ferrocyanide trihydrate, and Sodium Chloride [$K_3Fe(CN)_6$, $K_4Fe(CN)_6$, and NaCl]. The comparison was based on Open Circuit Voltage (OCV), Voltage Under Load (VUL), internal resistance, and power density. Variables investigated included the flow rate of the rinse solution, concentration, and composition. The flow rate of the ERS was varied from 9.15 to 18.3 L/h, and the concentration was varied from 5 to 30 g/L. But for the mixture, four of the most commonly used molar concentrations in literature were chosen. The experiments were conducted at room temperature (25 ℃ ± 0.5). The feed comprised of synthesized sodium chloride solutions flowing at a constant rate of 900 mL/min, with concentrations of 0.4 g/L for the less concentrated solution and 38 g/L for the more concentrated solution. The results indicated that the ERS significantly influences the power generation of the stack. The mixture demonstrated the best performance in terms of OCV, VUL, internal resistance, and power density. This superior performance can be attributed to the presence of redox species in the mixture. The highest recorded values for OCV, VUL, and power density were 4.354 V, 0.966 V, and 8.964 W/m^2, respectively, and these were exclusively measured when using the mixture as an ERS. When comparing the highest power density measurement for the mixture to the highest power density measurement for KCl solution, a notable difference of 73% was observed. Additionally, the lowest internal resistance recorded was 14.26 Ω, and it occurred with the mixture as the ERS.

The second part of the study involved using seawater and various river water samples as feed solutions, with manipulated variables including the temperature and flow rate of the feed. The temperature ranged from 25 to 40 ℃, and the flow rate varied between 900 and 1550 mL/min. The ERS was circulated at a constant flow rate of 153 mL/min. Results indicated that temperature had a more pronounced effect on power generation compared to flow rate. Notably, the highest increase in power density was 60.0% from a temperature of 25 to 40 ℃. On the other hand, the highest increase in power density was 31.3% from a flow rate of 900 to 1550 mL/min. Internal resistance was significantly influenced by temperature, with the lowest values consistently observed at the highest temperatures and flow rates.

In the final part of the study, a software tool, Design Expert, was employed to identify the optimum point for the system. uMkomaas river water sample was utilized for this analysis.

Data of the runs was feed to the Design Expert software under historical data. Low coded factors, which is -1, were 900 and 25 for flow rate and temperature, respectively. High coded factors, which is 1, were 1550 and 40 for flow rate and temperature, respectively. The responses of the system were OCV and VUL. ANOVA was used to analyze the system's historical data and optimize the process. The order of optimization was Quadratic. The adjusted R^2 for OCV and VUL were 0.8048 and 0.6484, respectively. The surface response was analyzed. The optimum conditions achieved a desirability of 92.7%. Four runs were conducted as confirmation.

Research output

Conference proceedings:

Peer-reviewed

M.P. Mbokwana, P.T. Ngema, A.T. Kaniki, N. Nkosi 'Comparison of reverse electrodialysis stack performance under a variety of experimental conditions using various electrode rinse solutions' in JCBEE-23 Nov. 16-17, 2023, Johannesburg (South Africa). International Institute of Chemical, Biological & Environmental Engineering, pp. (162-164). https://doi.org/10.17758/IICBE5.C1123051

Proceeding only

M.P. Mbokwana, P.T. Ngema, A.T. Kaniki, N. Nkosi. 'Comparison of reverse electrodialysis stack performance under a variety of experimental conditions using various electrode rinse solutions', in FRD-4 Oct. 23, Durban (South Africa). Faculty of Engineering and the Built-Environment Research Day.

Table of Contents

Preface ii

Declaration iii

Acknowledgments iv

Abstract v

Research output viii

Table of Contents ix

Nomenclature xv

CHAPTER 1: Introduction 1

1.1. Background on the renewable energy progress 1

1.2. Background on the RED technology 2

1.3. Motivation of the study 2

1.4. Scope of the research 3

1.5. Hypothesis and research questions 3

1.6. Aim and objectives of the study 4

1.7. Outline of the Dissertation 4

CHAPTER 2: Literature review 6

2.1. Background on renewable energies and their contribution in the South African grid 6

2.1.1. Salinity Gradient Energy (SGE) 8

2.2. Basics of Reverse Electrodialysis 10

2.2.1. Ion Exchange Membranes (IEMs) 10

2.2.2. Electrochemical and physical properties 13

2.3. Effect of Concentration polarization phenomena 17

2.4. Diffusion boundary layer 19

2.5. Electrode systems for RED 20

2.6. Effect of monovalent and multivalent ions on the RED system 23

2.6.1. Uphill transport 24

2.6.2. Fouling 25

2.7. Effect of spacer geometry 27

2.8. Effect of electric resistance 30

2.9. Fundamentals of reverse electrodialysis 31
2.9.1. Principles and mechanism of RED 31
2.9.2. Electrochemistry of RED 32
2.10. Review of power density, open circuit voltage, and key operational parameters affecting RED performance 33
2.10.1. Temperature 34
2.10.2. Feed flow rate 35
2.10.3. Influence of feed solution concentration 37
2.10.4. Effect of the feed composition 39
2.10.5. Effect of conductivity and pH 40
2.10.6. Power density 41
2.10.7. Open Circuit Voltage (OCV) 44
2.11. RED integration 45
2.11.1. Desalination and RED 45
2.11.2. Reverse Osmosis (RO) and RED 46
2.11.3. Microbial electrolysis cell-RED hybrid system 48
2.11.4. Microbial reverse electrolysis cell-RED hybrid system 49
2.11.5. Membrane distillation – RED hybrid system 49
2.11.6. Water electrolysis - RED hybrid system 51
2.11.7. Waste heat 52
2.12. Process optimization 53
2.12.1. Application of Response Surface Methodology 54
2.12.2. The historical data 55
2.13. Summary 55
CHAPTER 3: Materials and methods 56
3.1. Materials 57
3.1.1. Chemicals and materials 57
3.2. Collection, preparation, and characterization of samples 58
3.2.1. Synthetic samples 58
3.2.2. River and seawater samples 58
3.3. Characterization 59
3.4. Solutions chemistry 60
3.5. Experimental set-up 60
3.5.1. Main apparatus 61
3.5.2. Commissioning of RED Stack 61

3.6. Experimental measurements 62
3.6.1. Design of experiments 62
3.6.2. Experimental procedure 62
3.7. Modeling and Optimization 64
3.7.1. Empirical modeling 65
3.7.2. Optimization framework 66
CHAPTER 4: Results and discussions 67
4.1. Influence of ERSs 67
4.1.1. Effect of flow rate 68
4.1.2. The effect of concentration 72
4.1.3. The effect of composition 76
4.2. RED performance evaluation with natural water 78
4.2.1. Effect of temperature on the measure parameters 78
4.2.2. The effect of flowrate on…. 86
4.3. Performance evaluation between Natural and synthetic water 93
4.4. Summary 97
CHAPTER 5: Optimization 98
5.1. Exploring ANOVA Techniques for Performance Analysis 100
5.2. 3D surface graphs and contour plots 107
5.3. RED system variable optimization 109
5.4. Confirmation of runs 110
CHAPTER 6: Conclusion and recommendations 112
6.1. Major Findings of this Research 112
6.2. Recommendations 112
REFERENCES 114
Appendix A: Materials 134
Appendix B: Raw data and specification 138
Appendix C: Publications 141

LIST OF FIGURES

Figure 2-1: Renewable energy technologies 7
Figure 2-2: Schematic experimental set up for assessing membrane permselectivity through measurements of membrane potential ..... Error! Bookmark not defined.
Figure 2-3: A schematic representation of concentration polarization 18
Figure 2-4: The electrical double layer (EDL) and the diffusion boundary layer are formed between the solution and the membrane 20
Figure 2-5: The resistance of the stack plotted against the linear solution flow rate 29
Figure 2-6: Diagram of a RED stack 32
Figure 2-7: Ionic lattice of sodium chloride 33
Figure 2-8: Schematic diagram of the hybrid microbial electrolysis cell (MEC)-reverse electrodialysis (RED) cell 48
Figure 2-9: Schematic diagram showing integration of membrane distillation and reverse electrodialysis 51
Figure 3-1: The graphical methodology of the study. 57
Figure 3-2: A pH/Conductivity meter coupled with a thermostat probe. 59
Figure 3-3: A simplified schematic diagram of the RED system for the study. 60
Figure 3-4: RED stack that was used for the study. 61
Figure 4-1: The effect of flow rate on internal resistance at varying concentrations 69
Figure 4-2: The effect of flow rate on OCV at varying concentrations 70
Figure 4-3: The effect of flow rate on power density at varying concentrations 71
Figure 4-4: The effect of concentration on OCV for different ERS. 72
Figure 4-5: The effect of concentration on power density for different ERS. 74
Figure 4-6: The effect of concentration on internal resistance. 75
Figure 4-7: The effect of temperature on OCV. 79
Figure 4-8: The effect of temperature on power density. 82
Figure 4-9: The effect of temperature on internal resistance. 84
Figure 4-10: The effect of flow rate on internal resistance at varying temperatures. 87
Figure 4-11: The effect of flow rate on OCV. 90
Figure 4-12: The effect of flow rate on power density at varying temperatures 92
Figure 5-1: Correlation plot illustrating relationships between variables and runs. 98
Figure 5-2: Level of transformation signal for OCV. 99
Figure 5-3: Level of transformation signal for VUL. 100
Figure 5-4: The Normal % Probability Residual plots for the responses 104
Figure 5-5: Residual plots for the responses 104
Figure 5-6: Predicted vs. Actual plot for the responses 105
Figure 5-7: Box-Cox Plots for the responses 106
Figure 5-8: Cook's distance plot for the responses 107
Figure 5-9: Response surface plot showing the effects of temperature and flowrate on OCV as the response 108
Figure 5-10: Response surface plot showing the effects of temperature and flowrate on VUL as the response 109
Figure 5-11: Ramp plot displaying the optimized conditions of RED system variables at desirability of 92.7%. 110
Figure A-1: (a) uMkoomas River water sampling spot (b) Unfiltered River water sample 134

Figure A-2: (a) Natural water filtration process (b) filter Natural water sample 134
Figure A-3: Prepared electrode rinse solution of $K_3Fe(CN)_6$, $K_4Fe(CN)_6$, and NaCl....135
Figure A-4: End plates of the RED stack.....135
Figure A-5: Anion Exchange Membrane (AEM).....136
Figure A-6: Cation Exchange Membrane (CEM).....136
Figure A-7: Electrode rinse compartments 137
Figure B-1: Perturbation plot for OCV 139
Figure B-2: Perturbation plot for VUL 139
Figure B-3: Residuals v Runs plot for OCV. 140
Figure B-4: Residuals v Runs plot for VUL. 140
Figure B-5: Published paper. 141

LIST OF TABLES

Table 2-1: Major ion composition of sea water.....33
Table 3-1: Purity for all organic salts used in the study......58
Table 3-2: experimental run data.....65
Table 4-1: The characteristics of the ERSs and mixtures used. 67
Table 4-2: The triplicate preliminary runs......68
Table 4-3: Calculated power density values for the study. 77
Table 4-4: OCV values for the study......81
Table 4-5: Measured data from RED stack tests with temperature at ±25 ℃ and flow rate at 150 mL/min......94
Table 5-1: **Response data for OCV**.....100
Table 5-2: Response data for VUL 101
Table 5-3: Fit statistics for OCV......101
Table 5-4: Fit statistics for VUL......101
Table 5-5: Coefficients in terms of coded factors for OCV......103
Table 5-6: Coefficients in terms of coded factors for VUL. 103
Table 5-7: Conditions of optimization of RED system variables......110
Table 5-8: Confirmation runs that were conducted. 110
Table 5-9: Confirmation runs limits for responses. 111
Table B-5: General properties and specifications of the RED stack used in the analysis. 138
Table B-6: Properties of the ion-exchange membranes......138

Nomenclature

Symbols

E_m	Membrane potential
ΔG_{mix}	Gibbs energy of mixing
P_d	Power density
R_i	Internal resistance
Mm	Molar mass

Abbreviations

0.05 M	0.05 M $K_3Fe(CN)_6$, 0.05 M $K_4Fe(CN)_6$, 2.5 M NaCl
0.1 M	0.1 M $K_3Fe(CN)_6$, 0.1 M $K_4Fe(CN)_6$, 2.5 M NaCl
0.2 M	0.2 M $K_3Fe(CN)_6$, 0.2 M $K_4Fe(CN)_6$, 2.5 M NaCl
0.3 M	0.3 M $K_3Fe(CN)_6$, 0.3 M $K_4Fe(CN)_6$, 2.5 M NaCl
AEM	Anion exchange membrane
ANOVA	Analysis of variance
AR	Area resistance
CEM	Cation exchange membrane
CP	Concentration polarization
C.V.%	Coefficient of variation as a percentage
DBL	Double boundary layer
DOE	Design of experiment
ERS	Electrode rinse solution
FCD	Fixed charge density
HC	More concentrated

IEC	Ion exchange capacity
IEM	Ion exchange membrane
IR	Internal resistance
LC	Less concentrated
NOM	Natural organic matter
OCV	Open circuit voltage
OFAT	One factor at a time
PRO	Pressure retarded osmosis
PV	Photovoltaic
RED	Reverse electrodialysis
SD	Swelling degree
SGE	Salinity gradient energy
UV	Ultraviolet
VUL	Voltage under load

N.B

Mixture	The mixture of Potassium Ferricyanide anhydride, Potassium Ferrocyanide trihydrate, and NaCl

CHAPTER 1: Introduction

Chapter overview

This chapter provides a comprehensive overview of the study's context and objectives. The progress in renewable energy and current trends is highlighted. The background of Reverse electrodialysis is highlighted, its principles and applications. The motivation behind the study is then discussed, emphasizing the gap in knowledge or practical needs that necessitate the research. The scope of the research is outlined, defining the boundaries and focus areas of the study. Subsequently, the chapter presents the hypothesis and research questions guiding the investigation, providing a framework for analysis. Finally, the aim and objectives of the study are outlined, showing what the main goal is and what specific outcomes sought. The chapter concludes with an outline of the dissertation, offering a preview of the subsequent chapters.

1.1. Background on the renewable energy progress

The global population is projected to reach 8.1 billion by 2024, with emerging markets and developing economies, excluding China, contributing around two billion people by 2050. Sub-Saharan Africa's population is expected to double by 2050, indicating rapid growth. However, this increasing population strains global energy demand, posing challenges for both developed and developing economies. South Africa's state-owned utility, Eskom, exemplifies the energy-intensive nature of infrastructure development, contributing over 60% of the country's carbon emissions despite an unreliable grid supply. To address this, countries are considering sustainable energy options to meet future needs while reducing carbon emissions in alignment with COP21 commitments and UN sustainability goals (Szulejko *et al.*, 2017).

Clean energy technologies are becoming more affordable, offering opportunities for emission reduction and renewable energy development (Babayomi, Dahoro and Zhang, 2022). However, adoption of low-carbon technologies remains a challenge across various sectors, including mining, water, and manufacturing (Moshood *et al.*, 2021). Developing countries have yet to fully integrate renewable energy into industrial operations, facing limitations in natural gas and biofuel resources. Renewable energy sources in South Africa fall short of meeting the demands of its rapidly urbanizing and industrializing economy. To address this gap, sustainable and reliable alternatives are crucial. Salinity gradient technology, particularly reverse electrodialysis (RED), harnesses the abundant seawater resources and holds immense potential as a major renewable energy source (Post *et al.*, 2007; Pérez *et al.*, 2020). With global estimates

projecting significant technical exploitable energy, RED emerges as a transformative solution in South Africa's pursuit of renewable energy alternatives (Post *et al.*, 2007; Zhou *et al.*, 2022).

1.2. Background on the RED technology

RED offers a significant opportunity in South Africa by harnessing the vast energy potential inherent in the salinity gradient between seawater and river water. Its relevance is underscored by the country's high carbon emissions, intermittent power supplies, and commitment to sustainable energy sources (Cohen and Winkler, 2014). RED technology generates continuous and clean electricity from the salinity difference, addressing the urgent need for renewable energy (Daniilidis *et al.*, 2014; Avci *et al.*, 2018). Originally developed by Pattle in 1954 (Pattle, 1954), salinity gradient power utilizes the vast abundance of water in the oceans, making RED technology a transformative force in the renewable energy landscape. RED also facilitates renewable energy generation and desalination, showcasing its versatility (Trist *et al.*, 2020a; Li *et al.*, 2022). By leveraging the salinity gradient for both electricity generation and desalination, RED presents a sustainable alternative to thermal desalination, minimizing carbon footprint and addressing water scarcity in coastal regions effectively (Al-Sahali and Ettouney, 2007; Li *et al.*, 2022). Through integration with other renewable energy sources or existing desalination plants, RED offers a versatile and sustainable solution to water scarcity issues.

1.3. Motivation of the study

Electricity generation in South Africa is heavily dependent on coal. By using RED technology, local rivers and seawater can be harnessed to generate renewable energy. Through this diversification, the nation can reduce its reliance on coal and create a more sustainable energy mix. Research into RED technology, which generates power from clean, renewable water sources, offers a viable alternative to coal-based power generation. This way, coal combustion can be mitigated, and greenhouse gas emissions reduced. This context has led to the study's motives.

The study's focus on local rivers and seawater resources in KwaZulu Natal demonstrates the importance of tapping into readily available indigenous energy sources. This approach can reduce dependence on imported fuels and improve energy self-sufficiency in the region. Investigating and optimizing electrode rinse solutions and varying key operational parameters would immensely contribute to the advancement of RED technology. The findings from this research would benefit South Africa and other coastal regions seeking to harness renewable

energy through RED. Moreover, the research contributes valuable data and insights specific to the KwaZulu Natal region and South Africa. This data can inform evidence-based decision-making and support future initiatives to transition to cleaner and more sustainable energy sources.

1.4. Scope of the research

A critical component of this investigation is exploring electrode rinse solutions (ERSs), which play a pivotal role in the electricity generation process within a RED stack. The quality and composition of these solutions are paramount, as they can greatly affect the technology's overall efficiency and performance. Moreover, it is worth noting that this study does not encompass other renewable energy technologies, such as wind or solar power. It also does not extend its scope to the application of RED technology for purposes other than electricity generation, keeping the research tightly focused.

In the pursuit of optimizing RED technology for electricity generation, several key parameters were systematically varied during this study. These include the temperature of the feed, the flow rate of the feed, the flow rate of the electrode rinse solution, and the concentration and composition of the electrode rinse solution. This systematic variation allows for a comprehensive exploration of the factors that can enhance the efficiency of electricity generation through the RED stack. It is also essential to note that no experimental runs exceeded ten minutes, ensuring that the study maintains a controlled and consistent data collection and analysis timeframe.

1.5. Hypothesis and research questions

The following hypothesis was developed as part of this research:

- A variation in the RED stack feed input parameters will improve the performance of the stack and increase its power output.

The following research questions were addressed in support of the study’s hypothesis developed:

- What effects do variations in flow rate, concentration, and composition of the electrode rinse solution have on the performance and efficiency of the RED stack?
- For electricity generation in KZN, which river source produces better performance metrics?

1.6. Aim and objectives of the study

The aim of this research was to investigate and optimize the performance of Reverse Electrodialysis (RED) stacks for electricity generation, with a focus on enhancing efficiency and understanding the influence of various parameters such as flow rate, concentration, composition, temperature, and feed composition.

Objectives were as follows:

- to examine how changes in flow rate, concentration, and composition of the electrode rinse solution affect the performance and effectiveness of the RED stack in electricity generation.
- to determine the individual and interactive effects of temperature and flow rate on the performance metrics of a RED stack for salinity gradient power generation in KZN.
- to compare the performance of natural water feed with that of synthetic feed at similar operating conditions.
- to develop an empirical model and validate the optimal operating conditions, that maximize the electricity generation efficiency of the RED stack using the response surface methodology.

1.7. Outline of the Dissertation

Chapter 1: Introduction

This chapter provides an introductory overview and background for the entire study, emphasizing the study's necessity, the conceptual foundation, and the research aims.

Chapter 2: Literature Review

This chapter presents a comprehensive review of the literature with a primary focus on the assembly of RED stacks and the fundamental principles of RED. It explores the factors influencing RED stack performance, discusses the historical context of renewable energy technologies, and concludes by discussing technologies integrated with RED.

Chapter 3: Materials and Methods

This chapter covers the research methodology, detailing materials, methods, and equipment. The procedures for the experiments are clearly outlined.

Chapter 4: Results and discussion

In this chapter, the results are presented and discussed. Firstly, the findings from the

comparison study of electrode rinse solutions are discussed. This is followed by a discussion on the effect of using a natural water sample to operate the stack. The results of the synthesized water feed are then compared to those with natural waters and discussed.

Chapter 5: Optimization

The results obtained from the Design Expert software through response surface methodology are presented and discussed in detail.

Chapter 6: Conclusion

The conclusion and recommendations are presented in this chapter. This chapter summarizes the major results of the study and draws recommendations for future works.

CHAPTER 2: Literature review

Chapter overview

Climate change, exacerbated in large part by the excessive reliance on fossil fuels, is significantly altering the dynamics of our planet, with far-reaching consequences for both current and future generations. The alarming statistic that 71% of the world's energy is generated by fossil fuels underscores the urgency of addressing this critical issue (*Global Energy Review 2019*, 2020). The effects of climate change are already being felt across the globe, manifesting as extreme weather events, rising sea levels, more frequent and severe wildfires, and disruptions to ecosystems. These impacts pose a direct threat to the well-being and livelihoods of the current generation. However, the most profound implications of climate change will be borne by future generations. Without a concerted effort to mitigate the ongoing damage caused by fossil fuel emissions, future generations will inherit a world characterized by unprecedented challenges. They will face the daunting task of adapting to a rapidly changing climate, addressing resource scarcity, and coping with the social and economic ramifications of environmental degradation.

This chapter examines the literature concerning renewable energy technologies but focusing more on the RED stack providing an in-depth exploration of the existing body of knowledge. Through an in-depth analysis of the existing literature, the aim was to gain a profound understanding of the principles, applications, and potential innovations within the field of reverse electrodialysis. This review not only offers insights into the current state of reverse electrodialysis but also serves as a foundational resource for informing and contextualizing the research conducted in this study. In this section, special emphasis is placed on the literature related to the RED stack. The focus is directed towards comprehending its operational principles, internal mechanisms, historical development, the constituent elements comprising the stack, its synergies with other technologies, as well as the various factors and parameters that exert influence on power generation within the stack. Response surface methodology is highlighted as a versatile tool for experimental design, modeling, and optimization tool.

2.1. Background on renewable energies and their contribution in the South African grid

Energy has been a fundamental force since the dawn of time, serving as a crucial resource that has propelled human society forward, fostering progress, evolution, and prosperity (Sorensen,

1991). The sun, as the initial source of energy, provided both heat and light. The journey from the combustion of wood and coal to the utilization of nuclear power has played a pivotal role in advancing society (Alanne and Saari, 2006). However, these progressive steps have taken a toll on the environment (Dincer, 2000). Access to energy stands as a critical requirement for any society. In the early stages of human existence, reliance was solely on somatic energy—using muscles for securing basic food supplies, enhancing shelters, and acquiring modest material possessions (Sorensen, 1991). The era of dependence on animate power and biomass fuels gradually gave way, marking the significant transition to fossil fuels (Gaye, 2008).

The potential of renewable energy sources in **Figure 2-1** is enormous, as in principle it can be many times greater than the world's energy demand. Renewable sources such as wind energy, solar, biomass-to-energy, hydraulic, and geothermal energy can provide sustainable energy services based on the use of domestic resources available daily. The move to renewable energy systems seems more likely as oil and gas prices continue to fluctuate while costs fall (Herzog and Kammen, 2001). Governments around the globe are supporting the movement toward renewable energy technologies through favorable policies (Department of Energy, 2020) and investments (Hepbasli and Ozgener, 2004; Lund, 2007; Akinbami and Bodunrin, 2021)

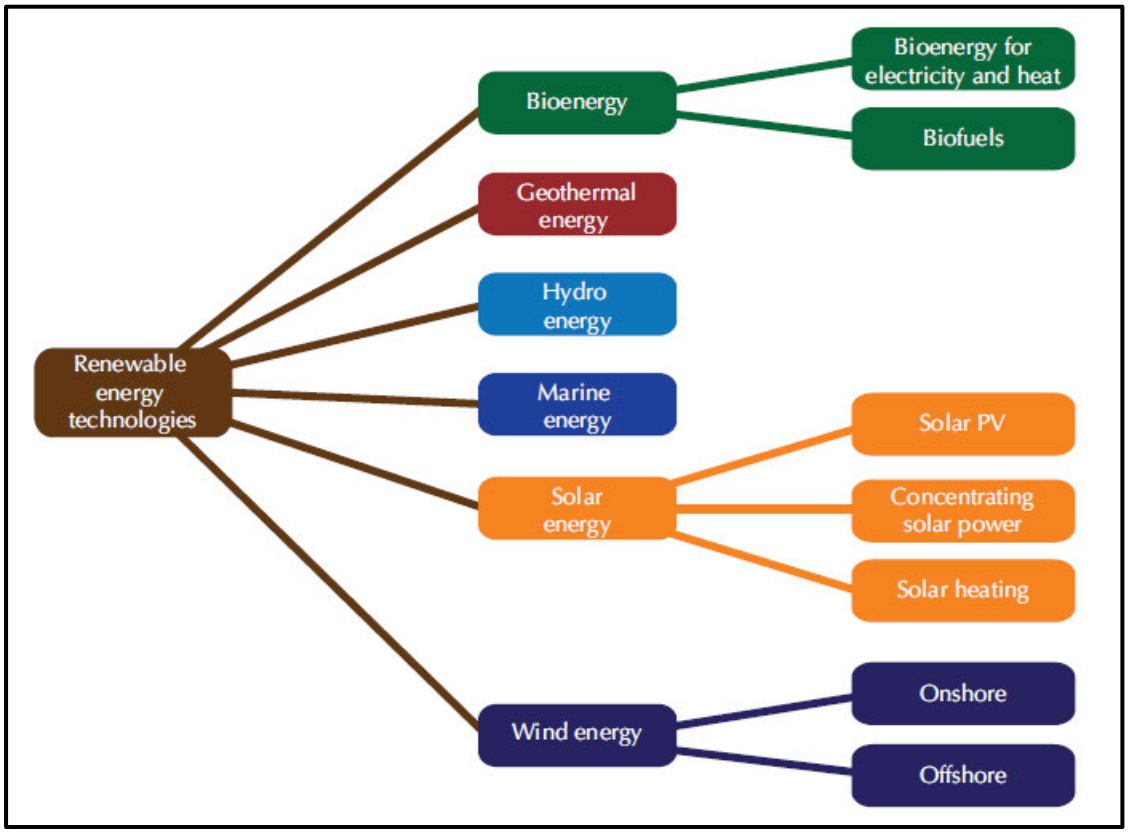

Figure 2-1: Renewable energy technologies (Dottoressa, 2016)

2.1.1. Salinity Gradient Energy (SGE)

The salinity gradient energy includes the reverse electrodialysis and pressure retarded osmosis.

2.1.1.1. Reverse electrodialysis

RED does not have a long rich history like other renewable technologies (Gross and Bauen, 2003; Mohtasham, 2015). The first time that RED was mentioned in literature was in 1954 by Pattle when he first described the concept of converting the difference between the chemical potentials of concentrated and diluted solutions to useful energy by RED (Pattle, 1954). In research it was noted that if a membrane separates two salt solutions of different strengths, a potential difference appears across it. The experiment he conducted showed the production of energy using an apparatus consisting of 47 cell pairs of membranes. Fresh and salt water was used at a temperature of 39 ℃. The maximum electromotive force obtained was 3.1 V and the maximum power was 15 mW. However, it wasn't until the 1970s that the scientific community began to take a serious interest in the potential of salinity gradient energy as a source of renewable power. Wick, 1978 published a paper where the author was investigating the viability of Salinity Gradient Power (Wick, 1977). It was discussed that the untapped energy available in the world while the author was also focusing on US rivers and salt deposit around the country. It was concluded that the SGP has certain features that makes it attractive as a source of energy but the cost of membranes suitable for the method was too high. The study of energy using RED where discussing the locations for sources of brine salt in United State of America (Wick, 1977; Principle, 2000). It was also discovered that geothermal brines can be potential sources of RED energy. In the 1990s, Audinos (Audinos, 1992) presented a study that showed that it was possible to convert the energy of mixing of two solutions of different salinities into electric power by RED. For the working solutions, the researcher used zinc sulphate ($ZnSO_4$) and sodium chloride (NaCl) in continuous flow operation. The energy obtained was 400 mW/m^2.

Although the concept of RED technology was first reported in 1954, the most significant research advancements have been documented since 2007 (Veerman *et al.*, 2008; Veerman *et al.*, 2009). The increase in fossil fuel energy costs over the last two decades has led to an increase in research on RED (Nagarale and Shahi, 2006). During this time lot of studies were focusing on IEMs (Długoł *et al.*, 2008; Besha *et al.*, 2019), stack configuration (Liu, Coronell and Call, 2017; Yasukawa *et al.*, 2020) and operational conditions (Veerman *et al.*, 2009; Zhu *et al*., 2015b) in RED. Improvement of stack design and the availability of IEMs led to a notable

development in power density (e.g., a maximum value of 0.93 W/m^2 was obtained using 1g NaCl/L of artificial river water and 30g NaCl/L of artificial seawater as feed solutions) (Veerman *et al.*, 2009). In 2012, the first tailor-made IEM specifically designed for RED showed a power density of 1.27 W/m^2 (Guler *et al.*, 2012). Over the years performance of IEMs has been improving (Daniilidis *et al.*, 2014).

In the last decade (2010–2019), RED pilot plants have been commissioned in the Netherlands and Italy (Tedesco *et al.*, 2016). This is an important step for large-scale commercialization but there are challenges for the full-fledged RED plant. Despite the progress made in the development of RED technology, the cost of electricity generated by RED is currently still higher than that of traditional power sources. However, advances in materials science, membrane technology, and system design are expected to the development of more cost-effective and efficient RED systems in the future (Tong *et al.*, 2018).

2.1.1.2. Pressure Retarded Osmosis

Pressure Retarded Osmosis (PRO) is a membrane process of harnessing osmotic energy to generate electricity. PRO is a technique for separating a solvent (e.g. fresh water) from a more concentrated (e.g. saltwater) pressurized solution (Achilli and Childress, 2010a). A semi-permeable membrane allows the solvent to pass through to the concentrated solution side by osmosis. The saline water draws the less concentrated water through the semipermeable membrane due to its higher osmotic pressure, increasing the volume of the flow. The energy in the pressurized permeate solution is then converted into a mechanical/electrical energy via a turbine-generator set (Helfer and Anissimov, 2014).

Professor Sidney Loeb invented PRO at the Ben-Gurion University of the Negev in Beersheba, Israel, in 1973 (Loeb and Norman, 1975). In the experiment, Loeb and co-workers used Dead Sea brine as the concentrated solution and fresh water in the low salinity stream. This study was followed by further experimental investigations from Mehta and Loeb. These studies successfully proved the PRO concept, but the power output was far below what was expected based on the osmotic pressure difference across the membrane. In 1981, a critical theoretical and experimental study on useful energy harvesting by PRO was published. The results from the experiments showed that a power density of 1.6 W/m^2 can be achieved. This led the authors to believe that a construction of a low-cost osmotic plant was justified. In the same year, Lee *et al.*, 1981 developed a model that used results from reverse osmosis and forward osmosis experiments to predict PRO performance. Loeb *et al.*,(2022), compared the mechanical

efficiency of several theoretical PRO plant configurations. With his colleagues, the researchers continued to evaluate a continuous-flow terrestrial PRO facility an alternating-flow terrestrial PRO facility, and a continuous-flow underground PRO facility to determine the most efficient method of pressurizing the PRO saltwater circuit. Loeb 1998, revitalized the interest in PRO by asking if PRO energy generation at the Dead Sea would be a challenge or a chimera (Achilli and Childress, 2010b). It was concluded that electricity generation depended on system configurations. Loeb, 2001 investigation of the potential for PRO technology use at the Great Salt Lake revealed that electricity can be produced at a cost of 0.15 $/kWh. Statkraft, 2008 opened the first prototype PRO installation in Norway. The plant configuration follows the original scheme proposed by Loeb 1975. This prototype was designed to develop and test new PRO technologies, especially new semi permeable membranes.

2.2. Basics of Reverse Electrodialysis

2.2.1. Ion Exchange Membranes (IEMs)

At the core of RED lie ion exchange membranes (IEMs), a vital component profoundly influencing the overall performance of the process (Pattle, 1954). The ion exchange membrane (IEM) is a primary component in the RED system for salinity gradient power generation. These membranes are electrically conductive and come in various types tailored for specific processes (Nagarale and Shahi, 2006). Essentially, IEMs consist of water-swollen polymeric films imbued with a high density of charged ionic functional groups affixed to the polymer chains (Długoł *et al.*, 2008; Luo, Abdu and Wessling, 2018; Jin *et al.*, 2021).

To make this technology a reality, innovation is needed to improve this critical subcomponent, particularly in the selection of appropriate membrane materials especially the design of appropriate RED membranes (Kotoka and Merino-garcia, 2020). Researchers have conducted numerous studies on IEMs (Galama *et al.*, 2014; Gi *et al.*, 2015; Zhang *et al.*, 2017; Fan and Yin, 2019), as exemplified by the work of Guler et al. (Guler *et al.*, 2012), who examined both commercially available and tailor-made IEMs, demonstrating that tailor-made IEMs yielded the highest gross power density. This was because of the reduce resistance of these membranes (Güler *et al.*, 2013). In 2012, the first tailor-made IEM for RED applications was developed and tested and it generated a power density of 1,27 W/m^2 (Guler *et al.*, 2012), which is a substantial improvement from most previous studies (Pattle, 1954; Veerman, Jong, *et al.*, 2009; Veerman *et al.*, 2009; Veerman, 2010).

IEM is a polymer film with anionic or cationic exchange groups that transport counter-ions, transports certain dissolved ions, while blocking other ions or neutral molecules (Tedesco and Biesheuvel, 2017). Ions with a fixed charge opposite to the fixed membrane charge density are called counter-ions, while ions with a similar charge are called co-ions, e.g., for a CEM, Na^+ ions are the counter-ions and Cl^- ions are the co-ions (Galama *et al.*, 2014). Ideally, only counter-ions can pass through the IEM, whereas the co-ions are rejected. However, In practical real-world applications IEMs are not 100% selective and can transport ions with the same charge (Tedesco *et al*., 2017; Nazif *et al.*, 2022). Tedesco et al. assessed the effect of co-ion transport through the membrane and found that there is a 20% reduction in power density (Tedesco *et al*., 2016a). RED employs two primary types of exchange membranes: anion-exchange membranes (AEM) (Wang *et al.*, 2019) and cation-exchange membranes (CEM) (Pal *et al.*, 2019). AEMs, possessing positively charged groups, facilitate the passage of anions while excluding cations. Moreover, AEM contain fixed cationic groups with predominantly mobile anions; because anions are the majority species, most of the conductivity is due to anion transport (Galama *et al.*, 2014) Conversely, CEMs, with negatively charged groups, permit cation passage while restricting anions (Moreno *et al.*, 2018).

These ion-exchange membranes can be further categorized based on the nature of the fixed charge groups (Mei and Tang, 2018). Strong CEMs incorporate sulfonic groups, while weak CEMs utilize carboxylic groups. AEMs, on the other hand, contain quaternary and tertiary amines as fixed positively charged groups (Galama *et al.*, 2014; Moreno *et al.*, 2018). The distribution of ion-exchange groups within these membranes also influences their classification as homogeneous or heterogeneous. Both categories have their advantages and disadvantages (Vermaas and Nijmeijer, 2011b; Hong and Chen, 2014).

Physical structure and fabrication method are used to classify homogeneous and heterogeneous structure. In homogeneous membranes, the ion-exchange component is directly incorporated into the polymer matrix during fabrication (Jang *et al.*, 2020). This category can be further divided based on the manufacturing process. Some involve polymerization or polycondensation of monomers, which must contain at least one cation or anionic moiety. Others start from a polymer state, such as polymer film or polymer solution (Nagarale *et al*., 2006). Homogeneous ion exchange membranes, characterized by a consistent fixed ion distribution across the entire polymer matrix and typically lower area resistances than their heterogeneous counterparts, generally exhibit superior performance in RED systems (Guler *et*

al., 2012). Homogeneous membranes exhibit strong electrochemical properties but tend to have lower mechanical strength (Jang *et al.*, 2020).

In contrast, heterogeneous ion-exchange membranes display a non-uniform charge distribution due to a distinct manufacturing process. In this method, a charged ion-exchange resin is mixed or melted into an uncharged bonded polymer, which is then pressed or cast onto a membrane (Wang *et al.*, 2019). Heterogeneous membranes offer advantages in terms of simpler preparation procedures, higher mechanical strength, and lower production costs. However, they often exhibit poorer electrochemical properties. Furthermore, The membrane specific properties are further influenced by the clear distinction between homogeneous and heterogeneous IEMs (Długoł *et al.*, 2008).

In real life RED applications, IEMs most desirable properties are high selectivity, low electrical resistance, good mechanical strength, and high chemical stability (Guo and Li, 2012; Hong and Chen, 2015). It is important for IEMs to have chemical stability to endure harsh pH environments (Gi *et al.*, 2015). There are several critical parameters that are required to have IEM that gives the best performance under severe pH conditions. Some of these parameters are conductivity, thermal and mechanical stability, selectivity, and chemical resistance (Hsu *et al.*, 2019; Culcasi *et al.*, 2021). The structure of IEMs is known to play an important role in membrane performance, especially ionic conductivity, and selectivity. In general, membranes with larger pores or higher porosity have better conductivity, but their selectivity decreases (Güler, 2014a). Denser membranes have higher selectivity, suffering from high membrane resistance as noted by Klaysom *et al*. (2011). Unfortunately, achieving one desired characteristic of an IEM usually comes at the expense of another. For example, to make the membrane more conductive, the membrane must absorb a large amount of water to support the movement of ions. On the other hand, due to high water absorption, the membrane becomes mechanically unstable, resulting in poor selectivity. Therefore, it is important to carefully optimize the manufacturing process to ensure that the prepared membranes are suitable for applications with specific requirements (Klaysom *et al.*, 2011).

In membrane science, it is generally accepted that membranes should be as thin as possible while remaining free of pinholes and maintaining mechanical strength (Ranade *et al.*, 2022). Ideally, reducing uniform membrane thickness linearly reduces electrical resistance, preferably without affecting other important membrane properties (e.g., ion exchange capacity, hydraulic permeability, or permselectivity). Membrane thickness is directly correlated with resistance

(Hulme *et al.*, 2021). Heterogeneous membranes with non-uniform charge distribution (Jang *et al.*, 2020) have much higher resistance than homogenous ones (Hulme *et al.*, 2021). Güler *et al*. (2014) explored the design and development of a RED process, with a strong focus on AEM preparation, characterization, and modification in relation to RED efficiency. During the research, he observed that the power output of the RED stack was strongly dependent on membrane thickness. The thinner the membrane, the better the performance, which resulted in the highest power density of 1.27 W/m^2 for the thinnest membrane (33 μm). However, Tedesco *et al*., (2018) showed that reducing the thickness of membranes below ~ 20μm for RED has a negative effect on the performance.

The features of the membranes' structural geometry are crucial since they directly affect how the flows mix and the resistances of boundary layers as well as how much energy the pumps use to operate (Güler *et al.*, 2014). Also, membrane mechanical stability can be improved by increasing the amount of cross-linking in the polymer matrix (Jiménez *et al.*, 2017). This improves permselectivity, but also makes area resistance more pronounced, which is undesired (Vanherck and Vankelecom, 2013; Pal *et al.*, 2019).

The distance between membranes is a crucial parameter influencing the power delivery in RED (Ranade *et al.*, 2022). A wider gap between membranes results in higher electrical resistance, impacting the efficiency of ion transport and subsequently diminishing the overall power output. On the other hand, reducing the distance between membranes can elevate the pressure drop across the compartment, a factor that, while potentially enhancing ion transport, also poses challenges (Długołe and Wessling, 2009; Ashu *et al.*, 2018). The delicate balance between membrane spacing and its consequential effects on resistance and pressure drop is pivotal for optimizing the net power output in RED systems. Therefore, careful consideration and fine-tuning of the membrane distance are essential in the design and operation of RED stacks to achieve the desired balance between electrical efficiency and hydraulic performance.

2.2.2. Electrochemical and physical properties

To enhance the efficiency of RED systems, the chemical and electrochemical properties of Ion Exchange Membranes must be strategically engineered. Key parameters play a pivotal role in evaluating IEM performance within RED systems, encompassing permselectivity, thickness, Fixed Charge Density (FCD), Ion Exchange Capacity (IEC), Permselectivity, Swelling Degree (SD), and Area Resistance (AR) (Hong and Chen, 2014). However, the modification of certain aspects of IEMs doesn't uniformly lead to improvement across all parameters, often resulting

in trade-offs that complicate the pursuit of optimal conditions (Klaysom *et al.*, 2011). Navigating these complexities requires a focused approach, involving the identification and prioritization of key membrane properties. Quantitative understanding of the relationships between these parameters is very crucial for effective optimization (Guler *et al.*, 2012; Zhao *et al.*, 2016).

2.2.2.1. Ion Exchange Capacity (IEC)

IEC represents the total number of active sites or functional groups responsible for ion exchange in polymer electrolyte membrane (Gi *et al.*, 2015). The IEC of an IEM is an important parameter because the ionic transport properties of the IEM depend on the amount and type of the ion exchange group (Strathmann, 2011). IEC is expressed as milliequivalent per gram of the membrane (meq/g-dry IEM) (Długoł *et al.*, 2008; Jang *et al.*, 2020). The IEC value of an IEM depends on the type of its counter ion. Most papers on ED and RED applications measure IEC for CEMs in sodium ions as the counter ion, and for AEMs in chloride ions. In general, increasing an IEM's IEC increases permselectivity and water content while decreasing membrane resistance and mechanical strength (Gi *et al.*, 2015). The IEC of the membrane can be calculated using the following equation (Hong and Chen, 2014):

$$IEC = \frac{C_{NaOH} \times V_{NaOH}}{W_{dry}} \qquad 2.1$$

Where C_{NaOH} is the concentration of NaOH solution (mol L^{-1}), V_{NaOH} is the volume of NaOH solution (L) used and W_{dry} is the dry weight (g) of the membrane.

A high IEC means that there are more ion exchange groups within the membrane. However, swelling can reduce the concentration of these groups because the distance between them increases when the membrane is immersed in a solution (Gi *et al.*, 2015). Therefore, the ratio of IEC to the degree of swelling, known as the fixed charge density (or fixed ion concentration), represents the overall impact of swelling on IEC and establishes a direct relationship between these two electrochemical properties of an IEM (Gi *et al.*, 2015).

The IEC of an IEM is typically measured experimentally using a titration method with a strong acid, such as HCl for CEM, or a strong base, like NaOH for AEM (Gi *et al.*, 2015). Klaysom et al. soaked the CEM in 1 mol dm^{-3} HCL and then rinsed it deionised water to remove excess HCl and after the CEM was subsequently immersed into 1 mol dm^{-3} solution of NaCl. When

this was done, the IEM was soaked in deionised water for 24 hours. After that, the membrane was taken out and the moisture on the surface was wiped off with tissue paper. The wet weight of the membrane was measured. The membrane was then placed in an oven at 50 ℃ for 10 hours which is when the weight of the membrane was not changing. They then recorded the dry weight of the membrane (Klaysom *et al.*, 2011).

2.2.2.2. Permselectivity

Permselectivity is a key property that contribute to the performance of ion exchange membranes in processes like RED. Permselectivity is a measure of the membrane's ability to distinguish between anions and cations (Gi *et al.*, 2015; Jin *et al.*, 2021). This can be determined by measuring the concentration potential generated between solutions of the same electrolyte at different concentration separated by the test sample (Nagarale *et al.*, 2006). When the membrane is in contact with an electrolyte solution, counterions can pass without interruption as illustrated by **Figure 2-2**. However, co-ions cannot cross the membrane due to the repulsion of fixed charge groups (i.e., the Donnan exclusion effect) (Jang *et al.*, 2020). An ideal ion-exchange membrane (IEM) would exhibit a permselectivity of one, completely blocking co-ions from passing through. However, based on Donnan's theory (Nagarale *et al*., 2006; Długoł *et al.*, 2008), some co-ions may still contribute to the transport current (Luo and Wessling, 2018). Additionally, permselectivity and ionic resistance are vital characteristics for RED, while other properties have a lesser effect on power generation (Gi *et al.*, 2015).

In the context of RED, higher permselectivity means that the membrane is more effective at selectively allowing the transport of specific ions, such as positive and negative ions, while inhibiting the passage of others. This selectivity is essential for maintaining the electrochemical potential difference across the membrane, which is crucial for generating voltage in the RED system.

When a membrane has high permselectivity, it facilitates the preferential movement of ions essential for the electrochemical process, allowing the creation of a concentration gradient across the membrane. A membrane with higher permselectivity allows for more efficient separation and movement of ions, leading to a greater potential difference and, consequently, an increased voltage in the RED system.

2.2.2.3. Fixed Charge Density (FCD)

Fixed charge density (FCD) is the calculation of fixed charge groups attached to the backbone of polymer (Długoł *et al.*, 2010). These groups are either anionic or cationic and they transport

cations or anions depending on the polymer type (Długoł *et al.*, 2010), meaning FCD helps in dictates the transport of counter-ions and the exclusion of co-ions through IEMs. Moreover, the counterion transport and ion permselectivity across the membrane are determined by the fixed charge density of the membrane (Długoł *et al.*, 2010; Guler *et al.*, 2012). The fixed charge density is expressed in milliequivalent of fixed groups per volume of water in the membrane (meq L^{-1}) and can be determined by the IEC over the SD of the membrane (Hong and Chen, 2014).

$$C_{fix} = \frac{IEC}{SD} \qquad 2.2$$

(Where C_{fix} is fixed charge density)

The concentration and nature of the fixed ionic charges determine the membrane's permselectivity and electrical resistance (Długoł *et al.*, 2008). The membrane resistance is significantly affected by fixed charge density (Tedesco *et al*., 2016b), i.e. as the membrane fixed charge increase, the resistance of the membrane decreases (Moya, 2016). Also, the membrane permselectivity increases with increasing charge density, this is because as charge density increase, the stronger is the exclusion of co-ions (Guler *et al.*, 2012).

Selectivity of IEMs depends highly on the pore size and fixed charge density on the pore walls (Luo *et al*., 2018). Moreover, The fixed charge density of membranes increase with reduced pore size and porosity (Klaysom *et al.*, 2011). On the other hand, with larger pore size and higher porosity in the membrane, the Donnan exclusion becomes less effective and therefore the ionic species with any signs can freely move across the membrane (Klaysom *et al.*, 2011).

According to Moya (2016), increasing the fixed charge concentration results in higher OCV and power density. This is because an increase in membrane fixed-charge concentration enhances the membrane's selectivity. There is a linear relationship between power density and selectivity. But Rijnaarts *et al*., (2019) found that a higher charge density in the polymer leads to larger swelling as well.

Tedesco *et al*., (2016b) noticed that the fixed charge density of the IEM significantly influenced the efficiency of the RED process, affecting the concentration of co-ions inside the membrane. They also reported that a decrease in fixed charge density leads to an increase of the co-ion transport and a reduction of the counter ion transport through the membrane.

2.2.2.4. Swelling Degree (SD)

The swelling degree of the membrane is defined as the water content or water uptake of the membrane under specific experimental conditions. It is quantified by the weight difference between its wet and dry states (Nagarale *et al*., 2006; Güler *et al*., 2014a). Swelling typically has a negative impact on the RED process because it tends to decrease the permselectivity of IEMs. However, in certain cases, especially for AEMs, it can also reduce membrane resistance (Nagarale *et al*., 2006; Gi *et al*., 2015; Zhu *et al*., 2018).

$$SD(\%) = \frac{m_{wet} - m_{dry}}{m_{dry}} \times 100 \qquad 2.3$$

Rijnaarts *et al*., (2019) investigated the RED performance of six AEMs varying in chemistry and characteristics. They found that AEMs with a low swelling degree exhibited a decrease in permselectivity along with an increase in membrane resistance. Furthermore, Enver Güler *et al*., (2014a) noticed that crosslinking reduced swelling and thus increased the charge density, but this apparently led to an increase in the resistance of the membrane.

2.3. Effect of Concentration polarization phenomena

Concentration polarization (CP) is one of the most important factors affecting the performance of membrane separation processes. Moreover, CP is determined by solute properties, membrane properties and fluid dynamics (Kim and Hoek, 2005). Solutes that are partially or fully retained will accumulate in a thin layer next to the membrane surface, creating a concentration gradient, i.e. a solute concentration near the membrane surface is much higher than that of bulk feed solution (Klaysom *et al.*, 2011; Gurreri *et al.*, 2014). As a consequence, a deficit flux of solute back to the feed bulk appears. The solute build up at the membrane's surface until the equilibrium between diffusive and convective solute flux is attained (Scientific and Company, 1980; Ashu *et al.*, 2018). As a result, the solute concentration changes from a maximum at the membrane surface to the bulk as depicted by **Figure 2-2**. Fouling is often the results of CP (Scientific and Company, 1980). This can reduce the potential difference established between electrodes, as the salt concentration gradient across the membrane is reduced (Pawlowski *et al.*, 2014). Membrane lifespan is also affected by CP (Sablani *et al*., 2001), this is because CP of solute at the membrane surface can lead to solute precipitation, solute adsorption, and gel layer formation which lead to increased operating costs since membranes must be cleaned frequently (Sablani *et al*., 2001).

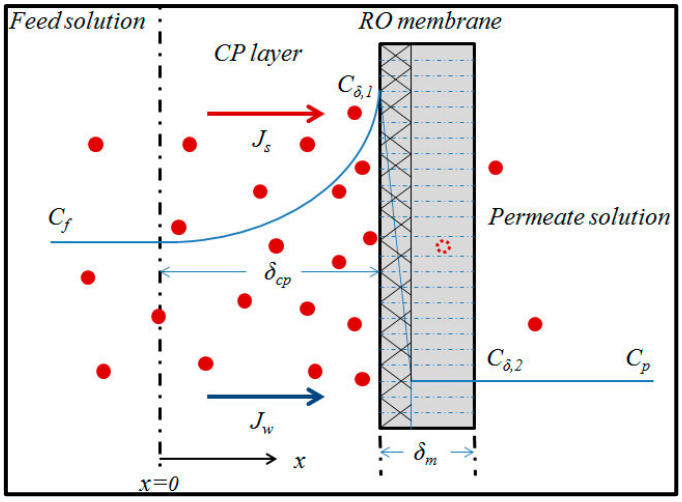

Figure 2-2: A schematic representation of concentration polarization (Chen and Qin, 2019).

CP increases resistance solvent flow and thus it's responsible for the water flux decline observed in many membrane separation processes (Sablani *et al*., 2001). It might also change the membrane separation properties as Matthiasson *et al*.,(1980) reported in their study. However, CP cannot be avoided in the membrane process but it can be minimize by varies methods (Ahmad *et al*., 2005; Bai *et al.*, 2023). It is also reversible and can be controlled by velocity regulation, pulsation, ultrasound, or electric fields within the membrane module (Sablani *et al*., 2001). In order to be able to deal with the problem of concentration polarization, it is crucial to understand mass (ion) transfer phenomena at the membrane-solute interface (Scientific and Company, 1980). To enhance mass (ion) transfer, the concentration polarization near the membrane interface should be reduced. This is typically achieved by increasing fluid mixing and encouraging convective phenomena (Ashu *et al.*, 2018). Increasing the feed flow enhances fluid mixing, which reduces the diffusion boundary layer resistance at the membrane interface due to the effect of tangential stress on the boundary layer thickness (Ashu *et al.*, 2018; Moreno *et al.*, 2018). This also results in a greater potential difference across the ion exchange membranes (IEMs) inside the stack, leading to higher power density (Ashu *et al.*, 2018). Hulme *et al*., (2020) also reported that increasing flow rate lead to a reduction of concentration polarization. Unfortunately, this increases pumping energy which is a negative factor (Zhu *et al*., 2015b; Mehdizadeh *et al.*, 2019).

2.4. Diffusion boundary layer

Diffusion boundary layer (DBL) refers to a thin region near a surface in which the concentration of a substance (such as heat or a solute) changes from its bulk concentration to zero or some other value at the surface (Długoł *et al.*, 2010; Zhang *et al.*, 2016). This change in concentration occurs due to diffusion, which is the process by which molecules move from regions of higher concentration to regions of lower concentration. In the diffusion boundary layer, the rate of diffusion is slowed by the close proximity of the surface, which impedes the movement of the diffusing species (Długoł *et al.*, 2010). The thickness of the diffusion boundary layer depends on various factors, including the properties of the diffusing species, the properties of the surface, and the conditions under which diffusion is occurring. **Figure *2-3*** illustrate the diffusion boundary layer on a membrane. It reduces the electrochemical potential difference, ultimately compromising the voltage generation in RED systems.

To enhance RED efficiency, mitigating the effects of the diffusion boundary layer is essential. Enhancing fluid mixing by increasing the flow rate and /or introducing spacers can reduce the thickness of the diffusion boundary layer (Pawlowski *et al.*, 2014). However, it was found that the presence of spacers not only reduces the boundary layer thickness, but also increases the ohmic resistance due to shadow effects at the membrane surface (Pawlowski *et al.*, 2014). Increasing the feed flow enhances hydrodynamic mixing (Długoł *et al.*, 2010) and reduces diffusion boundary layer resistance at the membrane interface due to the effect of tangential stress on the boundary layer thickness (Gurreri *et al.*, 2016). As a result, the potential difference across the IEM is increased, resulting in a higher power density (Zhu *et al*., 2015b). Boundary layer is also affected by temperature (Benneker *et al.*, 2018; Mehdizadeh *et al.*, 2019). As the temperature increases, the thickness of diffusion boundary layer decreases. This effect is due to an increase ion mobility that leads to a higher shielding effect of the electrical attraction between fixed charged groups and ions in the bulk solution (Zhang *et al.*, 2016).

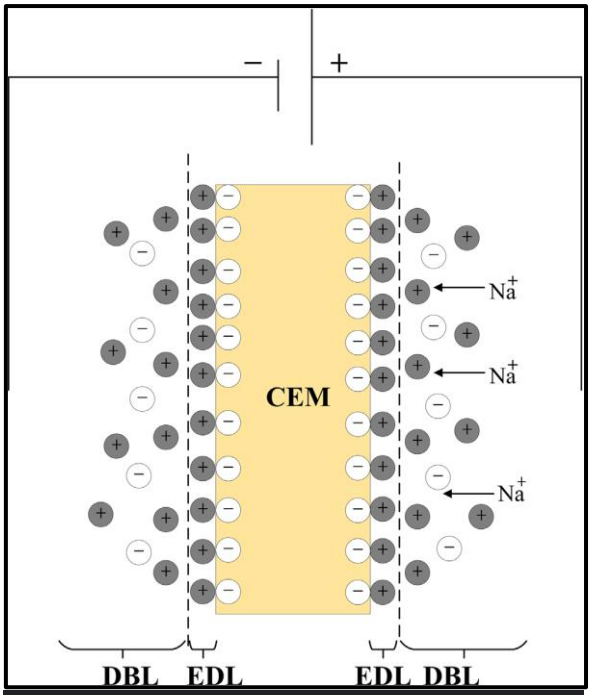

Figure 2-3: The electrical double layer (EDL) and the diffusion boundary layer are formed between the solution and the membrane (Zhang et al., 2016).

2.5. Electrode systems for RED

Electrodes play an essential role in energy conversion systems (Burheim *et al.*, 2012; Khalla and Suss, 2019; Nasir *et al.*, 2020). Recent papers (Simões *et al.*, 2020; Severin and Hayes, 2021; Wu *et al.*, 2023) have shown that a proper selection of redox species and of electrode materials is of paramount relevance in order to have a successful RED process (Scialdone *et al.*, 2013). The electrode is the place where electron transfer occurs (Scialdone *et al.*, 2012). Electrodes systems can be grouped in two categories: with or without opposite electrode reactions (Lee *et al.*, 2016) (e.g., the direct and the reversed reaction take place at the anode and the cathode, respectively). First, for systems with opposite electrode reactions and a recirculating electrode rinse, there is no net chemical reaction (Ashu *et al.*, 2018). These systems have a zero equilibrium voltage (Mei *et al*., 2018). Because there is no energy required for a net chemical reaction, a RED system with such an electrode system can produce electrical energy using only a few cells (Veerman *et al.*, 2010). The advantage of this system is there is no loss of chemicals and no gas production (Scialdone *et al.*, 2013). Fe^{2+}/Fe^{3+} and $[Fe(CN)_6]^{4-}/[Fe(CN)_6]^{3-}$ with inert electrodes are representative examples of this system (Jang *et al.*, 2020). Veerman *et al*., (2010) compared self-developed electrode systems and electrode systems that were described in the literature on safety, environment, health, economics, and technical

feasibility. They then presented a useful way of judging different system. The authors concluded that Fe^{2+}/Fe^{3+} couple in combination with graphite electrodes were a viable way but these systems were to be tested under real conditions to check for sufficient mechanical and electrochemical stability. In all these processes the electrode play an active role in the redox process: one electrode is growing and the other is dissolving (Veerman *et al.*, 2010; Ashu *et al.*, 2018). In such systems the feed solutions should be interchanged periodically to invert the direction of the electric current and with the electrode process (Veerman, 2010; Veerman *et al.*, 2010; Vermaas *et al.*, 2012). By combining homogenous redox couples with inert electrodes, this reversal may be prevented, which lowers the cost of the electrodes, improves the device's energy efficiency, and makes the stack easier to build (Scialdone *et al.*, 2013).

Reactive electrodes actively participate in reactions while inert electrodes do not participate in chemical reactions. Inside the RED stack, they are two electrode namely anode and cathode (Veerman *et al.*, 2010). Electrodes are classified as either cathodes or anodes, depending on the type of chemical reaction that occurs. When an oxidation reaction occurs at an electrode, the electrode is classified as an anode when a reduction reaction occurs at an electrode, the electrode is classified as a cathode (Yu *et al.*, 2018). Therefore, in a typical RED system, Chlorine ion is attracted to the anode because of the positively charged polymer in the anode and Sodium ion is attracted to the cathode. Oxidation and reduction reactions occur at each electrode by potential difference as a driving force, thereby the charge transfer (or ionic current) is converted to electric current (Post, 2009; Han *et al.*, 2019; Jang *et al.*, 2020).

In stacks with a large number of cell pairs in series, the voltage loss that is lost at the electrodes is negligible relative to the sum of the membrane potentials (Weiner *et al.*, 2015; Tedesco *et al.*, 2017). This is because as the number of cell increases, the energy efficiency of the system sharply increases and the larger RED stack voltage reduces the effect of electrode resistance on the electric power (Han *et al.*, 2019; Severin and Hayes, 2021). Looking at the literature, it seems there is no specific number that researchers agree on when it comes to what constitute a high number of cell pairs. According to Veerman *et al.*, (2010), a stack with 1000 cells pairs has a 3% power loss at the electrodes when considering the whole power output. But increasing cell pairs can come with some problems. Increasing number of cell pairs will increase the overall internal resistance of the RED stack (Culcasi *et al.*, 2020). The main reason for this is because of how the RED stack is fundamentally constructed. With an increase in membrane pairs, there are more channels for the feed, which could increase the internal resistance (Pawlowski *et al.*, 2014). On the other hand, ions driven by the electrochemical potential

difference between adjacent compartments migrate through the feed and drain channels, resulting in ion shortcut currents (Culcasi *et al.*, 2020). As the number of pairs increase, membrane pile up and the presence of ionic shortcut current becomes non-negligible, and the resistance increases significantly. With an increase membrane pairs, the accumulative effect of ionic shortcut current affects the electrical properties of RED and this reduces the maximum power density (Fu, 2020).

Ionic shortcut current refers to the electrical current that flows directly between the two electrodes in an electrochemical system, bypassing the ion exchange membranes that are intended to selectively allow the passage of certain ions (Veerman *et al.*, 2008; Culcasi *et al.*, 2020). This phenomenon occurs because the membranes are not perfect barriers and there are always some ions that can pass through them, creating a 'shortcut' path for electrical current (Culcasi *et al.*, 2020). In the context of RED, the presence of ionic shortcut currents can reduce the efficiency of the process by reducing the voltage that is generated across the system (Veerman *et al.*, 2008).

Platinum and iridium are two of the most widely used metals for electrodes (Kwon *et al.*, 2015; Guo *et al.*, 2018; Simões *et al.*, 2020), however these metallic electrodes are very expensive. Lee et al. compared the performance of graphite foil electrodes coated by porous carbon black with metal electrodes for RED applications. The study discovered that graphite foil electrode performed better than metal mesh electrode. They showed 5-10% higher power than the metal mesh electrodes (Lee *et al.*, 2016). Tedesco et al. used $[Fe(CN)_6]^{4-}/[Fe(CN)_6]^{3-}$ in their work, which is the most widely used redox couple in RED laboratory experiments due to its excellent stability in various experimental settings (Tedesco *et al.*, 2015). Scialdone *et al*. (Scialdone *et al.*, 2013) listed requirements for a good electrode system. They recommended iron-based electrodes because iron is abundant and is often non-toxic in low concentrations. The authors listed requirements for a redox couple that can be considered best candidate. This redox couple should have (i) high stability under operative conditions in terms of high concentrations of redox chemical species, low pH, and absence of air (ii) very low toxicity; (iii) low cost of components and electrodes and (iv) very low energy penalty.

Among the commonly utilized redox couples, the Fe(III)-Fe(II) system holds prominence due to several advantageous characteristics (Avci *et al.*, 2018; Jordi Moreno *et al.*, 2018; Bodner *et al.*, 2019; Ju *et al.*, 2020). Iron, a key component in this redox couple, is abundantly available, environmentally benign at low concentrations, and exhibits stability across a broad pH range,

particularly around neutrality. These attributes render Fe(III)-Fe(II) a preferred choice in various applications, aligning with the need for sustainable and safe energy solutions. Notably, Scialdone *et al*., (2013) examined the impact of selected redox processes on power density output. Their investigation revealed a significant correlation between the power output and the specific redox processes employed. This underscores the critical role that the choice of redox couple plays in influencing the efficiency and performance of RED systems.

2.6. Effect of monovalent and multivalent ions on the RED system

Although RED technology is advancing, power output remains limited, especially when using natural feed water sources (Kingsbury *et al.*, 2017). Since its application in practice requires the use of natural seawater and river water, the presence of multivalent ions is inevitable, and this currently limits RED performance (Ashu *et al.*, 2020). The presence of multivalent ions in natural waters leads to uphill ion transport within a RED stack (Post *et al*., 2009; Moya, 2020). In seawater, the most commonly found salt ions are sodium, magnesium, calcium, chloride, sulphate, and bicarbonate (Brennan and Lowenstein, 2002; Lowenstein *et al.*, 2005). Multivalent ions increase the membrane's electrical resistance and reduce the power generation. (Tufa *et al.*, 2014). Although natural seawater and river water contain a mix of monovalent and multivalent ions, laboratory research on RED typically uses artificial NaCl solutions (Vermaas *et al*., 2014; Tedesco *et al.*, 2015). This is not an accurate representation of what is happening in real world since seawater contains more than just sodium ions and chlorine ions (Tedesco *et al*., 2016). Natural water solutions contain other ions, including natural organic matter (NOM) (Kingsbury *et al.*, 2017; Suhendra *et al.*, 2023) and multivalent ions that adversely affect the performance of RED (Post *et al*., 2009; Guo *et al*., 2012). Kingsbury *et al*. (2017) measured power generation from five real water pairs (seawater, desalination brine, river water, treated wastewater, and saline wastewater from pickling plant) containing complex mixtures of ions and NOM in laboratory-scale RED stacks. Additionally, the performance of each real water pair was compared with that of synthetic control waters with the same conductivity for the investigation of the impact of inorganic constituents and natural organic matter. The result showed that the presence of NOM has greater effect on power density than ionic composition. In the study, NOM reduced power density by up to 43%. Furthermore, result showed that the pickling brine/storm water pair behaved differently from the other pairs in that the presence of NOM in the prickling brine improved the performance of the process.

The performance of the first RED pilot plant demonstrated that using real natural water reduces power output(Tedesco *et al*., 2016). This indicated how the presence of significant quantities of non-NaCl ions reduces the electromotive force of the membranes pile. Recently, significant work has been conducted on both the experimental characterization of multivalent ion transport effects in RED and the mitigation of these effects (Besha *et al.*, 2019; Kotoka *et al*., 2020; Moya, 2020).

2.6.1. Uphill transport

Uphill transport refers to the process of ion transport in the direction opposite to the concentration gradient, moving from low to high concentration (Rijnaarts *et al.*, 2017). In this phenomenon, multivalent ions are transported from the low concentration compartment to the high concentration compartment when a larger excess of monovalent is present on the concentrated side of the membrane. This process is purely entropic, in that, the entropy gained by the transfer of two monovalent ions from the concentrated side to the diluted side exceeds the entropy lost by the transfer of a single multivalent ion from the diluted side to the concentrated side (Rijnaarts *et al.*, 2017). Hence, the presence of multivalent ions in the process results in an irreversible loss of available energy from monovalent ions, leading to reduced performance (Ashu *et al.*, 2018). Put differently, a divalent ion (e.g., Mg^{2+}) can move towards the concentrated compartment and replace two monovalent ions (e.g., Na^{+}), without generating a net electrical current (Post *et al*., 2009; Vermaas *et al*., 2014). As a result, the salinity gradient for monovalent ions will be reduced and the produced voltage will decrease (Vermaas *et al.*, 2012; Vermaas *et al*., 2014). Therefore, the presence of multivalent ions in RED is counterproductive. Moreover, Uphill transport phenomenon causes a reduction in OCV and an increase in membrane electrical resistance due to lower diffusion coefficients of the divalent ions compared to monovalent ions (Vermaas *et al*., 2014). Additionally, multivalent ions can bond with fixed charged groups inside the membrane (Moreno *et al.*, 2018). A viable strategy to deal with multivalent ions is to use monovalent-selective membranes inside the RED stack, this will be useful especially in the case of a relatively high content of multivalent ions in the dilute (Vermaas *et al*., 2014). Avci *et al*., (2016) recommended special monovalent-selective IEMs to reduce the transport of divalent ions through the membranes. Furthermore, Mehdizadeh *et al*., (2021) used monovalent ion-selective membranes with a selective layer facing a low-concentrate compartment to prevent or reduce divalent ion's undesired uphill transport.

Rijnaart *et al.*, (2017) investigated the negative effects of the presence of divalent cations in RED. In that study, strategies to mitigate these effects were presented. Two of the strategies were (I) the use of monovalent-selective membranes and (II) multivalent-permeable membranes that were recently developed specifically for RED in natural water streams. Literature (Guler *et al.*, 2012; Güler *et al.*, 2014; Zhao *et al.*, 2016; Rijnaarts *et al.*, 2017; Gómez-coma *et al.*, 2019) has shown that that it is beneficial to use monovalent-selective membranes in RED processes especially in the case of a relatively high content of multivalent ions. Veerman *et al.*, (2009) tested various commercial membranes to assess the power density and thermodynamic efficiency of RED. In their study, they recommended using IEMs with enhanced monovalent ion selectivity for operating RED with real feed solutions..

Moreno *et al.*, (2018) investigated four cation exchange membrane types using three different magnesium concentrations. The results indicated that power density decreases in the presence of magnesium, which also has a negative effect on OCV. It was also found that the presence of magnesium significantly decreased both the power density (1.11 W/m^2, -64% with respect to pure NaCl) and OCV (2.73, -20% with respect to pure NaCl) and caused a significant cell resistance.

2.6.2. Fouling

The future prospect of employing RED system is in the use of natural feed water as that is the most abundance source. However, the use of real natural water sources present challenges, such as the presence of multivalent ions (Post *et al.*, 2009), membrane fouling (Pawlowski *et al.*, 2017) and spacer fouling (Rijnaarts *et al.*, 2019) that decreases RED performance. Fouling is one of the key bottlenecks for the practical implementation of RED. A study was conducted by Vermaas *et al.*, (2012) conducted a RED pilot study in Harlingen, Netherlands, where they investigated the impact of natural fouling using stacks with spacers or ridge-profiled membranes. The study revealed that the presence of organic matter may have contributed to a decrease in OCV and an increase in resistance. Also, a substantial pressure drop along the feed water compartment was observed. Others have also seen an increase in pressure drop over time due to fouling (Vermaas *et al.*, 2011b; Vermaas *et al.*, 2012; Moreno *et al.*, 2017; Luque *et al.*, 2018). In a study conducted at Afsluitdijk, The Netherlands, Moreno *et al.*, (2017) investigated the use of carbon dioxide-saturated water as a two-phase flow cleaning method for mitigating fouling in RED using natural feed water. An increase in the pressure drop between the feed water inlet and outlet was observed. This resulted in increased pumping energy requirements,

thereby reducing the net power density achievable. Fouling poses one of the most significant challenges to the design and operation of membrane processes.

Fouling in membrane separation occurs due to several mechanisms, including precipitation of sparingly soluble salts, adsorption, formation of cake or gel layers, and pore blockage (Matthiasson and Sivik, 1980; Sablani *et al*., 2001). Depending on where the foulant is deposited, fouling is usually divided into external and internal fouling. Fouling of the RED stack has a strong influence on the gross power density output (Moreno *et al.*, 2017). This is even more severe when natural feed waters are used (Vermaas *et al.*, 2012). Various types of fouling can occur, such as scaling, biofouling, adhesion of organic substances, and deposition of colloids (Guo *et al*., 2012; Rijnaarts *et al.*, 2019). Both CEMs and AEMs are susceptible to various types of fouling, which are primarily influenced by differences in the charge characteristics of the membranes (Rijnaarts *et al.*, 2019). In general, CEMs are primarily affected by organic and colloidal fouling (Vermaas *et al.*, 2014). Fouling increases pressure drop, which in turn raises hydraulic losses, thereby increasing the pumping energy required to move the feed (Moreno *et al.*, 2017). A number of studies on strategies for fouling prevention have been done (Guo *et al*., 2012; Wang *et al.*, 2019; Nazif *et al.*, 2022). Wang *et al*., (2019) modified AEMs by poly (Sodium 4-Styrene Sulfonate) (PSS) with titanium dioxide nanoparticles using the one-step electrode position method to enhance the antifouling ability of the membranes. This method promoted the fouling reversibility in the membrane, while at the same time improving negative charge density and the hydrophilicity of the membrane. This was the result of using Ultraviolet (UV) irradiation through photocatalytic decomposition. The modified AEMs showed some increase in membrane resistance due to PSS modification, electric resistance was lower than the pristine membranes after 100 minutes of fouling. Other researchers have also used Ultraviolet to induce antifouling properties (Güler *et al*., 2014b; Salters and Piola, 2017; Ryan *et al*., 2020).

Fernandez-Gonzalez *et al*., (2017) investigated the enhancement of organic fouling resistance of nanocomposite AEMs made from a commercial polyethylene anion exchange membrane and a negative thin layer. They evaluated the effects produced by the introduction of negatively charged nanocomposite layer on the fouling resistance of the AEMs. They used sPPO, Fe_2O_3-SO_4^{2-} and CNTs-COO^- to allow for a highly negative charge within a very thin layer, this in turn improved conductivity and reduced the resistance of the membrane. The enhancements led to a 53% improvement in fouling resistance and energy savings between 49% and 60%.

Choi *et al*., (2022) Investigated the effect of reducing fouling using patterned IEMs based of changes in pressure drop and membrane resistance. In the study, patterned membranes that consisted of ultra-thin pore-filling were used to determine whether the RED system was operating steadily when using sewage and natural underground seawater. Performance of the pattern stack, which consists of patterned membranes with mirror-imaged wavy lines, were compared to those of the flat stack, which consists of flat membranes and woven-type spacers. The process was in operation for 14 days. The results showed that patterned membranes that were used created a uniform fluid-flow environment that could reduce fouling in the stack. Moreover, it was also observed that switching the flow direction of the feed water in the inlet and outlet was an effective cleaning method.

Various membrane related fouling studies rely on the implementation of membrane fouling simulator (MFS), which is useful when measuring pressure-driven processes, but not very useful when monitoring the current driven RED process using IEMs. Bodner *et al*., (2019) introduced the RED Fouling Monitor proof of concept to the scientific community, in which one side of a single ion-exchange membrane in contact to a foulant-containing feed stream can be studied under OCV and current conditions. This tool was able to give a detailed, defined, real-time fouling analysis for RED applications. This tool followed the progression of fouling-relevant operational parameters for one side of a single ion-exchange membrane. Prior to the fouling investigation, river or seawater were chosen as the salt bridge electrolyte solution and the ambient medium of choice to test the operational stability using artificial feed water in two different configurations. This tool was able to detect immediate performance changes in real-time, thus detecting detailed differences in fouling behaviour. What this study demonstrated was that RED Fouling monitor has a potential use in identifying the fouling potential of different feed water sources and seasonal changes.

2.7. Effect of spacer geometry

A RED stack consists of many pairs of cells, each cell pair consisting of alternating CEMs and AEMs separated by spacer-filled channels, allowing fluid to flow across the membrane surfaces. The membranes are supported by a spacer, which also form the flow channels for the diluted and concentrated stream while also promoting the mixing of solutions through inertial forces imposed by the mesh filaments (Wagholikar *et al.,* 2017). The mixing process reduces concentration polarization (Nazif *et al.,* 2022), thereby minimizing non-Ohmic resistance (Kwon *et al*., 2017). Spacers are typically porous materials placed between adjacent IEMs and

electrode pairs inside the stack. Pawlowski *et al*., (2014) noticed that the presence of spacers reduced the diffusion boundary layer compared to the case without spacers in the channels. But, spacers also cause an increase in pressure drop inside the compartments (Pawlowski *et al*., 2014).

The spacers are usually placed between membranes to maintain membrane distance (Gurreri *et al.*, 2014), but their presence also has a significant impact on RED stack resistance, often referred to as the spacer shadow effect (Pawlowski *et al.*, 2014). Dlugolecki *et al*., (2010) investigated the influence of the spacer shadow effect on the RED stack and revealed that 30-40% of the available energy is lost due to the spacer shadow effect when commercially available, non-conductive spacers are used. The inclusion of spacers notably reduces power generation due to membrane area loss caused by blockage from non-conductive spacers. (Długoł *et al.*, 2008; Gi *et al.*, 2015). Furthermore, spacers causes a larger increase in friction coefficient which leads to an increase in channel thickness and decrease in optimum velocities as was observed by Ciofalo *et al*., (2019). Space geometry plays a huge role on the performance of the RED process because it impacts pressure drop, mass transfer and resistance as previously mentioned. For these negative reasons, Profiled membranes have been proposed as alternative to traditional spacers because of their ability to improve the performance of RED systems by reducing hydraulic losses and removing the spacer shadow effect (Güler *et al.*, 2014; Pawlowski *et al.*, 2016; Jin *et al.*, 2021). The power output in RED stacks fitted with profiled membranes is greater than in equivalent RED units equipped with non-conductive spacers (Ashu *et al.*, 2018).

One possible remedy to reduce the spacer shadow effect is to use ion-conductive spacers instead of the conventional inert spacers as illustrated by **Figure *2-4***. Dlugolecki *et al*., (2010) developed and applied ion conductive spacers for RED. Substituting commercially available, non-conductive spacers with ion-conductive spacers resulted in a notable decrease in stack resistance and an increase in power density of a factor 3 compared to the use of non-conductive spacers made of PVC with the same open area and shape. In addition, when using non-conductive spacers, the stack resistance was significantly increased. This was because non-conductive spacers reduce the area available for ion transport. However, this did not reduce hydraulic friction as the spacer design was far from optimal. This was in agreement with Pawlowski *et al*., (2016) study where they investigated different types of membranes including profiled membranes. The results of the study were compared with the performance of RED stacks with non-conductive and conductive spacers. There was a 76% net power gain relatively

to channels with non-conductive spacers. Pawlowski et al., (2017) conducted a similar study where they experimentally verified the CFD modelling predictions. The study compared the performance of six different RED stacks formed by different combinations of flat membranes with spacers. Profiled membranes with pillar corrugations and profiled membranes with chevron corrugations were experimentally evaluated in terms of OCV, resistances, net and gross power density and hydraulic friction in the feed channels. The findings showed that stacks with profiled membranes have a 25% lower Ohmic resistance compared to those with a spacers-only setup. The reason for this is because the main electric resistance of a RED stack is located in the diluted compartment because of the much lower conductivity compared to the concentrated compartment (Mehdizadeh *et al.*, 2021). The highest achievable gross power density values were obtained in stacks with chevron-profiled membranes. Additionally, In comparison to other stacks with net spacers or pillar profiled membranes, stacks with chevron profiled membranes have shown higher net power density values (Pawlowski *et al.*, 2017).

The non-conductive spacers (**Figure *2-4***), which are traditionally used to keep the membranes apart, greatly increase the internal resistance and the hydraulic friction of the feed solution (Vermaas *et al.*, 2011b), this is because spacers partially cover the membrane surface, creating longer paths for ion transport in solutions (Ashu *et al.*, 2018). This phenomenon is called spacer shadow effect (Nazif *et al.*, 2022).

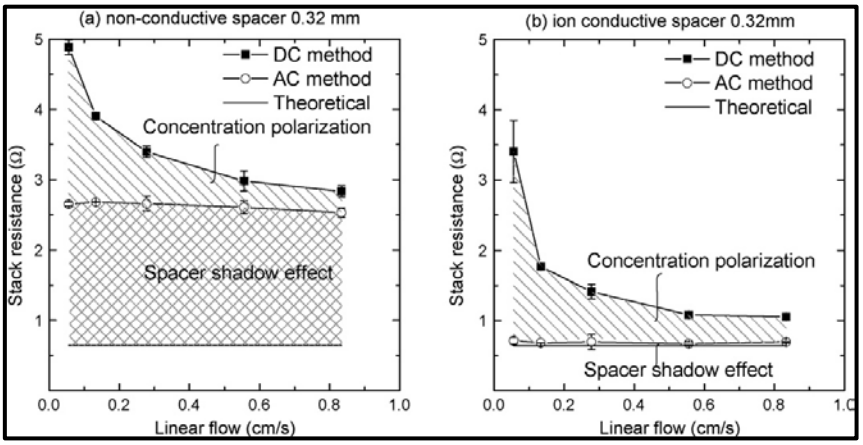

Figure 2-4: The resistance of the stack plotted against the linear solution flow rate is depicted for two scenarios: (a) using a non-conductive 0.32 mm spacer and (b) employing an ion-conductive 0.32 mm spacer in the normal configuration, where the anion exchange part is positioned on the anion exchange membrane and the cation ion exchange part is situated on the cation exchange membrane (Długołe, Gambier and Wessling, 2009)**.**

Mehdizadeh *et al.*, (2019) investigated the spacer shadow effects on both membrane and solution compartment resistances using 16 spacers having different geometries with 0.100-

0.564 mm thickness and 56-84% porosity. The results of the study showed that there is a quantitative way to estimate the RED stack resistance with varying spacer dimensional characteristics. Additionally, it was discovered that using a spacer that is thinner than the gasket can reduce the shadow effect contribution on the membrane. This is because the contact area of the membrane and the resulting shadow effect depends on the difference in spacer and gasket thickness. As the spacer thickness becomes thinner than the gasket, the contact area decreases, resulting in less shadow effect.

2.8. Effect of electric resistance

To achieve a high net power density in RED, it is important to keep the internal resistance of the stack and the hydraulic friction of the feed waters in the compartments low (Rijnaarts *et al.*, 2017). The electrical resistance is a measure of the driving force (voltage) required to transport charge (ionic current) through the membrane. The resistance of the membranes increases when the driving force needed to transport ions increases (Rijnaarts *et al.*, 2017). Internal resistance is the resistance within the system that causes a drop in the source voltage where electricity is flowing. Theoretically, the resistance of the RED stack is the sum of all component resistances in series, including electrodes, membranes, spacers, electrolytes, and the DBL (Joanna, *et al.*, 2010; Gi *et al.*, 2015). Minimizing internal resistance reduces electrical losses in the stack, whereas hydraulic friction in the feed water increases pumping power requirements. For an ideal RED stack, the maximum power density is obtained when the load resistance equals the internal stack resistance (Moya, 2016).

In RED, the internal resistance of the stack is composed of several components: Ohmic resistance, non-Ohmic resistance, and the resistance of the electrode system (Moreno *et al.*, 2016). A non-ohmic resistance is a resistance which does not follow the ohm's law, i.e., the non-ohmic resistance has a non-linear relationship between voltage and current. Non-ohmic resistance is due to diffusion boundary layer resistance (R_{dbl}) and electrical double layer resistance (R_{edl}). R_{dbl} and R_{edl} can be measured experimentally by using electrochemical impedance spectroscopy (EIS) (Długoł *et al.*, 2010; Zhang *et al.*, 2016). In practice, the contribution of non-Ohmic resistance to the stack's internal resistance is minimal, especially when working with highly concentrated salt solutions (Długoł *et al.*, 2010).

In the RED stack, the salt concentration near the membrane surface is lower than the bulk on the concentrated side and the concentration near the membrane is higher than the bulk on the diluted side. Therefore, the Ohmic resistance of a cell pair is mainly determine by the diluted

side (Takagi *et al*., 2014; Zhu *et al*., 2015b). The thin depletion layer on the concentrated side and the thin enrichment layer on the diluted side have little effect on the total Ohmic resistance of the cell pair (Rijnaarts *et al.*, 2017).

Most of the RED stack resistance comes from the diluted side (Galama *et al.*, 2014; Geise *et al.*, 2014; Wu *et al.*, 2022). Furthermore, when operating the RED stack with natural waters, the river water compartment contributes more to the overall resistance. The reason is because river water has low electric conductivity due to the low salt concentration (Długołe *et al*., 2009; Moreno *et al.*, 2016).

Sugimoto *et al*., (2022) used low-area-resistance IEMs that resulted in lower internal resistance and higher power density. Another way to reduce non-Ohmic resistance is to not use non-conducting spacers, but use ion-conductive spacers (Vermaas *et al*., 2011b; Sharma *et al.*, 2022), this enhances the mixing process which leads to the minimization of non-Ohmic resistance (Długoł *et al.*, 2010).

2.9. Fundamentals of reverse electrodialysis

2.9.1. Principles and mechanism of RED

In a typical RED system, an alternating series of cation exchange membranes (CEMs) and anion exchange membranes (AEMs) are stacked between two electrodes, with each ion exchange membrane separated by a spacer as depicted by **Figure 2-5**. Spacers are used to maintain an appropriate distance between the membranes, create compartments for feed solutions and to promote turbulence (Ortiz-imedio *et al.*, 2019). The ion-selective membranes used in RED are typically made from a variety of materials (Koter *et al*., 1999; Nagarale *et al*., 2006; Güler *et al.*, 2014; Kowsari *et al*., 2015; Zhang *et al.*, 2017). These membranes are strategically designed to facilitate the passage of specific ions while preventing the mixing of the two solutions. Consequently, a concentration gradient is established between two solutions with differing salt concentrations. When these solutions are positioned on opposite sides of the ion-selective membranes, ions move through the membrane towards the solution with lower concentration driven by the concentration gradient.

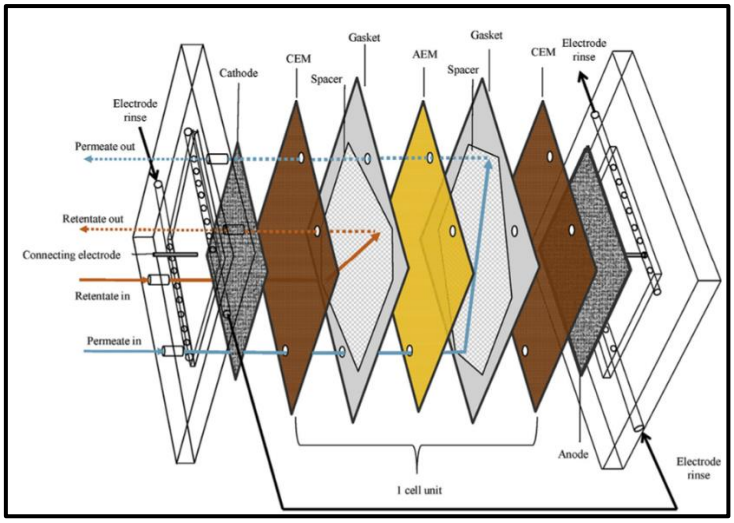

Figure 2-5: Diagram of a RED stack (Mercer et al., 2019)

Between two adjacent IEMs there is an AEM, a low concentration compartment, a CEM and a high concentration compartment. This forms what is called a cell and a RED stack typically contains a large number of cells (Daniilidis *et al.*, 2014). The driving force for the movement of ions is the potential difference across the membranes (Güler *et al.*, 2013; Tedesco *et al.*, 2015). This potential difference is created by applying an electric field across the membranes, which is achieved through the use of electrodes (Veerman *et al.*, 2010; Simões *et al.*, 2020). The electrodes are typically made from a conductive material, such as platinum (Turek and Bandura, 2007), and are placed at the ends of the stack (Scialdone *et al.*, 2013). When a potential difference is applied, ions are driven through the membranes towards the electrode with the opposite charge (Khalla and Suss, 2019). This movement of ions creates a flow of current, which can be harnessed to generate electrical power. Here, the principles of Donnan equilibrium come into play (Galama *et al.*, 2013; Tedesco *et al.*, 2016a). The concentration imbalances of ions across the IEMs, influenced by fixed charges, lead to the establishment of a Donnan equilibrium within each cell (Ashu *et al.*, 2018). The electrode rinse solution circulates through the electrode section at a constant flow rate (Zhu *et al.*, 2015a; Avci *et al.*, 2016).

2.9.2. Electrochemistry of RED

Generally, electrons have to travel through a wire in order to create electricity but in RED stack, the electrons travel through a membrane to generate electricity. RED is practically a salt battery that use the transport of ions through membranes. The seawater contains various chemical

compounds, with NaCl, or sodium chloride, being a significant contributor to seawater salinity, as depicted in **Table *2-1***. Sodium chloride is an ionic compound characterized by cube-shaped crystals, comprising the elements sodium and chlorine, as illustrated in **Figure *2-6***. An ionic compound such as sodium chloride is held together by an ionic bond. This type of bond is formed when oppositely charged ions attract. An ion or charged atom is formed when the atom gains or loses one or more electrons. It is called a cation if a positive charge exists and an anion if a negative charge exists. Sodium is an alkali metal and tends to lose an electron to form the positive sodium ion. Chlorine is a non-metal and tends to gain an electron to form the negative chloride ion.

Table 2-1: Major ion composition of sea water (Emmanuel *et al*., 2012)**.**

Major ion composition of sea water		
Common name	Ions	(g)
Sodium	Na	10360
Magnesium	Mg^{++}	1.294
Calcium	Ca^{++}	0.413
Potassium	K^{+}	0.387
Strontium	Sr^{++}	0.008
Chloride	Cl^{-}	19.353
Sulphate	SO_4^{2-}	2.712
Bromide	Br^{-}	0.008
Boron	N_3B_3	0.001
Bicarbonate	HCO^{3-}	0.142
Fluoride	F^{-}	0.001

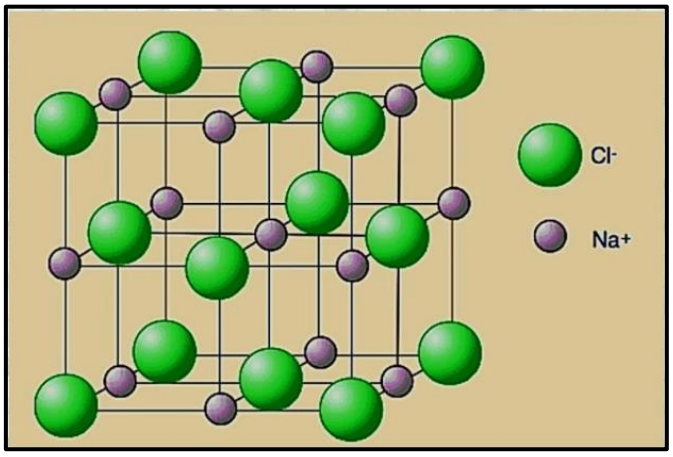

Figure 2-6: Ionic lattice of sodium chloride (Bashyal, 2023).

2.10. Review of power density, open circuit voltage, and key operational parameters affecting RED performance

The performance of RED is primarily influenced by the characteristics of the feed solutions and the operating conditions. Things like the concentration and type of ions present in the

feed solutions directly affect the ion exchange process. The temperature of the feed affects the kinetics of the ions and how they interact with the membranes.

2.10.1. Temperature

Temperature changes throughout the year and for RED technology to be of practically use, experiments that are being conducted must account for that. Temperature plays a significant role in RED performance as it has been evidenced in previous work (Daniilidis *et al.*, 2014; Tedesco *et al.*, 2015; Benneker *et al.*, 2018; Guo *et al.*, 2018). Previous literature has shown that working in warmer conditions enhances the performance of the RED stack (Długołe *et al*., 2009; Mei and Tang, 2017). As the temperature of the liquid increases, the viscosity decreases because the cohesive force between water molecules decrease (Mei and Tang, 2017; Cui *et al.*, 2022), which leads to less pumping power (Nazif *et al.*, 2022). Temperature also affects the internal resistance (Benneker *et al.*, 2018), i.e., High temperature lowers the resistance and vice versa (Mei and Tang, 2017).

Conductivity is temperature dependent, when water temperature increases, the conductivity is affected (Ashu *et al.*, 2018). Furthermore, temperature affects conductivity by increasing ionic mobility and solubility of many salts and minerals (Nazif *et al.*, 2022) and this leads to the decrease in water viscosity, which leads to easier ion migration (Nazif *et al.*, 2022). Benneker *et al*., (2018) experimentally studied the effect of imposing temperature gradients in Electrodialysis (ED) and RED systems. In the study, they discovered that conductivity of the solution is increased by approximately 27% when temperature is increased from 20 ℃ to 40 ℃. They also discovered that at 40 ℃, the river water resistance is decrease by approximately 27% and the power density is increased for the cases in which at least one of the feed streams has an elevated inlet temperature. In one case they had an increase of 38% in power density.

Mei and Tang (2017) reported a 60% increase in power out when both concentrated and diluted solutions were heated from 25 to 60 ℃. This temperature increase increased the electrochemical potential by about 9%. This agreed with Cui et al. who observed that increasing the LCC temperature from 5 ℃ to 40 ℃ led to power density increasing from 0.29 Wm^{-2} to 0.42 Wm^{-2}, which is an increase of 44.8%. This is in agreement with the result of the study that was done by Michal *et al*., (2018) where it was demonstrated that increasing temperature from 15 to 35 ℃ doubled the maximum power density from 0.11 W/m^2 MP to 0.22 W/m^2 MP. Additionally, Ju *et al*., (2020) theoretically and experimentally investigated the effect of operating conditions on the performance of a RED system. The study showed that temperature

increased both power and voltage. Furthermore, the power increased by 12% when temperature was increased from 293 to 313 K. a further increase to 333 K resulted in the power increasing by 16%.

While temperature generally enhances RED performance, higher temperatures can introduce challenges. Increased temperatures may lead to more prevalent ionic shortcut currents, reducing RED's permselectivity and energy efficiency (Moreno *et al.*, 2018; Cui *et al.*, 2022). Ortega-Degaldo *et al*., (2019) noted that an increase in temperature led to an increase of co-ions and water permeation through the IEMs. This led to a variation of power density.

Permselectivity is one of the properties that is affected by temperature (Guo *et al.*, 2018). Daniilidis *et al*., 2014 noted that permselectivity decreases with rising temperatures. The experimentally work highlighted that ionic shortcuts increase with higher temperatures. This increase was due to higher conductivity of the solutions, as well as because of increased mobility of the solution ions and the membrane polymers. This also agrees with Moreno *et al*., (2018) results where they found that high temperature might increase ionic shortcut currents that reduces the permselectivity and energy efficiency of RED. Also, energy efficiency decreased drastically when the temperature was increased from 25 ℃ to 60 ℃.

Moreover, the additional energy needed to heat up the feed solution may not be economically feasible, but waste heat from industrial sources can provide supplementary energy (Luo *et al.*, 2012; Benneker *et al.*, 2018; Giacalone *et al.*, 2019). Furthermore, the increase of the temperature should take into consideration the withstanding temperature of the membrane; too high a temperature will damage the membrane and compromise the whole process.

2.10.2. Feed flow rate

To make RED a commercially attractive renewable energy source, the power of the RED stack needs be maximized while the feed water flow rate is minimized to reduce energy losses due to pressure drop in the stack and energy losses for pumping water (Zhu *et al*., 2015b; Michal *et al.*, 2018). The flow rates not only affect the performance of a RED process, but they also impact energy required to pump the solutions through the RED stack (Zhu *et al*., 2015b; Ashu *et al.*, 2018). An optimal flow rate value is required to achieve a high power density (Ashu *et al.*, 2018). The flow rates not only affect power generation, but also net energy yield (Zhu *et al*., 2015b). Pressure drop is very dependable on the flow rate. A high flow rate of the feed solution can lead to an increase in pressure drop within the stack (Ortiz-imedio *et al.*, 2019; Ju *et al.*, 2020). When the feed solution flows at a higher flowrate, it encounters greater resistance

from the membranes and the channel walls, this increases frictional force. Moreover, as the flowrate keeps increasing, the kinetic energy also increases, and this contribute to the pressure within the stack. Both the frictional resistance and the elevated pressure leads to an increase in pressure drop. Zhu *et al*., (2015b) suggested varying the flow rates of the solutions with different concentrations. To adjust pressures that are created in adjacent channels, they recommended pressure regulators to be used to avoid damage to the membrane.

Increasing the feed water flow rate leads to increase in power density and OCV (Kang *et al.*, 2017; Long *et al.*, 2018). Tedesco *et al*., (2017) achieved a power of 147.6 W with a flow rate of 23 L/min for both solutions of low and high concentration, and 137.2 W with a flow rate of 16 L/min for both solutions. Furthermore, Kang *et al*., (2017) noticed that maximum power density increased as the flow rate of the salt and fresh water feed to the RED stack increasing. The study also revealed that RED stack resistances generally decreased as a flow rate increased, which is something that a number of researchers agree with (Luo *et al.*, 2012; Membranes *et al.*, 2021). On the other hand, Zhu *et al*., (2015b) noted that at lower flow rates OCV decreased, likely as a result of the decreased ion concentrations in concentrated channel and the increased ion concentration in the diluted channel.

High flow rates lead to a shorter residence time of feed in the stack (Tedesco *et al.*, 2017), which reduces the energy efficiency (Ashu *et al.*, 2018). A longer residence time allows a faster transfer of ions from the concentrated compartments to the diluted compartments (Zhu *et al*., 2015b; Ortiz-imedio *et al.*, 2019). Tristán *et al*., (2020) noted that increasing flow rates of both concentrated and diluted streams help maintain a consistent concentration difference across membranes and enhance fluid mixing in the compartments. They also discovered that the power delivered is more sensitive to diluted stream flowrate variations than concentrated one. However, Zhu et al., (2015b) noticed that the use of lower flow rates greatly reduced hydrodynamic power losses, and provided higher energy recovery. This is because operating the RED stack with low flow rate leads to a lower power consumption for pumping the feed water, but this will lead to a relatively high value for the double boundary layer thickness (Moya, 2016).

Energy efficiency measures the utilization of Gibbs free energy from concentrated and diluted solutions, while net power density quantifies the power that can be extracted from these solutions (Long *et al.*, 2018). Energy efficiency decreases with higher solution flow rates entering the system. This is because the Gibbs free energy of the solution is more effectively

utilized at lower flow rates given a constrained membrane area (Long *et al.*, 2018). Furthermore, Energy recovery is another important parameter, which is how much energy can be extracted from the feed water used in the process. Higher energy recovery means less pumping energy to transport feed water from the source to RED stack (Zhu *et al*., 2015b). Energy recovery and flow rate have an inverse relationship.

While a higher flow rate can enhance ion transport and potentially increase power density, the associated rise in pressure drop should be carefully considered and balanced in the design and operation of a RED system. Finding the optimal balance is crucial for maximizing both performance and effectiveness in the RED process.

2.10.3. Influence of feed solution concentration

RED depends on the salinity gradient between the feed solutions. The higher the difference between the two solutions, the higher will the driving force which will lead to an increase in power output (Tufa *et al.*, 2014; Tedesco *et al.*, 2015). One of the critical factors that influence the performance of the RED stack is the concentration of the feed solution. The concentration of the feed plays an important role determining the electromotive force of the RED stack power out. Large Concentration gradient between diluted and concentrated compartment is beneficial for power output because it increases the OCV, but achieving a high concentration gradient ratio generally requires the use of very low concentrations in the diluted compartment. However, low concentration is usually characterized by low values of conductivity which is a major contributor to the total stack resistance and that undermines power output (Kingsbury *et al.*, 2017), since an increase in internal resistance exceeds the gains that are made on the salinity gradient side (driving force) (Tristán, Pérez, *et al.*, 2020). Kingsbury *et al*., (2017) observed that the resistance of the dilute feed water accounted for 21-75% of the total stack resistance, while the resistance of the concentrated feed water compartment accounted for only 1-6%. This is because the dilute concentration has more influence on RED's electromotive force (e.m.f) and internal resistance than the concentrated compartment (Mei and Tang, 2017; Tristán *et al.*, 2020).

Permselectivity is another parameter that is dependent on concentration gradient (Daniilidis *et al.*, 2014; Tristán *et al.*, 2020). Very high concentration of the feed waters results in a gradual decrease of the membrane permselectivity (Michele Tedesco *et al.*, 2017). Wu *et al*., (2022) observed that high solution concentration significantly reduced permselectivity and affected the energy efficiency of RED. This occurs because highly concentrated solutions diminish the

effectiveness of co-ion exclusion (Donnan exclusion), thereby reducing the permselectivity of the IEM (Daniilidis *et al.*, 2014; Tristán *et al.*, 2020). This also leads to the diminishing of energy conversion efficiency in a RED stack (Zhu *et al*., 2015a). Nevertheless, the use of saline feed solutions is advantageous in reducing ohmic losses, especially for lower concentrated compartment (Ashu *et al.*, 2015; Tedesco *et al.*, 2015). However, this increases the risk of fouling, especially scaling caused by sparingly soluble salts deposited on the membrane surface. Daniilidis *et al*., (2014) used salt concentrations ranging from 0.01 M TO 5 M in two stacks with identical specifications. Results on the study showed a decrease in permselectivity with higher salt concentrations and higher gradients. The membranes showed permselectivity readings below 90% for diluted solution levels of more than 0.5 M and for concentrated solution it was above 2 M.

Tufa *et al*., (2015) combined DCMD and RED to simultaneously produce water and energy using DCMD brine (4 - 5.4 M) and seawater (0.5 M). They found that when increasing the HCC concentration from 2 M to 5 M, the maximum power density increased more than two folds. A 71% increase in OCV (from 1.23 to 2.1 V) and a 67% increase in power density was observed when the brine concentration was increased from 4 M to 5.4 M at 0.7 cm/s and 20 ℃. Furthermore, Zhu *et al*. (2015a) reported an increase in power generation by the RED stack when NaCl concentration was increased from 0.6 M to 3.6 M in the concentrated solution.

Tedesco *et al*., (2015) investigated the effect of feed concentration, temperature and flow rate on the process performance parameters using two different stack size. Concentrated brine was used as the concentrated feed water, while brackish water served as the diluted feed water. An increase in OCV from 1 to 3V was observed when concentrated brine solution was increased from 1 M NaCl to 5 M NaCl, at a fixed brackish water concentration of 0.5 M NaCl. When using a larger stack size, a 100% increase in the OCV values was observed. This was attributed to the doubled number of cell pairs in the larger stack.

Ortiz-Martínez *et al*., (2020) suggested using a fraction of the high salinity solution to increase the salinity of diluted solution. Also, Mei and Tang (Mei and Tang, 2017) reported that stack internal resistance decreased sharply from 10.5 Ω to 3.8 Ω when the diluted concentration was increased from 0.002 M to 0.02 M. However, a further increase in diluted water concentration was less effective in reducing the stack resistance. This is because increasing diluted water concentration while keeping the concentrated side still, decreases concentration gradient which

leads to a decrease in electromotive force. Furthermore, Tedesco *et al*., (2017) noticed that the higher inlet concentration of dilute solution led to a reduction in the OCV.

2.10.4. Effect of the feed composition

The composition of the feed solutions significantly influences the power output of the stack (Lowenstein *et al.*, 2005; Zhu *et al.*, 2018). The selection and characteristics of the feed solutions play a pivotal role in power generation. Feed solutions containing multivalent ions have been shown to have a negative effect on the power production of the stack (Moreno *et al*., 2018; Besha *et al.*, 2019).

Post *et al*., (2009) investigated the effect of feed composition on the performance of a RED stack. Four experiments were performed to determine the effect of different ionic composition of diluted feed water on the stack voltage. During each experiment, a different salt was added to the solutions: NaCl, $MgSO_4$, Na_2SO_4 and $MgCl_2$, respectively. Concentrated solution with a concentration of 0.45 mol/L NaCl was enriched with 0.05 mol/L of $MgSO_4$. During the whole experiment, 0.2 - 0.4 mmol/L of $MgSO_4$ was added to the dilute stream. A reduction in OCV from 0.78 V to 0.74 was observed when increasing the concentration of $MgSO_4$ from 2 mmol/L to 4 mmol/L in the diluted side.

Tufa *et al*., (2014) investigated the effect of ionic composition on SGP-RE using brine and brackish water from solar ponds as a sources for high concentration compartment and low concentration compartment of the RED stack, respectively. The stack was able to generate a maximum power density of 3.04 W/m^2 MP when operated with pure sodium chloride aqueous solutions. However, a significant reduction in power density of -63% was observed when the stack was fed with artificial multi-ion solutions mimicking real brine and brackish water. Furthermore, the presence of magnesium drastically decreased both OCV and power density.

Fontananova *et al*., (2017) investigated the effect of solution concentration and compositions on permselectivity, membrane and interface resistance, for both AEMs and CEMs. The study focused on the most common multivalent ions in seawater and their role on the electrochemical properties on the membranes. The results of the study highlighted a strong negative effect of magnesium on the CEM. This is because Na^+ has a higher mobility than Mg^{2+} and the increase of the molar fraction of Mg^{2+} leads to an overall reduction of water mobility. Moreover, because of its small ionic radius and high charge, magnesium is a strongly polarizing cation which makes it to strongly interact with the negative sites of the CEM.

2.10.5. Effect of conductivity and pH

The conductivity of water is a measure of its ability to conduct electricity. This ability depends on the concentration of ions or charged particles in the water. River water and seawater have different conductivity levels due to difference in the types and amounts of dissolved substances they contain. River water is typically less conductive than seawater because it contains fewer dissolved salts and minerals. River water is primarily composed of freshwater from precipitation and surface runoff (Olume and Renberth, 2002; Vörösmarty *et al.*, 2005). The concentration of ions in river water varies depending on the geology and soil characteristics of the surrounding area. In general, river water contains low levels of dissolved salts, typically less than 0.5 grams per liter (Cañedo-Argüelles *et al.*, 2013). Seawater, on the other hand, is highly conductive due to its high concentration of dissolved salts and minerals. The high salt content of seawater allows it to conduct electricity more efficiently than river water. The conductivity of river water is about 25 times lower than that of seawater (Ashu *et al.*, 2018). The performance of a RED stack depends heavily on the electrical conductivity of solutions that are used (Gurreri *et al.*, 2017).

The electrical conductivity of water increase with increase in temperature (Nazif *et al.*, 2022). This is because higher temperatures contribute towards increasing ion mobility, allowing ions to move more freely through the solution. Benneker *et al*. (2018a)reported an increase in conductivity of approximately 27% when the temperature was increase from 20 ℃ to 40 ℃. Furthermore, Tedesco *et al*., (2015) observed the same thing when studying the effect of temperature on the membrane resistance.

Kingsbury *et al*., (2017) measured power generation from five real water pairs (seawater, desalination brine, river water, treated wastewater, and saline wastewater from pickling plant) containing complex mixtures of ions and NOM in laboratory-scale RED stacks. Additionally, the performance of each real water pair was compared with that of synthetic control waters with the same conductivity for the investigation of the impact of inorganic constituents and natural organic matter. They noticed that lower conductivity of the less concentrated feed water limits power output by increasing the stack resistance. The study also showed that the diluted feed water conductivity may be used as a predictor of differences in stack resistance among water pairs.

Because of the low conductivity of the dilute solution compartment, it accounts for a larger portion of the stack resistance (Güler *et al.*, 2014; Nazif *et al.*, 2022). One way to increase ionic

conductivity of the diluted side is to use a slightly concentrated solution than normal. This automatically means using an even more concentrated solution in the concentrated compartment to avoid a reduction in concentration gradient (Kingsbury *et al.*, 2017). Some researchers used brine and seawater as a high concentration and a low concentration solution respectively (Kwon *et al.*, 2015; Santoro *et al.*, 2021). Others used brine and brackish water to deal with low conductivity of the less concentrated solution (Turek *et al*., 2008; Tufa *et al.*, 2014; Tedesco *et al*., 2016; Kingsbury *et al.*, 2017; Nam *et al.*, 2019).

The pH of the feed solution is another critical factor that affects the performance of the RED stack. The pH of the feed solution influences the ionization of the functional groups on the IEMs (Hsu *et al.*, 2017; Roman *et al.*, 2020). The ionization of the functional groups affects the transport of ions across the membrane, which influences the electrical potential difference across the RED stack (Zhang *et al.*, 2021). At low pH, the function groups become protonated, which reduces the transport of anions and cations across the membrane. At high pH, the functional groups become deprotonated, which increases the transport of anions and cations across the membrane (Hsu *et al.*, 2017). Therefore, there is an optimum pH range for the feed solutions that maximizes the ion transport rate and power output of the RED stack. Moreover, the pH of the feed solution affects the stability of the IEMs (Zhang *et al.*, 2021). At extreme pH values, the ion exchange membranes can degrade or lose their functionality, which leads to reduced ion transport rates and lower power output. Therefore, it is crucial to maintain the pH of the feed solution within acceptable range to ensure the long-term stability and performance of the RED stack.

Tedesco *et al*., (2017) dosed a minimal amount of HCl to keep the pH between 2 and 3 to prevent iron compound precipitation. The study investigated different conditions of inlet conductivity and flow rates for the diluted stream. It was found that reducing feed conductivity to 0.7 mS/cm leads to an increase in the stack resistance, thus resulting in an overall reduction in the power out. Moreover, when using real brine as the concentrated solution and tap water as the diluted solution, the conductivity of the diluted stream feed led to higher OCV values, while slightly increasing the stack resistance.

2.10.6. Power density

Power density is a measure of the electrical power produced per unit of surface area of the membranes. It is calculated as the product of current density and voltage (Vermaas *et al.*, 2012; Pawlowski *et al.*, 2017; Elmakki *et al.*, 2023). The voltage generated by the RED stack is a

critical factor in determining power density. Maximum power density is a key parameter for assessing the commercial viability of RED technology. Net power density is influenced by various factors, including IEM-specific electrochemical performance, hydrodynamics, stack configuration, characteristics of available saline streams, and pumping energy requirements. In recent decades, power density has grown from 0.05 W/m^2 (Pattle, 1954) to 12 W/m^2 (Tedesco *et al.*, 2015), which is a huge improvement for this technology. However, achieving high net power density requires low internal resistance of the system and low hyraulic friction of the feed solution in the compartments (Rijnaarts *et al.*, 2017).

One of the parameters that have a positive effect on power density is temperature. Guo et al. investigated the influence of coexisting ions, temperature and their synergistic effect on energy generation by RED, two series of cells dividing with Yadeshi membranes were fed with different solutions at 10 ℃, 25 ℃ and 40 ℃. When the temperature increased for 10 ℃ to 40 ℃, the maximum power densities increased from 0.13 Wm^{-2} to 0.22 Wm^{-2}. Furthermore, Cui *et al*. (2022) found that the maximum power density increased from 0.31 Wm^{-2} at 5 ℃ to 0.39 Wm^{-2} at 40 ℃.

Adding more cell pairs increases power density (Scialdone *et al.*, 2013; Tedesco *et al.*, 2015; Han *et al.*, 2019). This is because at high values of current density and cell voltage, the energy loss due to redox processes is less impacted compared to the total current production, resulting in significantly improved power density performance (Scialdone *et al.*, 2013). Tedesco *et al*., (2015) used two different size RED stack units that were fed with concentrated brine and artificial saline waters. The effects of feed concentration, flow rate and temperature on the process performance parameters were analysed. Furthermore, the larger stack with 100 cell pairs of 20×20 cm^2 membrane area was fed with 0.1 M NaCl and 5 M NaCl at 40 ℃. It generated a maximum power density of 12 $W/m^2_{\text{cell pair}}$ which is the highest value that has been reported thus far. Furthermore, Ju *et al*., (2020) theoretically and experimentally investigated the effect of operating conditions on the performance of a RED system. The study showed power density is dependent on the number of cells, i.e., the power density increased with increasing number of cells. In the study, the maximum power density changed from 0.02 to 0.11 Wm^{-2} with an increase in the number of cell pairs from 5 cells to 20 cells.

Long *et al*., (2018) proposed a model that will maximize power density while also maximizing energy efficiency. To achieve this objective, optimization using the Non-Dominated Sorting Genetic Algorithm II (NSGA-II) was performed to determine the Pareto frontiers of the RED

system employing various membranes. In the study, Qianqiu homogeny stack of 25 cells and Fumasep FAD/FKD stack of 50 cells were used. The result of the study revealed that there exist optimal flow rates of the concentrated and diluted solutions that will lead to a maximum net power density, however the energy efficiency achieves its maximum value at lower flowrates due to more sufficient ion transfer through the membranes.

Ciofalo *et al*., (2019) presented a simplified model of a RED stack which was coupled with an optimization algorithm in order to determine the conditions that will give maximum net power density. In this model, correlations of physical properties suitable to concentrated brines were adopted in order to extend the model capabilities to the simulation of situations such as saltworks. In the study, membrane permselectivity was assumed to be independent of concentration in the feed water, however, the dependence of permselectivity on feed concentration was poorly known for the membranes. The effects of multivalent ions and uphill transport on the membrane resistance were not considered. This was because this simplified the model, and they were using artificial solutions. The results of the study showed that flow velocity and thickness of the channels yielding maximum values of net power density were sensitive to the inlet concentration and the stack length.

Moreno *et al*., (2018) investigated the influence of stack size and membrane type on power density, energy efficiency, and thermodynamic efficiency. Four stacks with different active area per membrane were used. Each stack contained 50 cell pairs, corresponding to a total active membrane area of 0.36, 1.00, 4.84, and 19.36 m^2 per stack. Moreover, stacks were compared in terms of power density and efficiency, and the influence of membrane types and stacks size. The results showed that the larger stack (44 × 44 cm) produced a slightly higher gross power density at the same residence time compared to that of the smaller stack (6 × 6 cm). This was because the larger stack needed a higher flow velocity to achieve the same residence time in the feed water compartments. The smallest stack achieved the highest gross power density at the residence time of 3 seconds with a flow velocity of 2 cm/s. This was expected because at higher flow velocities, the salinity gradient along the flow compartments is high. But the smaller stacks showed relatively higher hydrodynamic losses. This was because the smaller stack required a higher pumping power density to pass the water through the compartments at the same flow velocities compared to that of the larger stacks. Also, the study showed that gross energy efficiency increased with an increasing stack size.

2.10.7. Open Circuit Voltage (OCV)

The open circuit voltage (OCV) is the voltage generated by the RED stack when there is no external electrical load connected to it (Długoł *et al.*, 2010; Benneker *et al.*, 2018). It represents the maximum voltage that the RED stack can generate under ideal conditions. OCV is determined by the concentration gradients between the more concentrated and the less concentrated solutions, the selectivity of the IEMs, and other factors related to the specific RED system design. Due to electrochemical equilibrium, an IEM immersed between two solutions of different concentrations experiences a voltage difference (Donnan exclusion) (Strathmann, 2004), and the total membrane potential across the stack constitutes the OCV.

OCV mainly depends on membrane permselectivity, temperature, flowrate of the feed, concentration gradient, and valence of transported ions (Ashu *et al.*, 2018; Guo *et al.*, 2018). Cui *et al*., (2022) observed that when temperature was increased from 5 ℃ to 40 ℃, the OCV increased from 1.27 V to 1.43 V.

Tufa *et al*., (2015) reported that OCV increased by up to 35% (from 1.7 V to 2.3 V) and power density increased by up to 47% (0.75-1.1 W/m^2) when the feed flow rate was increased from 0.7 to 1.1 cm/s. Moreover, Fu *et al*., (2020) observed that when increasing flow velocity from 0.24 cm/s to 1.19 cm/s, the OCV increased from 1.25 V to 1.39V. Regarding the influence of concentration, Fu *et al*., (2020) observed that the OCV increased linearly with HCC concentration from 0.75 V in 6.67 g/L to 1.38 V in 66.70 g/L of NaCl.

Multivalent ions have a negative effect on OCV. These ions increase membrane resistance since they have a charge that is more than +1. Additionally, these ions contribute to the fouling of the membranes inside the stack. Rijnaarts *et al*., (2017) investigated the effect of divalent cations ($Mg^{2+}$and Ca^{2+}) on RED. The study showed that when Mg^{2+} was present in the feed stream the OCV decreased. This is caused by the uphill transport and the decrease in permselectivity when there is divalent ions (Moreno *et al.*, 2018). Avci *et al*., (2018) also observed a 63% (from 3.04 W/m^2 to 1.13 W/m^2) reduction in power density when Mg^{2+} was present.

Kingsbury *et al*., (2017) measured the RED performance of five real water pairs with a laboratory-scale RED stack. They compared the performance of each real water pair containing complex mixture of ions and NOM with that of synthetic control waters to investigate the individual impacts of inorganic constituents and NOM. The findings showed that the presence of NOM in the real waters negatively impacted OCV.

Divalent ions have a negative effect on the OCV as Rijnaarts *et al*., (2017) demonstrated when investigating the effect of divalent cations ($Mg^{2+}$and Ca^{2+}) on RED. The study showed that when Mg^{2+} was present in the feed stream the OCV decreased. This is caused by the uphill transport and the decrease in permselectivity when there is divalent ions (Moreno *et al.*, 2018). Avci *et al*., (2018) also observed a 63% (from 3.04 W/m^2 to 1.13 W/m^2) reduction in power density when Mg^{2+} was present.

Increasing a number of cell pairs in the stack leads to a higher OCV (Han *et al.*, 2019). This is evidenced by the experiments carried out by Ju *et al*., (2020) to measure the OCV and maximum power in a bench-scale RED system. The study showed that OCV increased linearly with the number of cell pairs, e.g. the OCV was 0.8 V with 5 cells and increased by more than 3 times with 20 cells. Also, the OCV increased with an increase in flow rate of up to 40 ml/min. At higher flow rates, the shorter residence time for ion exchange maintains a more significant salinity gradient along the cell. Han *et al*., (2019) observed that increasing the number of cell pairs from 25 to 100 led to an increase in maximum current density from 26 A/m² to A/m² and maximum power density from 15 mW to 366 mW. Altiok *et al*., (2021) came to the same conclusion in their study. However, in a study that was done by Pawlowski *et al*., (2014) it was found that the net power density decreased when the number of cell pairs was increased. The reason for that was because the partial pressure drop in the branches became dominant. Also, with an increase in number of cell pairs, the probability of a non-uniform fluid flow distribution inside the system increases significantly.

2.11. RED integration

An emerging and promising trend involves harnessing the potential of RED by integrating it with other complementary technologies, thus creating a powerful combination. In addition to generating electrical energy, integrating RED systems with other technologies is increasingly attractive for producing essential resources such as water and hydrogen. RED's hybrid process maximizes productivity and enables diverse applications of technology at lower capital cost, while also minimizing environmental impact (Mei and Tang, 2017).

2.11.1. Desalination and RED

The combined production of renewable energy and drinking water is among the most promising applications of the RED concept in hybrid systems. Desalination is the process of removing mineral components from salt water. Saline water (particularly sea water) is desalinated to produce water that is suitable for human consumption and irrigation. The by-product of the

desalination process is brine (Ashu *et al.*, 2019), Which is being disposed back to the sea in huge amounts, with dramatic negative environmental impact (Ashu *et al.*, 2015; Wenten, 2016). This brine can be used as a high-salinity solution to enhance power generation in RED systems (Nazif *et al.*, 2022). Desalination plants that are operated by fossil-based energy sources are associated with the emission of greenhouse gases. Seawater desalination is generally more costly than fresh water from surface water or groundwater, water conservation, and water recycling.

2.11.2. Reverse Osmosis (RO) and RED

Reverse osmosis is a pressure driven membrane process which has received widespread use and is recognised as the leading technology of desalination process. Improvements in RO technology, including module and process design, energy recovery, and advance membrane material, has resulted in cost being reduced, which as increased interest in its commercial uses (Anis *et al*., 2019). Today, RO employed in numerous processes including purification, concentration processes, and selective separation (Hailemariam *et al.*, 2020). Despite significant advances in RO technology towards higher production efficiencies, RO processes still feature energy-intensive approaches for harvesting freshwater from various brackish water resources. This large energy expenditure is primarily caused by the pumping work required to overcome the high osmotic pressure of the feed solution (Kravchenko *et al*., 2021). Moreover, RO processes create a lot of problems concerning environmental and ecological issues when disposing the concentrated brine (Mei and Tang, 2017). Combining RED and RO makes a lot of sense, since the RED-treated high salinity solution has a low salinity and acts as a feed solution for the RO unit, reducing pumping work (Li *et al.*, 2013). The concentrated RO brine provides the RED unit with a better high-saline source for energy recovery compared to seawater. Additionally, the environmental impact of the RO brine is minimized by reducing the salinity of the discharged brine via the RED process.

Kwon *et al*., (2015) used brines discharged from RO and forward osmosis (FO) as a high salinity solutions to demonstrate power enhancement of RED. They used river water and seawater as the diluted solution. Maximum power density was obtained when seawater was used as a diluted solution, 1.40 W/m^2 for RO brine and 1.86 W/m^2 for FO. The power density was significantly lower when river water was used a diluted solution, 0.09 W/m^2 for RO and 1.86 W/m^2 for FO.

Li *et al*., (2012) introduced a novel concept for a hybrid desalination system that combined RO and RED processes. To investigate the performance of this integrated system, a model with variety of configurations with different operating conditions was carried out. The results of the integrated model indicated that the model was superior to the conventional SWRO processes in many aspects including the easy of configurability of the system to accommodate new requirements. In addition, the results indicated that the hybrid process could substantially reduce the specific energy consumption and better control the outlet brine concentration.

Tufa *et al*., (2019) investigated the energy performance of a system combining Seawater Reverse Osmosis (SWRO), Membrane Distillation (MD) and RED for simultaneous production of water and energy. This was done through the assessment of the energy performance of a conceptually integrated reverse osmosis-membrane distillation-reverse electrodialysis desalination system designed based on the experimental results they obtained from lab-scale tests. They found that when increasing the HCC concentration from 2 M to 5 M, the maximum power density increased more than two folds. This gain in power was due to a decrease in resistance from the HCC side because of an increase in conductivity. This increased power density confirms that the use of concentrated brine supplied by Direct Contact Membrane Distillation (DCMD) has significant benefits in improving RED performance. But the issue with using highly concentrated brine is permselectivity which is negatively affected. Highly concentrated solution block the pores in the membrane (Fan and Yin, 2019). Also, during the experiment they ran the system without the RED unit and with the RED unit, and the result showed that electrical energy consumption was reduce by 17% when the hybrid system incorporated RED.

In Okinawa Island (Japan), seawater desalination was integrated with the RED process because of the large amount of RO brine production, which is usually discharge into the sea. The plant had a pilot-scale RED stack, with 299 cell pairs and 179.4 m^2 of effective membrane area. It was the first time that an asymmetric monovalent selective membrane with a monovalent selective layer directly on the side of the membrane was used as the IEM in the RED stack (Membranes *et al.*, 2021). Additionally, Mei and Tang (2017) investigated the effects of co-locating RED with RO. The authors suggested applying RED as an RO pretreatment, so that less saline seawater that comes from a RED stack can be desalinated by RO at significantly reduced energy consumption.

2.11.3. Microbial electrolysis cell-RED hybrid system

Microbial electrolysis is a process for the production of green hydrogen from organic matter (Jeremiasse *et al*., 2010). In a microbial electrolysis cell (MEC), electrochemically active microorganisms convert organic matter into CO_2, H^+, and electrons. These electrons move to the anode and flow from anode to the cathode through a circuit containing a power supply. At the cathode, hydrogen is produced by reduction of protons or water. The flow of negative charge outside the cell is balanced by cation transport from anode to cathode inside the cell. In theory, 0.14 V has to be applied to promote hydrogen production under biological conditions. However, in practice, more than 0.14 V has to be applied, partly due to the cathode overpotential (Zhu *et al.*, 2013; Jafary *et al.*, 2015; Song *et al.*, 2021).

Jwa *et al*., (2020) conducted a two-phase experiment on a MEC-RED hybrid for enhanced energy production as illustrated by **Figure *2-7***. Firstly, a continuous-flow tubular MEC was constructed and operated to remove multivalent cations from seawater during hydrogen production. Secondly, seawater effluent from the MEC was fed to the RED stack as a high concentration solution. OCV and power density were measured to evaluate RED performance under continues flow of pure NaCl, treated and untreated seawater. To show how the power decreases in the presence of divalent ions, a NaCl solution with the same conductivity as that of untreated seawater was used. The study demonstrated that MECs can enhance divalent ions removal rates while simultaneously producing hydrogen and treating biological water. Additionally, the study showed how this technology can be used as a pretreatment of water before solution if fed to the RED stack.

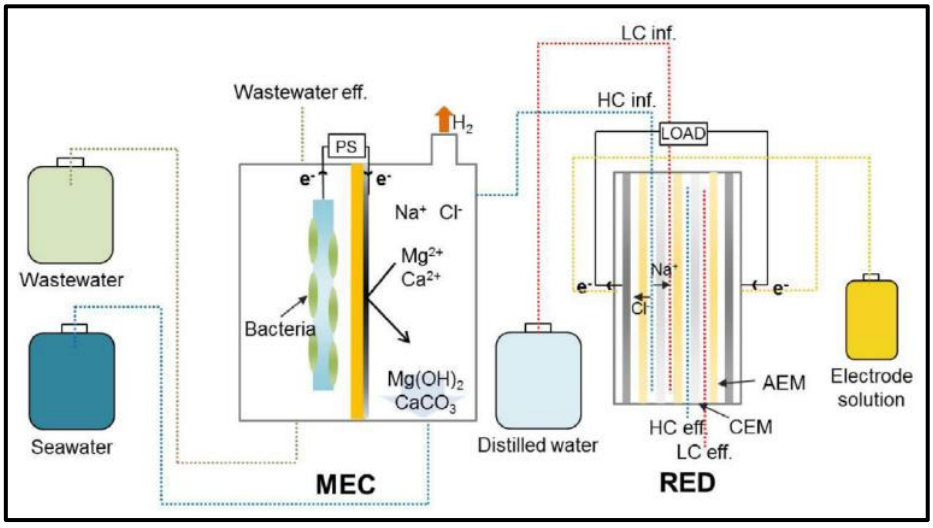

Figure 2-7: Schematic diagram of the hybrid microbial electrolysis cell (MEC)-reverse electrodialysis (RED) cell (Jwa et al., 2020).

2.11.4. Microbial reverse electrolysis cell-RED hybrid system

Kang *et al*., (2017) investigated the influence of RED flow rates on MRC electrochemistry and power production. The MRC system consisted of an anode chamber, cathode chamber and RED stack. The stack with five cell pairs was located between the anode and cathode chamber. In the study, four different flow rates of concentrated and diluted solutions were tested. As flow rate increased, maximum current density and maximum power density increased. Also, the study showed that charge transfer resistance in the anode and ohmic resistance in the cathode is more affected by the stack flow rate. The study didn't consider the effect of the energy for pumping the solution to the stack, which has a huge role when calculating the net energy of the whole system. Unlike Kang *et al*., (2017), Yasukawa *et al*., (2020) considered pumping energy in a study where they evaluating performance of a bench-scale RED stack regarding power generation at steady state. They used natural seawater RO brine and natural municipal wastewater as the feed solution. Furthermore, they examined how varying feed flow rates influenced power density and OCV. The results indicated that the flow rate of the sewage treated water side has a higher impact on the resulting OCV than that of the seawater RO brine. The study showed that using RO brine and municipality wastewater as a feed in RED before discharging will be helpful in that the RED process enables dilution of the highly concentrated brine that may causes harm to the environment.

Song *et al*., (2021) demonstrated the possibility of simultaneously producing hydrogen and struvite crystallization at the cathode of an microbial reverse-electrodialysis electrolysis struvite-precipitation cell (MRESC) under no additional external energy. Struvite is a phosphate mineral that is commonly used to make fertilizer (Hertzberger *et al*., 2020). In order to accomplish this, a RED stack with 10 cells was sandwiched between an anode and a cathode chamber. Interestingly, in the study they neglected the energy that is required to pump concentrated and diluted solutions. This was because the pumping energy was smaller compared to the hydrogen gas energy produced. Maybe the next part of the study will be to supply the hydrogen energy to another system like present one and eliminate the external power usage completely.

2.11.5. Membrane distillation – RED hybrid system

The integration of membrane distillation (MD) and RED is a novel approach that leverages the strengths of both technologies to enhance the overall efficiency of desalination and power

generation. This combination addresses some of the limitations of each individual method. This is an ongoing study that most researchers are embarking on as illustrated by **Figure *2-8***.

Ashu *et al*., (2015) combined membrane distillation with RED to test for the simultaneous production of energy and water from SWRO brine, while having a near-zero liquid discharge in seawater desalination. Part of the study was to obtain highly concentrated NaCl brines as inlet to concentrated compartment of a RED stack. To do this, the brine rejected from the reverse osmosis stage was further concentrated by DCMD and used to feed the concentrated compartment of the RED stack for electrochemical energy generation, while seawater was feed to the diluted compartment side of the stack . The study demonstrated that increasing the concentration gradient of the solutions lead to high OCV measurements. The results also showed that temperature gradient has a huge effect on the main operative parameters of the performance of DCMD in terms of transmembrane flux. Moreover, feeding the RED stack with high temperature solution leads to a high OCV. Additionally, the study also demonstrated that combining the hot brine produced by DCMD with a RED stack unit will result in a high overall water recovery and higher power density especially at higher temperatures.

Ortega-Delgado *et al*., (2019) investigated the performance of a RED-MED heat engine by comparing two different salts, sodium chloride and potassium acetate, using different working solutions concentration and temperature in the RED unit. The study showed that using potassium acetate aqueous solution as the working fluid of the RED heat engine leads to higher thermal efficiency than when using sodium chloride under same conditions. However, there is an abundance of sodium chloride than potassium acetate in nature and sodium chloride is easily accessible (Emsley, 2010).

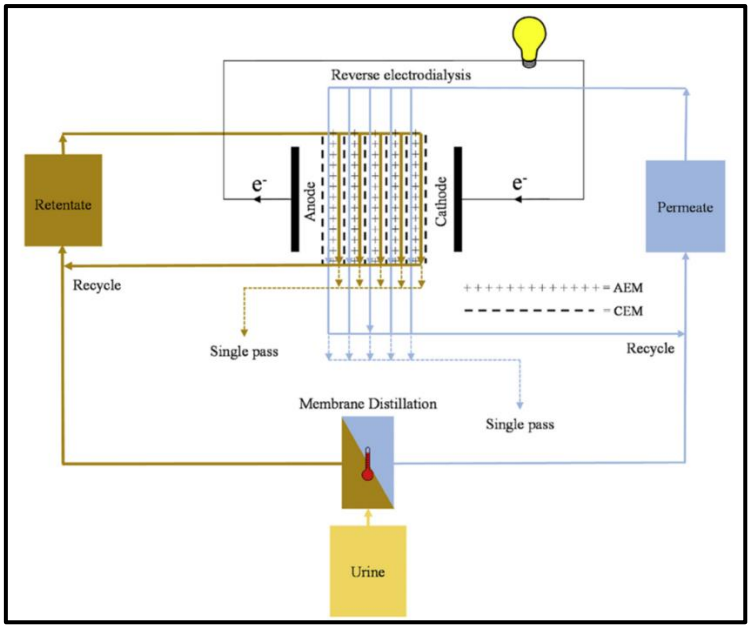

Figure 2-8: Schematic diagram showing integration of membrane distillation and reverse electrodialysis (Mercer et al., 2019).

2.11.6. Water electrolysis - RED hybrid system

Electrolysis water, also called electrochemical water splitting, is the process of using electricity to split water into oxygen and hydrogen gas through a process called electrolysis (Grigoriev *et al.*, 2020). The hydrogen gas thus released can be used as hydrogen fuel or remixed with oxygen to produce oxyhydrogen used for wielding and other applications. Electrolysis of water requires a minimum potential difference of 1.23 V (Nadeem and Idriss, 2020), but this voltage requires external heat from the environment. This energy (heat) can be provided by RED power.

Michal *et.al.*, (2018) combined RED and alkaline polymer electrolyte water electrolysis (APWEL) to demonstrate the feasibility of converting the electrochemical potential of industrial waste streams into clean energy and hydrogen by an integrated RED-APWEL energy system. The performance of a pilot-scale RED unit with 200 cells was evaluated using salt solutions mimicking sulphate-rich waste streams. Furthermore, the performance of the RED stack was evaluated in terms of voltage and power density at varying flow rates and temperatures of the feed. APWEL was fuelled by salinity gradient power derived from sulphate-rich industrial wastewater.

Wu *et al.*, (2022) recently proposed a complete mathematical model of a Reverse electrodialysis – Air-gap diffusion distillation (AGDD) integration system that converts low-

grade thermal energy to hydrogen. The process was driven by the membrane voltage that was sourced from the salinity gradient of KAc solutions.

Tufa *et al*., (2016) tested the potential of an innovative SGP-RED-APE system for hydrogen production driven by salinity gradient energy. In the study, a laboratory-scale RED unit consisting of 27 cell pairs was fed with various NaCl solutions to simulate brine (5 M), seawater (0.5 M), brackish water (0.1 M), and RO retentate (1 M). The unit was coupled with an alkaline polymer electrolyte (APE) water electrolysis cell to serve as a power source. The RED stack produced an OCV of 3.7 V and maximum power density of 3.2 W/m^2. But it was observed that the pumping energy required to recirculate electrolyte and concentrated/diluted solution was 23 W, which resulted in a negative net power density generated by the RED unit overall.

Han *et al*., (2019) investigated the amount of hydrogen that can be produced at maximum power of the RED system using a batch-type electrode chamber with a gas bag. In the study, they evaluated the interrelation between hydrogen energy and the electric power with varied cell pairs. The system was fed with artificial NaCl solution and had more than 50 cells in which the membrane voltage was large enough to achieve water electrolysis. They noted that while hydrogen collected from the process was expected to be pure, the gas pack of conventional RED contains mixture of oxygen and hydrogen gas. This means that hydrogen produce from conventional RED should be separated from oxygen and other gases which adds to costs. The authors concluded that pilot-scale RED systems many cell pairs, i.e. 50 +, can be operated in a stable long term for water electrolysis with a neutral-pH electrolyte.

Ranade *et al*., (2022) investigated the feasibility of producing hydrogen and chlorine in addiction to electricity while identifying potential levers that could improve the process economic feasibility. To do this, a techno-economic model was adopted, and a number of simulations were done. In the study they considered the impact of varying number of cell pairs, resistance, membrane price, discount rate and permselectivity.

2.11.7. Waste heat

Integrating RED with other processes that generate waste can improve the efficiency of the RED system. Temperature plays a critical role in power density. An increase in temperature directly affects power density in a positive way but the energy needed to increase this temperature comes at the cost and that cost decreases the attractiveness of RED as a technology.

Luo *et al*., (2012) proposed a concept called a thermal-driven electrochemical generator (TDEG) that used ammonium bicarbonate solutions as working fluids in which heat is first transformed to SGP by distillation column and afterward converted to electricity by a RED stack. This system consisted of a RED stack and a thermal separation unit. The passing of the concentrated and diluted solution in the stack generates electricity and a distillation column utilizing waste heat is then used to remove the increased amount of ammonium bicarbonate from the effluent diluted solution in the form of CO_2 and NH_3, which afterward dissolved into the effluent concentrated solution, resulting in renewed concentrated and diluted solution. The maximum power density that was achieved is 0.33 Wm^{-2} which proved the possibility of converting the waste heat into electricity by this process.

Olkis *et al*., (2018) combined RED membrane with an Adsorption desalinator in a closed-loop system. The aim of the system was to generate electricity from more concentrated and less concentrated solutions in a closed-loop system by utilising low-grade heat between 60-100 ℃. The study investigated the efficiencies of 227 salts with a range of different valences. The results showed that the optimized system can achieve an exergy efficiency of up to 30%.

Jande *et al*., (2014) integrated RED with capacitive deionization (CDI) to simultaneously generate electricity while producing highly pure water and fresh water. The CDI cell generates a high concentration stream during discharging and purified water during charging. The RED stack achieved a power density of 0.57 W/m^2. Moreover, the excessively high concentration of brine from CDI can have huge negative impact on the environment if the brine is directly disposed to the environment. The brine concentration from the CDI cell was minimized by the installation of the RED stack to the system.

2.12. Process optimization

Process optimization is a crucial aspect in various industries. This is because optimization enhances the efficiency of a process, ensuring that the resources such as raw material, time and energy are utilized effectively. This can result in cost savings, reduced waste, and improved overall productivity. Furthermore, by identifying and elimination inefficiencies, unnecessary steps, or overutilization of resources, process optimization can ensure that these resources are used effectively to achieve the desired output.

2.12.1. Application of Response Surface Methodology

Response Surface Methodology (RSM) is a statistical and mathematical technique used in experimental design and optimization. It is particularly employed in fields such as engineering, manufacturing, chemistry, and other sciences to model and optimize complex processes (Almeida *et al.*, 2008; Tetteh *et al*., 2017; Tetteh and Rathilal, 2021). The primary goal of RSM is to understand the relationship between multiple independent variables and a response (output) variable (Iqbal *et al.*, 2016). This tool is valuable in situations where the relationship between variables is not well-understood, and it provides a systematic approach to optimize processes with multiple factors (Tetteh and Rathilal, 2021). It is widely used in industries where experimentation is costly or time-consuming.

Before the adoption of RSM, the prevalent method was OFAT, which stands for One Factor at a Time (Tetteh *et al*., 2017). OFAT focuses on adjusting one variable at a time while keeping the other variables constant. However, this approach is not ideal for capturing potential interactions between variables. OFAT is less efficient as it requires running a series of experiments, each concentrating on a single factor. This method tends to miss interactions between variables since they are not investigated concurrently, which has the potential to overlook optimal conditions (Tetteh and Rathilal, 2018).

Response Surface Methodology:

- RSM typically involves designing a set of experiments based on a mathematical model. The design includes varying the input variables at different levels to observe the response variable's behavior.
- A mathematical model is developed to represent the relationship between the input variables and the response variable. The model is often a polynomial equation that approximates the true behavior of the system.
- Conducting experiments based on the designed experimental plan and collecting data on the response variable for each combination of input variables.
- ANOVA (analysis of variance) is used to analyze the collected data and determine the significance of each variable and interaction terms. This helps identify which factors have a significant impact on the response.
- Graphical representations, such as response surface plots and contour plots, are used to visualize the relationship between the input variables and the response. These plots help in understanding the optimal conditions for the response variable.

- ❖ The goal of RSM is often to find the optimal set of input variables that maximize or minimize the response variable. Optimization techniques, such as gradient-based methods or desirability functions, may be employed for this purpose.
- ❖ Once the optimal conditions are identified, further experiments may be conducted to verify the predicted values and ensure the reliability of the model.

In this study design expert software was used to find the optimal point. RSM was used to systemically investigate the effect of independent and dependent variables.

2.12.2. The historical data

On the design expert software, historical data was used. Runs were first design and conducted. The data that was obtained was then imported to the software from the Excel spreadsheet. The reason for using Design Expert software was to find the optimal point. The software than develops a mathematical model to represent the relationship between the input variables and the response variables. In this study there were two response variables which were OCV and voltage under load.

2.13. Summary

In this section, the background of various renewable sources was explored, along with their contributions to the South African electricity grid. While diverse renewable energy sources exist, each carries its own set of challenges. With the global demand for energy continually rising, the integration of these green energies becomes imperative to devise sustainable solutions.

Within the literature, RED stands out as a promising energy source. The exploration of the RED stack extended to a comprehensive examination of its components, from Ion Exchange Membranes to the RED stack geometry. Furthermore, a thorough review of key parameters affecting power generation in the RED stack, such as the temperature and flow rate of the feed, was undertaken. Additionally, the literature delves into an extensive discussion on technologies that are integrated with RED. Design expert was chosen as tool for process optimization and statistical data analysis and modeling.

CHAPTER 3: Materials and methods

Chapter overview

This chapter describes the experimental approach used to achieve the study's objectives. This exploratory study was divided into two distinct parts. The first part of the study investigates the performance of reverse electrodialysis stacks under various experimental conditions using electrode rinse solutions (ERSs). The main operating parameters were the concentration, the flow rate, and the composition of the electrode rinse solutions. A second part of the project involved the generation of power using Indian ocean and water samples from different rivers in KwaZulu Natal. The feed flow rate and temperature of the feed were primarily examined in the RED system. A comparison of ERSs conducted in Part A informed the choice of ERS for Part B. ERS pump settings in Part B were carefully selected based on the optimal results achieved in Part A, i.e., those that produce the highest Voltage Under Load (VUL) while having the lowest internal resistance. Further details about the experimental setup and operating procedures are provided in the following sections. The installation, troubleshooting, and commissioning processes for the RED stack are included in this process. Response surface methodology (RSM) was adapted from Design Expert software (Stat-Ease Inc, Minneapolis, USA) to investigate and optimize the individual effects and interactions of the parameters. This study was conducted following the methodological steps outlined in **Figure *3-1***.

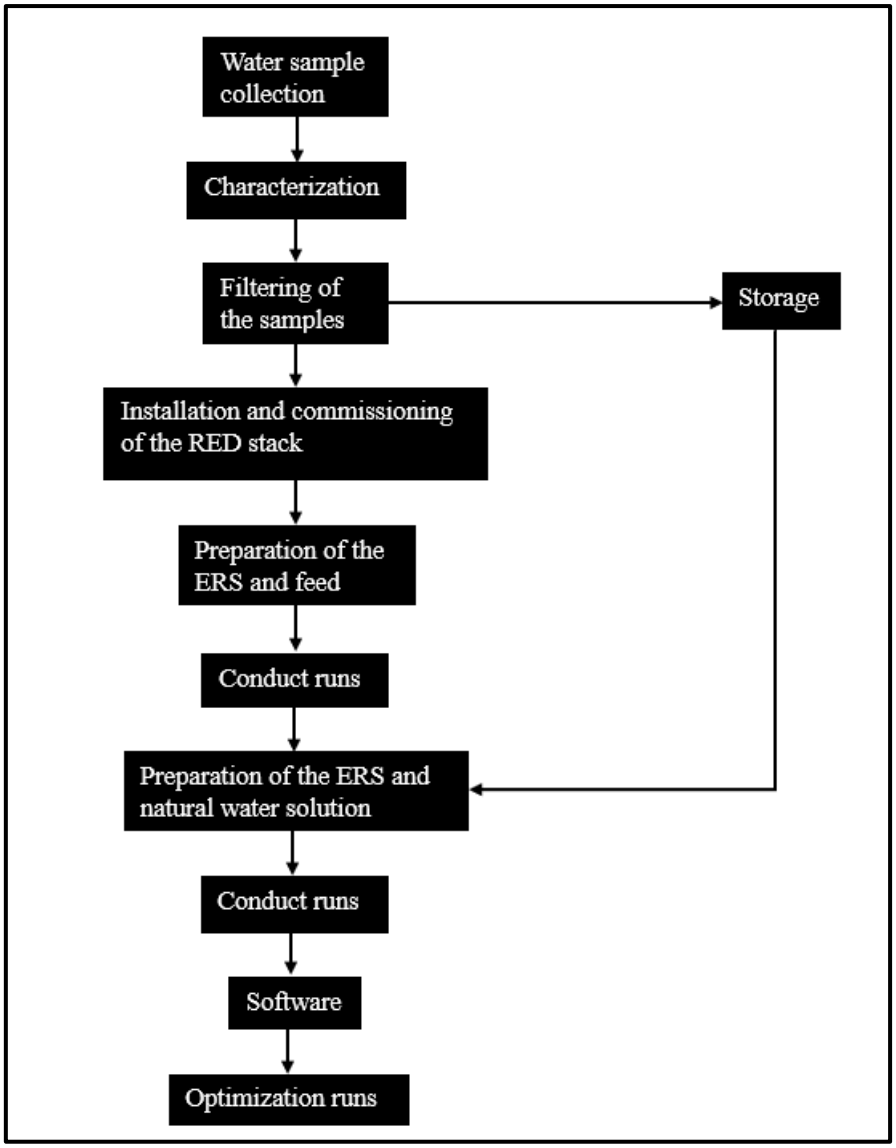

Figure 3-1: The graphical methodology of the study.

3.1. Materials

3.1.1. Chemicals and materials

All chemicals (***Table 3-1***) used in this research were of analytical grade and used directly as received. Both high and low-concentration solutions were prepared by dissolving NaCl in deionized (DI) water. All the chemicals that formed ERSs were mixed and appropriately dissolved in DI water. Deionized water (ELGA PureLab Option-Q water deionizer, UK) was used in the solution preparation. Chem Lab Supplies supplied Sodium Chloride (99.5%), Potassium Ferricyanide anhydride ($K_3Fe(CN)_6$), Potassium Ferrocyanide trihydrate [$K_4Fe(CN)_6$], Potassium Chloride (KCl) as well as the other chemicals used to prepare ERSs.

Table 3-1: Purity for all organic salts used in the study.

Compound	Purity (wt.%)	Supplier†	CAS no.
$K_3Fe(CN)_6$	≥ 99.0	United Scientific SA	13746-66-2
$K_4Fe(CN)_6$	≥ 99.0	United Scientific SA	14459-95-1
Na_2SO_4	≥ 99.0	United Scientific SA	7757-82-6
KCl	≥ 98.0	United Scientific SA	7447-40-7
NaCl	≥ 99.9	United Scientific SA	7647-14-5

† Supplier quoted purity

3.2. Collection, preparation, and characterization of samples

3.2.1. Synthetic samples

Literature suggestions were used to select ERSs (Tufa *et al.*, 2014; Long *et al.*, 2018; Ashu *et al.*, 2019; Buckingham *et al.*, 2020; Mehdizadeh *et al.*, 2021). Salts (NaCl, KCl, and Na_2SO_4) were dissolved in deionized water to prepare electrode rinse solutions. For an example, Precise amounts of $K_3Fe(CN)_6$, $K_4Fe(CN)_6$, and NaCl (0.2, 0.2 and 2.5 M) were prepared to create solutions with specific molar concentrations. Impurities were removed from the solutions by filtering at least three times. Furthermore, artificial aqueous solutions were prepared to recreate river water and seawater's ionic composition without altering their strength. For example, the ERS was prepared on a weight-per-volume basis and reported as 31 g/L for 31 g-NaCl in 1L of DI water. The solids were dispersed in 1L of DI water by adding 5 g of NaCl and stirring (Stuart UC152 Hot plate stirrer) until completely dissolved. A similar procedure was performed with 10, 20, and 30 g of NaCl in 1L of DI water. Finally, high (38 g/L) and low (0.4 g/L) salinity concentrations mimicking river water and seawater were prepared. Before the experiments, the solutions were filtered and stabilized for 24 hours. The samples prior to their use were characterized by measuring their pH and conductivity.

3.2.2. River and seawater samples

Samples for this study were collected from the uMgeni, uMzimkhulu, and uMkomaas rivers. uMgeni, uMzimkhulu, and uMkomaas River samples had conductivities of 821, 1460, and 1849 µS/cm, respectively. Seawater samples were collected south of Durban at Blue Lagoon Beach, KwaZulu Natal. Upon collection, a series of tests were conducted on the water, including pH and conductivity. This was carried out using a Thermo Scientific Orion Star A215 pH/conductivity meter, as illustrated in **Figure *3-2***. For electrical measurements, a multimeter

was used. To prepare the water for the RED stack, it was pre-filtered through a series of microfilters, with a final filter having a median diameter of 20 µm. No additional measures were taken to prevent fouling. The samples were kept in a cool place overnight and used the following day. In this project, conductivity was a key parameter.

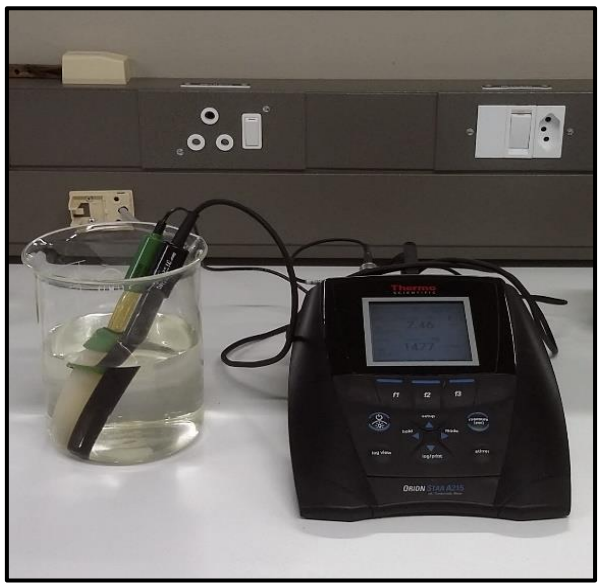

Figure 3-2: A pH/Conductivity meter coupled with a thermostat probe.

To accommodate all experimental runs efficiently, a 250 L drum was used to prepare two homogeneous solutions (river and seawater samples). The solutions were filtered again using a filter bag and filter paper to avoid fouling the membranes. Both solutions were prepared at least 24 hours before the experiments began. By extending the mixing and stabilizing time, the experimenter was able to ensure that the solutions were homogeneous and uniform in composition before starting the runs. Afterwards, a black cloth was placed over the container of the solution to prevent it from reacting with sunlight and from possible degradation (Scialdone *et al.*, 2012).

3.3. Characterization

The samples were characterized both before and after the experiments. The first step in the analysis was to measure the pH and conductivity of synthetic and collected samples (river water and seawater) as these data were heavily relied upon. Similarly, the pH and conductivity of samples drawn from two-channel outlets were determined. As described above, a pH/conductivity meter was used.

3.4. Solutions chemistry

In the presence of water molecules, the electrostatic attraction between potassium and chloride ions becomes weaker when KCl dissolves in water, allowing the ions to become surrounded by water molecules and move freely in solution (Marcus, 2009; Benjamin, 2014). Dissociation of KCl in deionized water results in K^+ and Cl^- ions in solution. The presence of these mobile ions results in the solution conducting electricity. A similar phenomenon occurs with the compound Na_2SO_4. Two Na^+ and one SO_4^{2-} ions form when Na_2SO_4 dissolves in deionized water. NaCl dissociates into Na^+ and Cl^- ions. The reactions involving Fe^{2+} and Fe^{3+} are redox reactions. During this redox reaction, an electron is transferred from one oxidation state of the ferrocyanide ion to another.

3.5. Experimental set-up

The experimental setup for this study's RED stack technology is shown in ***Figure 3-3***. The experimental setup is similar to that used by other researchers (Altıok *et al.*, 2021; Cui *et al.*, 2022).

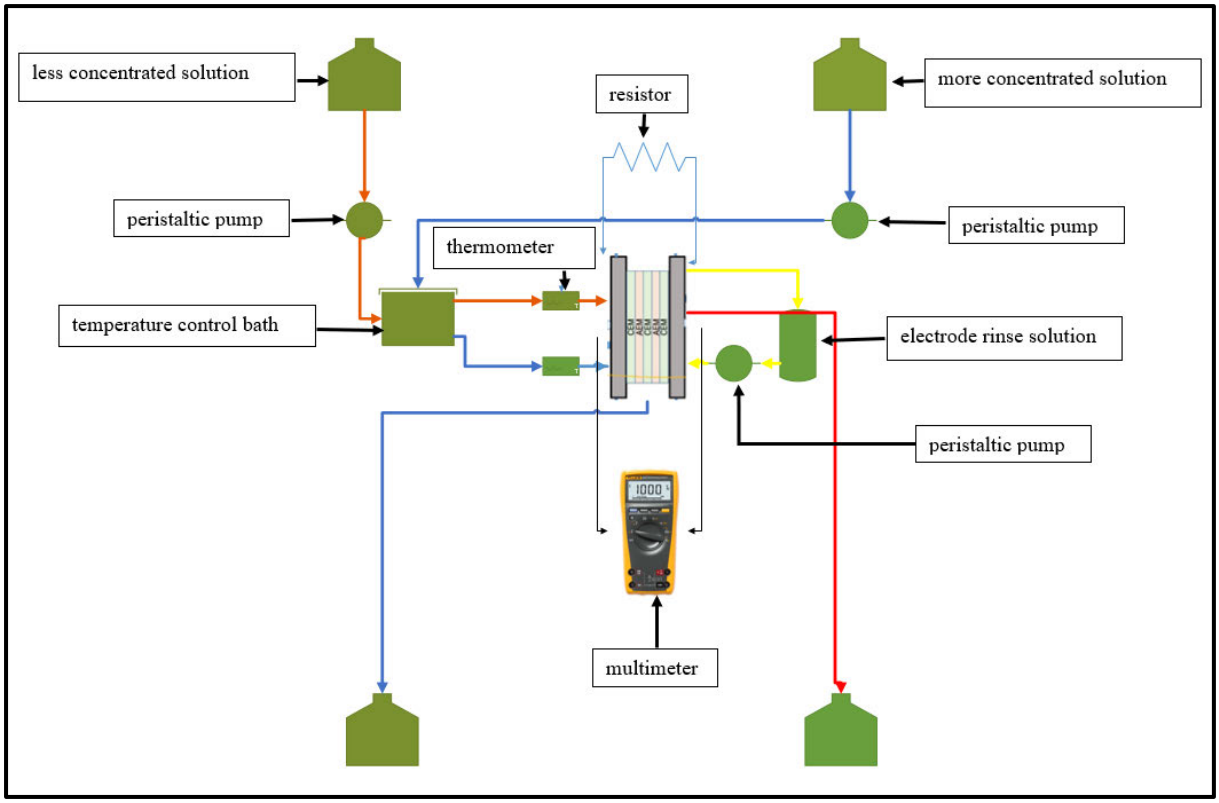

Figure 3-3: A simplified schematic diagram of the RED system for the study.

3.5.1. Main apparatus

RED stack

A RED stack (as shown in **Figure *3-4***), with 30-cell pairs, was used (supplied by Beijing Jingo Desalination, China). To ensure efficient electron transfer, the stack had titanium mesh electrodes coated with platinum and iridium (Ti/Pt-Ir). Cation Exchange Membranes (CEMs) and Anion Exchange Membranes (AEMs) were combined in the stack, each offering an active membrane area of 0.0297 m² (0.11 × 0.27). A CEM was used as a shielding membrane on the stack's outer sides to prevent the transfer of negatively charged iron complexes (Scialdone *et al.*, 2012; Simo *et al.*, 2023). The total membrane area of the cell was 0.0594 m². A woven spacer of 0.5 mm thickness improved solution flow and mixing and maintained stability. To prevent leaks and maintain a sealed environment, rubber seals were installed. RED stack and membrane characteristics are illustrated in ***Table 3-2*** and ***Table 3-3***.

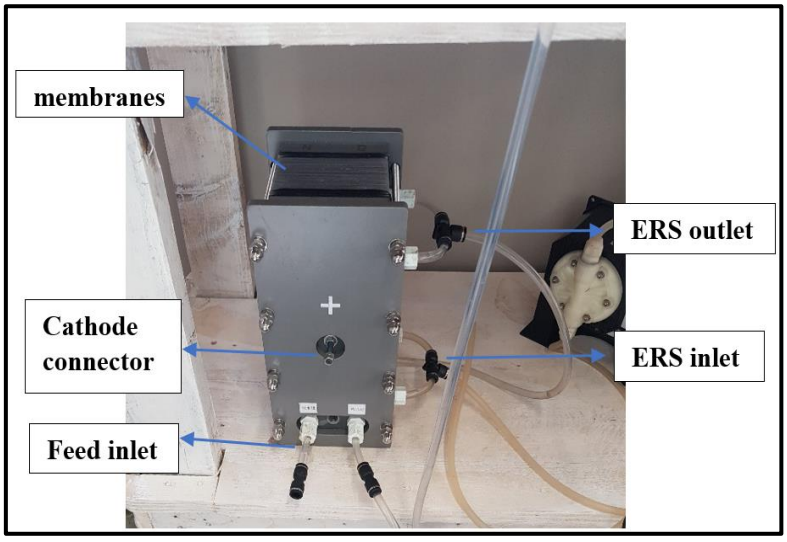

Figure 3-4: RED stack that was used for the study.

3.5.2. Commissioning of RED Stack

Upon delivery, the RED stack was carefully inspected for visible damage that might have occurred during transportation. The inspection included a detailed check of all components, including membranes, spacers, and electrodes. It was confirmed that all necessary components were in place and undamaged. After reassembling the stack, the peristaltic pump lines were connected, along with the feed and ERS lines. Deionized water was then recirculated within the ERS compartment while simultaneously being fed into both the low concentration and high concentration compartments. This procedure was carried out to check for any potential leakage.

The manufacturer's manual specified that the RED stack should generate OCV of 3 V when operated with a more concentrated solution of 30g NaCl, a less concentrated solution of 0.5g NaCl, and an ERS of 0.3 M $K_3Fe(CN)_6$, 0.3 M $K_4Fe(CN)_6$, 2.5 M NaCl. At ambient temperature of around 25 ℃ and a flow rate of 400 mL/min for the feed solutions and a flow rate of 180 mL/min for the ERS. Three runs were conducted, resulting in OCV values of 3.01, 2.981, and 3.09 V. These values closely align with the expected 3 V, demonstrating consistent performance.

3.6. Experimental measurements

3.6.1. Design of experiments

For the first part the study used the One Factor at a Time (OFAT) experimental design method. Methods such as this involve systematically varying one parameter (in this case, the rinse solution's flow rate or solution concentration) without changing any other factors. In this approach, each parameter's impact on the electrochemical process is analyzed in detail and focused by changing one at a time. In this way, it is possible to understand how changes in each specific parameter affect the system's performance and response while keeping other variables constant. It was decided to use the OFAT method because it facilitates a systematic and methodical investigation of the variables of interest, allowing a comprehensive understanding of their effects on electrochemical processes.

3.6.2. Experimental procedure

Before commencing the experimental runs, the system underwent a stabilization process involving the circulation of deionized (DI) water through both high concentration (HC) and low concentration (LC) compartments for five minutes. This ensured optimal wetting of all membranes and flow channels, similarly done for the electrode rinse solution compartment. To ensure the reliability and validity of the results while minimizing biases and variabilities, the runs were randomized. Two peristaltic pumps (Altimus, SA) were used to feed HC and LC solutions into the RED stack in a co-current arrangement. The thermostated liquid bath (with an uncertainty of ± 0.5 °C) was used to maintain the system temperature. Thermometers at the inlet of the stack monitored the temperature. The ERS was continuously recirculated from a 1L container to the cathode and anode chambers in the RED stack at a chosen flow rate via a peristaltic pump (Blackstone, Hanna Instruments, SA). To introduce a load, a 4.7 Ω resistor was connected to the ERS anode and cathode chambers. Electrical performance measurements,

such as OCV and VUL, were recorded once the system reached a steady state, confirmed by 30 seconds of stable measured variables which was approximately 4 minutes. Real-time voltage outputs were monitored continuously. Effluent samples were collected post-experiment for pH and conductivity measurements. When changing the type of ERS, the RED stack was opened, and membranes were submerged in deionized water for 2 hours before subsequent runs. When the RED stack dried, it was reassembled, and the electrode rinse solution and feed solution lines were connected back. Prior to each run, the pH of the feed solution and ERS was measured using a pH meter. The experimental runs were repeated three times to ensure accuracy and reliability. Averages were used to report the data. Samples taken from the outlet points were collected and analysed.

In the initial phase of this investigation (Part A), ERS and synthetic feed solutions listed in the previous sub-sections were used. A total of forty-eight runs were carried out under ambient conditions (± 25°C), varying the flow rate of ERS from 9.15 to 18.3 L/h and its concentrations from 5 to 30 g/L. The flowrate range was chosen based on the capacity of the ERS pump, and it was also selected because it did not damage the membranes of the stack. Meanwhile, the mixture concentrations ranged from 0.05 M to 0.3 M. Additionally, the flow rate of the feed solutions was consistently maintained at 900 mL/min. This study's second part (B) used the best conditions obtained in the first part. These conditions comprised of flow rate, concentration and type of ERS used. Power density was the determining factor for these conditions. During Part B of this study, actual river water and seawater samples were used as feed solutions following the abovementioned procedure. The flow rate of the feed solutions was varied between 900 to 1550 ml/min, with temperatures ranging from 25 to 40°C. The flowrate range was chosen based on the capacity of the feed pumps, and this range also did not damage the membranes of the RED stack. The temperature range aligns with the average regional temperatures, making it relevant to local conditions and enhancing the real-world applicability of the study. This alignment is especially important when using natural feed sources, as it reduces the need for additional heating or cooling, thus making the process more energy-efficient and environmentally friendly. The river water and seawater flow rate were similar in all the runs. For wetting the membranes, the river water and seawater were circulated through both high HC and LC compartments for five minutes. Forty-eight runs were conducted with the ERS flow rate constant at 153 mL/min. Equation (3.1) was used to calculate power density (Weinstein, 1976) while equation (3.1) was used to calculate internal resistance (Elmakki *et al.*, 2023).

$$P_{d,max} = \frac{(V^o)^2}{4AR_i} \quad (3.1)$$

where A, R_i and V^o denote the membrane area, the stack's internal resistance, and stack open circuit voltage.

$$R_{internal} = \frac{OCV - V_{load}}{I_{load}} \quad (3.1)$$

where OCV, V_{load} and I_{load} denote the voltage value, voltage under load and current under load. The current was calculated using the following equation.

$$I = \frac{V_{load}}{R_{load}} \quad (3.2)$$

3.7. Modeling and Optimization

Developing an empirical model is a fundamental step in understanding and optimizing the complex interplay of variables influencing electricity generation in a RED system. The RSM is employed to assess the combined effects of temperature and flow rate on power density. This empirical model provides comprehensive insight into the relationships between input variables and resulting power density, allowing for a nuanced understanding of their interactions within the RED system. Through RSM, key factors influencing electricity generation can be identified, which is crucial for optimizing the system and achieving high power density.

Furthermore, empirical models play a pivotal role in guiding future experiments. They highlight areas of interest and indicate potential trends, ensuring that subsequent experiments are more targeted and resource efficient.

Optimizing input variables is paramount in achieving the dual objectives of maximizing power density while minimizing operational costs. It's not just about enhancing performance; it's also about ensuring cost-effectiveness. Striking a balance is imperative to keep the process economically viable, with minimized operating costs, particularly related to energy

consumption. By minimizing resource consumption and operational costs, the system becomes more environmentally friendly and economically sustainable.

3.7.1. Empirical modeling

Table 3-2 shows the results obtained after the experimental runs. OCV and VUL are the responses that were used for the model. Temperature and flow rate are the manipulated variables.

Table 3-2: Experimental run data

Run#	Temperature (°C)	Flow rate (mL/min)	OCV (V)	VUL (V)
1	25	1370	3,553	0,664
2	35	1370	3,605	0,898
3	40	1550	3,775	0,904
4	30	950	3,498	0,767
5	25	1550	3,535	0,687
6	30	900	3,454	0,791
7	40	1370	3,722	0,885
8	35	950	3,56	0,816
9	30	1370	3,502	0,736
10	25	900	3,313	0,632
11	35	1550	3,61	0,781
12	40	900	3,564	0,881
13	25	950	3,362	0,634
14	40	950	3,607	0,834
15	30	1550	3,535	0,69
16	35	900	3,395	0,652

$$OCV = 3.56 + 0.1085\,A + 0.0775\,B - 0.0006\,AB + 0.0382\,A^2 - 0.0489\,B^2 \quad (3.3)$$

$$VUL = 0.7672 + 0.1071\,A + 0.0148\,B + 0.0123\,AB \quad (3.4)$$

A and B are the coded factors. The coded factors represent the values of the independent variables scaled to a dimensionless form, usually in terms of standard deviations from the centre point.

Equation (3.3) and (3.4) are the equations in terms of coded factors which are used to make predictions about the response for given levels of each factor. Additionally, the coded equation is used for identifying the relative impact of the factors by comparing the factor coefficients.

3.7.2. Optimization framework

In the pursuit of achieving net power generation in the RED system, it is crucial to carefully address the impact of key variables on energy consumption. The optimization of these variables, namely temperature and flow rate, plays a pivotal role in attaining a balance between maximizing power generation and minimizing operational costs.

A high-temperature feed requires additional energy input, specifically in terms of heating up the feed solutions. The trade-off between increased power density at higher temperatures and the associated energy cost needs to be carefully considered. The model aims to identify an optimal temperature range that enhances power density while ensuring that the added energy cost does not overshadow the benefits.

Similarly, a higher flow rate of the feed solution necessitates more pumping energy. The RSM facilitates the assessment of the correlation between flow rate, power density, and the energy required for pumping. The model seeks to identify a flow rate that maximizes power density while maintaining a balance between increased electricity generation and the energy expended in the pumping process.

CHAPTER 4: Results and discussions

Chapter overview

This chapter presents and discusses the results of the study. Firstly, the effect of the electrode rinse solution on the power generation of the RED stack is discussed. The effect of rinse flowrate, concentration and composition is discussed extensively. Raw data and corresponding graphs are presented for a comprehensive understanding. This is followed by a discussion on the effect of using natural water as feed for power generation. The discussion focuses on various parameters that influence power generation.

4.1. Influence of ERSs

The OCV and VUL were measured at various flow rates and concentrations of ERS to assess the influence of each ERS. ERSs were further examined by evaluating the effect of varying compositions. Mixtures do not have the same mass concentration as other ERSs. **Table *4-1*** shows the conductivities and concentrations of the ERSs and mixtures used in this study.

Table 4-1: The characteristics of the ERSs and mixtures used.

Concentration (g/L)	NaCl (mS/cm)	KCl (mS/cm)	Na_2SO_4 (mS/cm)	Mixture (mS/cm)
5	9.00	10.44	9.16	74.8
10	17.12	20.10	17.72	95.71
20	31.50	36.54	32.91	105.87
30	46.33	54.10	48.22	122.56

A set of 3 preliminary runs under identical conditions was conducted before each set of runs to ensure repeatability. Test solutions were selected with consistent parameters, including a 5 g concentration and a 153 ml/min flow rate. Mixture concentrations were 0.05 M $K_3Fe(CN)_6$, 0.05 M $K_4Fe(CN)_6$, 2.5 M NaCl. The results of these triplicate runs are presented in **Table *4-2***.

Table 4-2: The triplicate preliminary runs.

Component	Run no.	OCV (V)	VUL (V)
NaCl	1	4.362	0.508
	2	3.950	0.460
	3	4.090	0.495
Na_2SO_4	1	3.250	0.425
	2	3.405	0.385
	3	3.520	0.410
KCl	1	3.938	0.411
	2	4.001	0.435
	3	3.920	0.451
Mixture	1	4.213	0.725
	2	4.475	0.740
	3	4.542	0.690

4.1.1. Effect of flow rate

4.1.1.1. Internal resistance

As shown in **Figure *4-1***, increasing the rinse solution flow rate decreases the internal resistance.

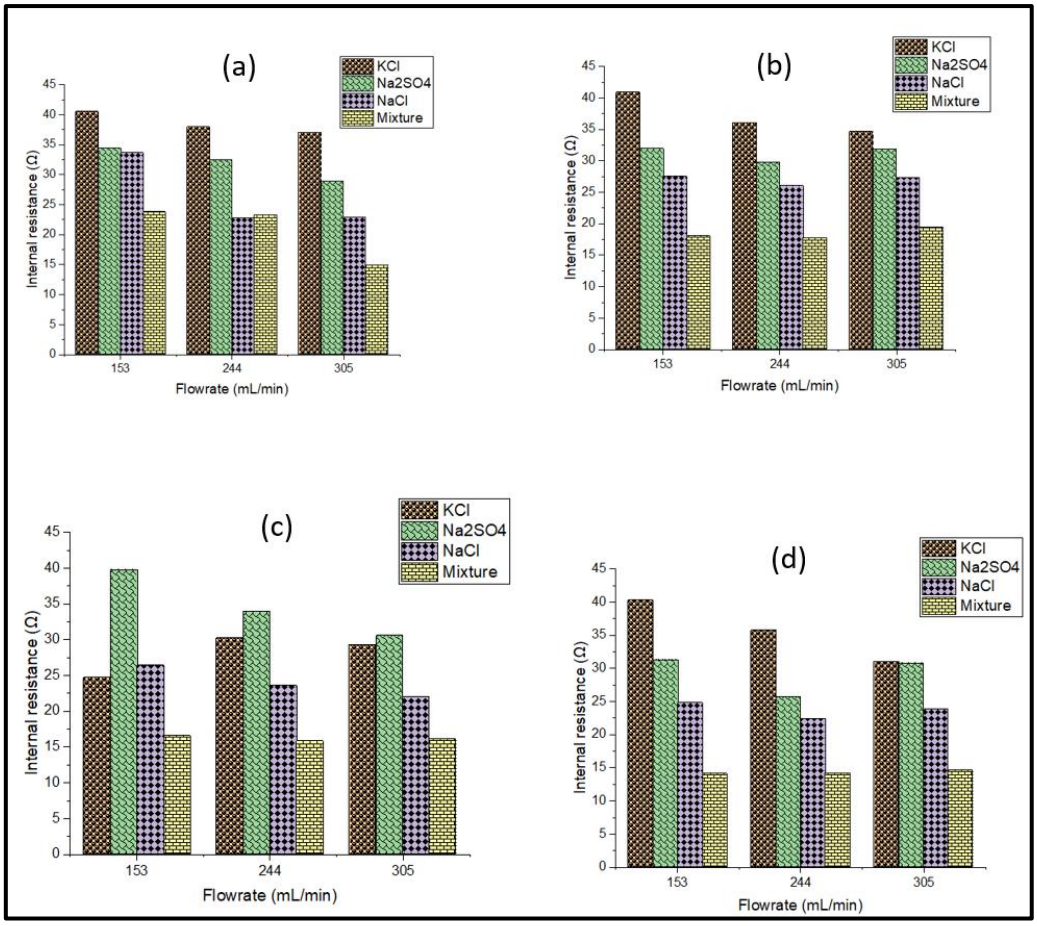

Figure 4-1: The effect of flow rate on internal resistance at varying concentrations : symbols 'a, b, c, and d' denote 5g, 10g, 20g, and 30g, respectively. Similarly, for the mixture, symbols 'a, b, c, and d' denote 0.05 M, 0.1 M, 0.5 M, and 0.3 M, respectively.

This is due to continuously replenishing ions at the electrode interface, which reduces concentration polarization. As a result, ion accumulation is minimised, reducing resistance (Wu *et al.*, 2023). This behaviour may also be attributed to reduced electrode fouling at higher flows, reducing the deposition of undesired materials on the electrode surface. Increased flow rates prevent material buildup on electrode surfaces, minimising fouling. An electrode interface with less fouling allows ions to interact better, lowering internal resistance.

4.1.1.2. OCV and Power density

Figure 4-2 depicts a decreasing trend in measured OCV as the rinse flow rate increases. There is a significant drop in OCV as the flow rate increases from 153 ml/min to 244 ml/min, with a more pronounced decrease than the shift from 244 ml/min to 305 ml/min.

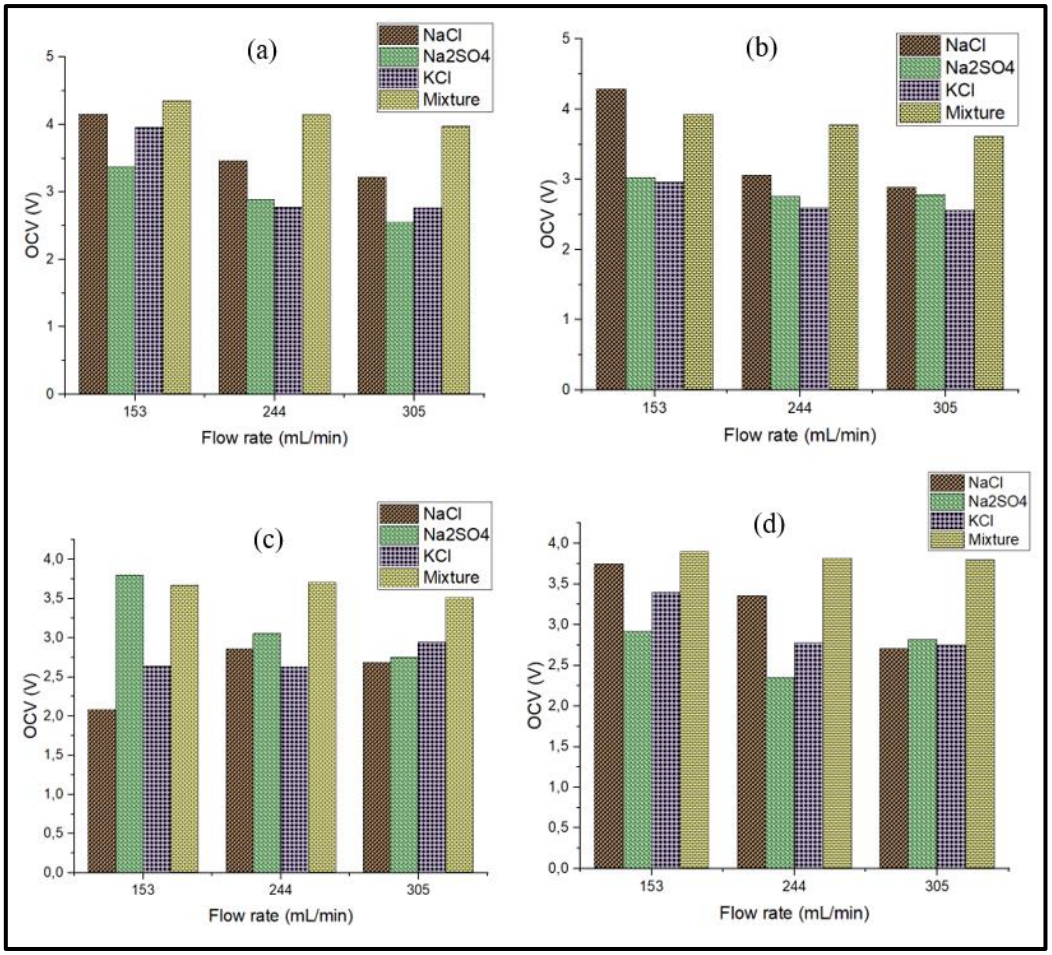

Figure 4-2: The effect of flow rate on OCV at varying concentrations : symbols 'a, b, c, and d' denote 5g, 10g, 20g, and 30g, respectively. Similarly, for the mixture, symbols 'a, b, c, and d' denote 0.05 M, 0.1 M, 0.5 M, and 0.3 M, respectively.

This occurs because the residence time is reduced as the flow rate increases. This reduction in residence time results in a lower OCV because efficient electrochemical reactions generating OCV depend on ions staying close to the electrode. The faster flow carries ions away from the electrode vicinity. Higher flow rates cause the electrode rinse solution to pass over the electrode more rapidly, diluting the ion concentration near the electrode surface. This rapid flow effectively mixes the ions near the electrode with the incoming rinse solution, leading to an even distribution of ions within the electrode rinse solution. There were mixed results regarding this relationship for all ERSs in the 20 g concentration level (**Figure 4-2**(c)). Only the Na_2SO_4 solution had consistent results. At this level, Na_2SO_4 had the best results of 3.805 V, followed by the mixture with 3.672 V.

NaCl consistently produces the highest OCV among the three electrode rinse solutions that were not redox, with Na_2SO_4 showing the highest OCV at 20 g and a trend of decreasing OCV

with increasing flow rate. The highest OCV for each electrode rinse solution is observed at the lowest flow rate. This can be attributed to the increased residence time, which allows for more ion interaction between the electrodes and the ERS. However, lower flowrate can contribute to electrode fouling, which refers to the accumulation of undesired materials, such as precipitates, on the surface of the electrodes. Lower flow rates mean the solutions spend more time contacting the electrodes. This extended residence time provides a longer period for the interaction between ions in the solution and the electrodes. If specific ions have the potential to form solid compounds (precipitates) or adhere to the electrode surfaces, the likelihood of these processes occurring increases with longer residence times.

Error! Reference source not found. shows a general decreasing trend in power density as the flow rate of the ERS increases.

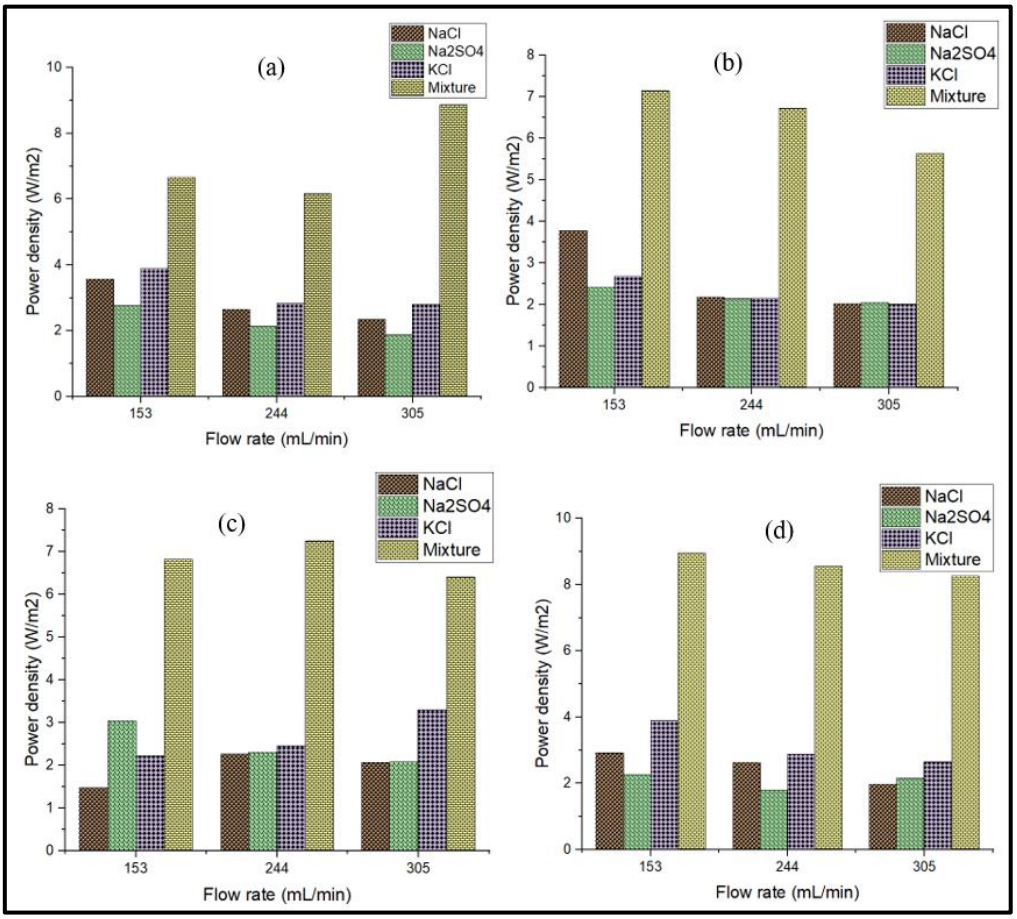

Figure 4-3: The effect of flow rate on power density at varying concentrations : symbols 'a, b, c, and d' denote 5g, 10g, 20g, and 30g, respectively. Similarly, for the mixture, symbols 'a, b, c, and d' denote 0.05 M, 0.1 M, 0.5 M, and 0.3 M, respectively.

This may be attributed to the reduced residence time due to the increasing flow rate. Decreased residence time reduces power density because the electrodes do not have enough time to interact with the rinse solution. Therefore, this indicates that no reactions occurred at the electrodes. Furthermore, the highest power density values were achieved at a lower flow rate of 153 mL/min throughout the experiment, except for a few cases.

4.1.2. The effect of concentration

4.1.2.1. Power density and OCV

In **Figure *4-4*(a to d)**, when analysing the relationship between OCV and the concentration of the ERS for the three solutions that were not redox, it is evident that no linear relationship exists.

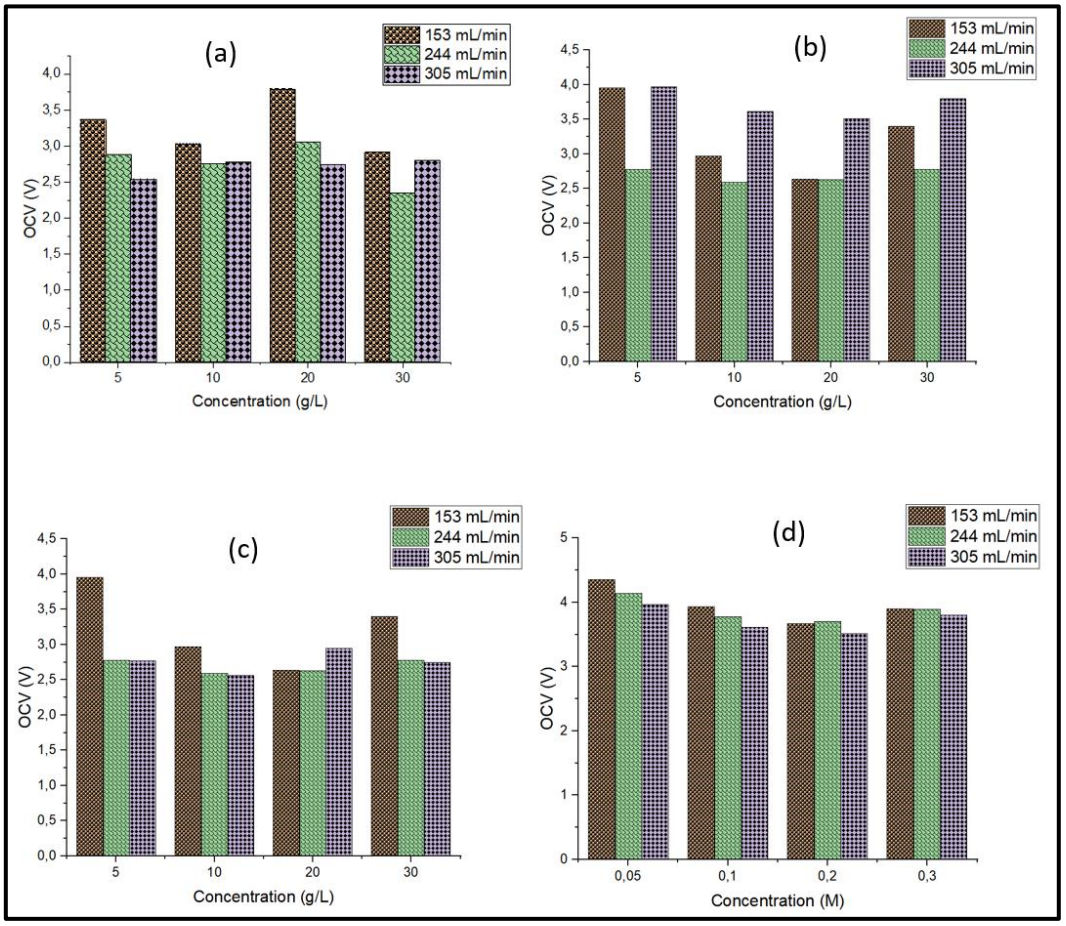

Figure 4-4: The effect of concentration on OCV for different ERS. Symbols "a, b, c and d" denote NaCl, KCl, Na_2SO_4 and mixture, respectively.

This lack of linearity may be attributed to concentration levels not well-suited for the electrodes. Another reason for this observed behaviour could be that the electrode rinse solutions were incompatible with the electrodes. The compatibility between electrodes and the

electrode rinse solution is critical to electrochemical systems' overall performance and stability. Electrodes interact with ions in the solution during electrochemical reactions. If the ions in the ERS are not conducive to the desired electrochemical processes, it can lead to inconsistencies and inefficiencies. Incompatibility between the electrode material and the ERS can contribute to fouling, where unwanted deposits accumulate on the electrode surfaces. This fouling can alter the electrode's properties and impede electrochemical reactions, resulting in inconsistencies in performance.

In **Figure *4-4*(d)**, a noticeable trend emerges as the concentration of the ERS, specifically the mixture, increases—a corresponding decrease in the OCV. This observation highlights an inverse relationship between ERS concentration and OCV, suggesting that higher concentrations may diminish the OCV. The observed phenomenon may be attributed to excessive concentration of the ERS. Excessive concentration of the ERS can induce saturation effects, wherein the electrodes become saturated with ions. When saturation occurs, inconsistent reactions may result due to current over-limitation (Deng *et al.*, 2013). Uneven ion transport and over-limiting currents can result in non-linear behaviour in the relationship between the concentration of ions in the ERS and the OCV. The OCV may not increase proportionally with increasing concentration due to the limitations imposed by over-limiting currents and uneven ion transport.

Figure *4-5* shows no linear relationship between the electrode rinse solutions and power density.

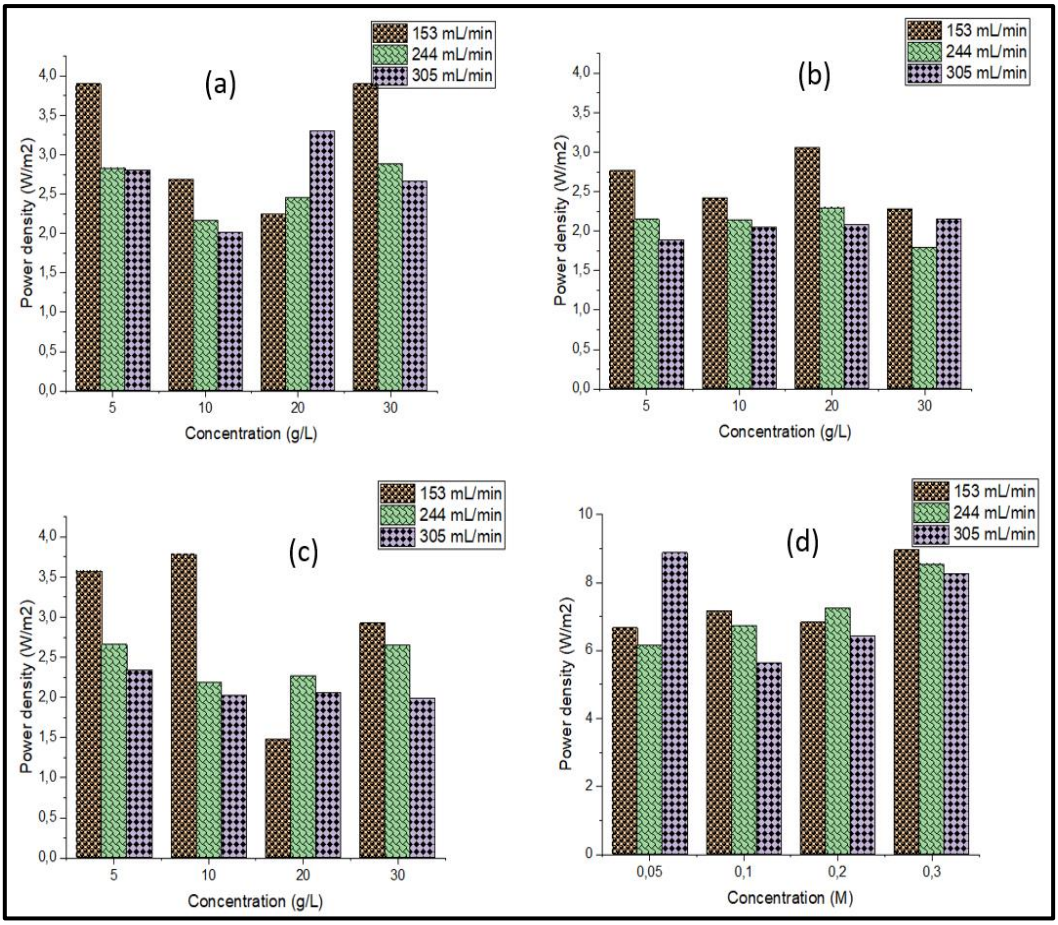

Figure 4-5: The effect of concentration on power density for different ERS. Symbols "a, b, c and d" denote NaCl, KCl, Na_2SO_4 and mixture, respectively.

This is because power density is the product of OCV and internal resistance (see Eq.3.1). Since there is no visible trend between OCV and the concentration of the ERS, this will lead to power density not having any visible relationship with the concentration of the ERS.

In **Figure *4-5*(d)**, when the concentration of the ERS increases, the power density also increases. Increasing concentration reduces internal resistance, leading to increased power density. This trend was observed when a mixture was used as an ERS. A system's internal resistance is affected by various factors, including ion mobility. A higher ion concentration in the ERS can reduce internal resistance, improving energy conversion efficiency and power density. Contrary to other electrode rinse solutions, which are less commonly used, this mixture contributes to a better understanding of its properties.

4.1.2.2. Internal resistance

Figure 4-6 depicts a decreasing trend in internal resistance as the concentration of the rinse solution increases.

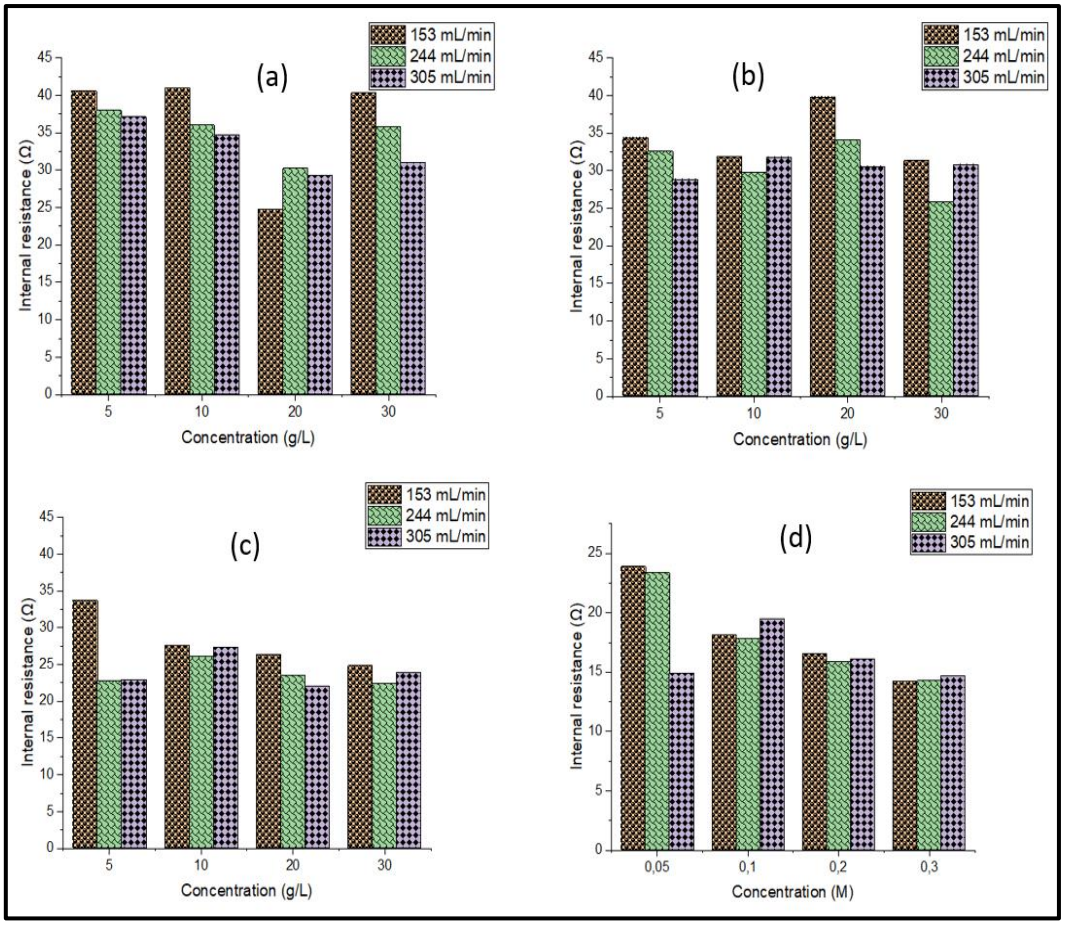

Figure 4-6: The effect of concentration on internal resistance. Symbols "a, b, c and d" denote NaCl, KCl, Na_2SO_4 and mixture, respectively.

An increase in solution concentration increases conductivity. Conductivity is inversely related to electrical resistance. Higher conductivity corresponds to lower electrical resistance. Lower resistance indicates that electrons encounter fewer obstacles or hindrances as they move through the solution, leading to more efficient electron transfer. Conductivity is a measure of how well a solution can conduct electric current. The higher the conductivity, the better the solution conducts.

On the other hand, electrical resistance measures how much a solution opposes the flow of electric current. The higher the resistance, the more difficult it is for electric current to flow through the solution. Ohm's Law, a fundamental principle in electrical engineering, states that the current flowing through a conductor between two points is directly proportional to the

voltage across the two points and inversely proportional to the resistance.

Among the three ERS that were not the redox mixture, NaCl showed the best performance when reducing internal resistance. This might be because sodium ions (Na^+) are generally more electrically conductive than potassium ions (K^+). This is due to differences in their respective properties. Sodium ions are smaller than Potassium. Smaller ions can move more easily through a solution because they experience less resistance from neighbouring ions and water molecules. This increased mobility makes sodium ions better conductors of electricity.

In **Figure 4-6**(d), the mixture's internal resistance decreased by 24% when the concentration increased from 0.05 M to 0.1 M at a 153 mL/min flow rate. However, for concentrations of 0.1 to 0.2 M and 0.2 to 0.3 M, there was less than a 20% decrease in internal resistance. A similar trend was observed with NaCl at the same flow rate. This suggests that doubling concentrations does not necessarily lead to a proportional improvement in performance, specifically in terms of internal resistance reduction. It indicates a diminishing return and may suggest an optimum concentration for minimizing internal resistance. As the concentration increases, there is a tendency for it to deviate further from the optimum point.

4.1.3. The effect of composition

The mixture had superior results in terms of Power density, OCV, and internal resistance, as shown in **Figure *4-1*** to **Figure 4-6**. Fe^{2+}/Fe^{3+} or ferri-/ferrocyanide are the most used redox species in the studies that involve RED. These redox species have low over potential for electron transfer, which leads to low electrode resistance and maximum electric power (Han *et al.*, 2019). Conversely, it is important to note that the mixture did not have the same concentration by mass as the other ERS.

When comparing the highest power density measurement for the mixture to that of the KCl solution, a notable difference of 129.35% was observed. Additionally, the percentage difference between the mixture and NaCl was 136.54%, while the difference between the mixture and Na_2SO_4 was 193.33%, as shown in **Table *4-3***.

Table 4-3: Calculated power density values for the study.

Flow rate (mL/min)	Power density (W/m^2)				Concentration (g/L)	Concentration (M)(mixture)
	KCl	Na_2SO_4	NaCl	Mixture		
153	3.910	2.781	3.579	6.670	5	0.05
244	2.836	2.155	2.657	6.174		
305	2.808	1.889	2.353	8.880		
153	2.689	2.425	3.789	7.163	10	0.1
244	2.164	2.151	2.189	6.740		
305	2.017	2.052	2.029	5.640		
153	2.224	3.054	1.482	6.834	20	0.2
244	2.461	2.313	2.271	7.267		
305	3.311	2.083	2.073	6.422		
153	3.909	2.285	2.931	8.964	30	0.3
244	2.886	1.802	2.645	8.573		
305	2.657	2.164	1.989	8.262		

The choice of electrode rinse solution can impact the system's performance and efficiency in RED. $K_4Fe(CN)_6$ (potassium ferricyanide) and $K_3Fe(CN)_6$ (potassium ferrocyanide) are often used as electrode rinse solutions in RED, and they differ from using simple salts like NaCl (sodium chloride) alone. The differences arise from the redox properties and conductivity of the specific compounds. Both $K_4Fe(CN)_6$ and $K_3Fe(CN)_6$ are redox-active compounds. They can undergo reversible redox reactions, transitioning between the ferricyanide (Fe^{3+}) and ferrocyanide (Fe^{2+}) states. This redox activity can influence the electrochemical processes occurring at the electrodes. $K_4Fe(CN)_6$ and $K_3Fe(CN)_6$ are generally more electrochemically stable than simple salts like NaCl (Scialdone *et al.*, 2012; Tedesco *et al.*, 2015). This stability can reduce the likelihood of side or undesired reactions at the electrodes during the RED process. The conductivity of the electrode rinse solution is crucial for the efficiency of the RED system. Both potassium ferricyanide and potassium ferrocyanide exhibit higher conductivity than NaCl, KCl and Na_2SO_4, as shown in **Table *4-1***. Higher conductivity allows for better electron transfer and overall system performance. The higher conductivity of a solution allows for better electron transfer because conductivity measures how well a substance can transmit

an electric current, which is essentially the flow of electrons. The presence of ions or free electrons in a substance influences conductivity.

The mixture demonstrated the highest OCV due to a redox couple. Redox-active species engage in reversible oxidation-reduction reactions at the electrodes, generating or consuming electrons and increasing OCV. Redox couples possess a higher electrochemical potential than simpler ions like Cl^- or K^+, resulting in a greater voltage and higher OCV. Additionally, redox reactions exhibit enhanced kinetics at the electrode surface, promoting more efficient charge transfer and further elevating the OCV.

4.2. RED performance evaluation with natural water

Only the temperature and flow rate of the feed were varied. The ERS's flow rate was kept constant at 153 mL/min for all the experimental runs. The average time for a single run was 4 minutes.

4.2.1. Effect of temperature on the measure parameters

4.2.1.1. OCV

In **Figure 4-7**, the effect of temperature on OCV is visible. These results are in agreement with what other researchers have found (Daniilidis *et al.*, 2014; Guo *et al.*, 2018; Mehdizadeh *et al.*, 2019).

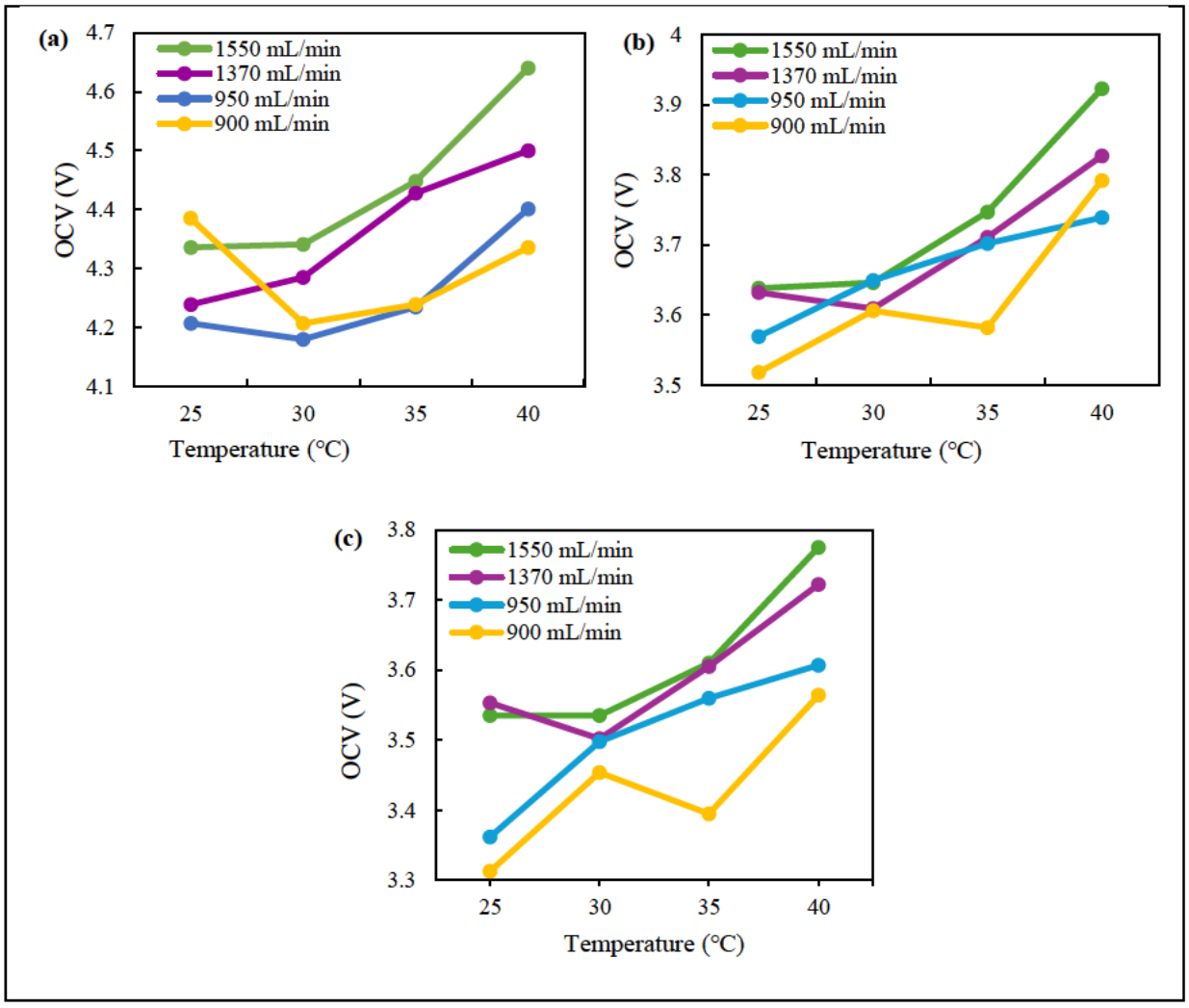

Figure 4-7: The effect of temperature on OCV. Symbols (a, b and c) denote uMgeni, uMzimkhulu and uMkomaas river, respectively.

This is because temperature affects the mobility of ions in rivers and seawater. As the temperature of water increases, its viscosity decreases, facilitating more effortless movement of ions. This is because high viscosity can impede the mobility of ions through a solution. Higher temperatures increase the kinetic energy of the ions, allowing them to move more freely through the IEMs and the waters. This phenomenon results from the increased thermal energy associated with higher temperatures. Their thermal motion drives the movement of ions in water. At higher temperatures, the ions have more energy, and this increased energy causes them to move faster and diffuse more readily. This is commonly observed in the context of ionic conductivity, where the electrical conductivity of water increases with temperature due to the greater mobility of ions. Benneker *et al.,* (2018a) reported an increase in conductivity of approximately 27% when the temperature was increased from 20 to 40 °C.

The increased mobility results in higher OCV and power density as ions move easily between the electrodes, reducing internal resistance. Increasing the temperature of the river and seawater can also lead to heat being transferred to adjacent electrode compartments. This leads to the electrode rinse gaining heat, affecting the electrochemical reactions at the electrode. Electrode kinetics, the rate and mechanisms of electrochemical reactions that occur at the surface of electrodes, generally improve with increasing temperature, meaning that the electrochemical reactions occur more rapidly and efficiently. This can result in higher power output from the RED stack. Additionally, at higher temperatures, the electrochemical reactions at the electrodes can have lower activation energy, meaning they occur more readily (Vyazovkin, 2020). This leads to a more efficient conversion of the ionic potential energy into electrical energy, resulting in a higher OCV.

The relationship between OCV and internal resistance is crucial in determining power density (see Eq. 3.1). When internal resistance is reduced and OCV increases, there is a corresponding boost in power density. As temperature rises, OCV, found in the numerator of the equation, increases. Simultaneously, internal resistance in the denominator decreases with a rise in temperature. Consequently, it is anticipated that power density will increase with higher temperatures.

Dlugolecki *et al.,* (2009) conducted a study that quantified the contribution of concentration polarization phenomena and resistance of the RED stack under different hydrodynamic conditions. In the study, an increase in temperature from 10 to 40 ℃ increased power density. Furthermore, Mehdizadeh *et al*., (2019) evaluated the effect of the feed solution temperature on the RED performance. The study revealed that at the highest temperature, 35 ℃, the stack generated the highest power of 0.57 W/m^2.

Figure 4-7(a) shows that the highest OCV of 4.64 V was observed at the highest temperature (40 ℃), while the lowest OCV of 3.313 V was recorded at the lowest temperature (25 ℃). This is consistent with what other researchers have found, namely, that the highest power density values of the systems are measured at higher temperatures (Daniilidis *et al.*, 2014; Guo *et al.*, 2018; Mehdizadeh *et al.*, 2019).

In all experimental cases, the observed order of performance for OCV among the rivers was uMgeni > uMzimkhulu > uMkomaas, as seen in **Table *4-4***. However, when considering power

density, the results were mixed. This variation can be attributed to internal resistance being inversely proportional to power density (see Eq. 3.1).

Table 4-4: OCV values for the study.

Temperature (°C)	uMgeni (W/m^2)	uMzimkhulu (W/m^2)	uMkomaas (W/m^2)	Flowrate (mL/min)
25	4,239	3,632	3,553	1370
35	4,5	3,711	3,605	1370
40	4,64	3,923	3,775	1550
30	4,18	3,649	3,498	950
25	4,336	3,638	3,535	1550
30	4,194	3,606	3,454	900
40	4,428	3,827	3,722	1370
35	4,235	3,702	3,56	950
30	4,285	3,609	3,502	1370
25	4,385	3,518	3,313	900
35	4,448	3,747	3,61	1550
40	4,327	3,792	3,564	900
25	4,207	3,569	3,362	950
40	4,401	3,739	3,607	950
30	4,341	3,646	3,535	1550
35	4,218	3,582	3,395	900

4.2.1.2. Power density

Figure *4-8* shows that an increase in temperature of a certain magnitude does not proportionally translate into an equal percentage increase in power density.

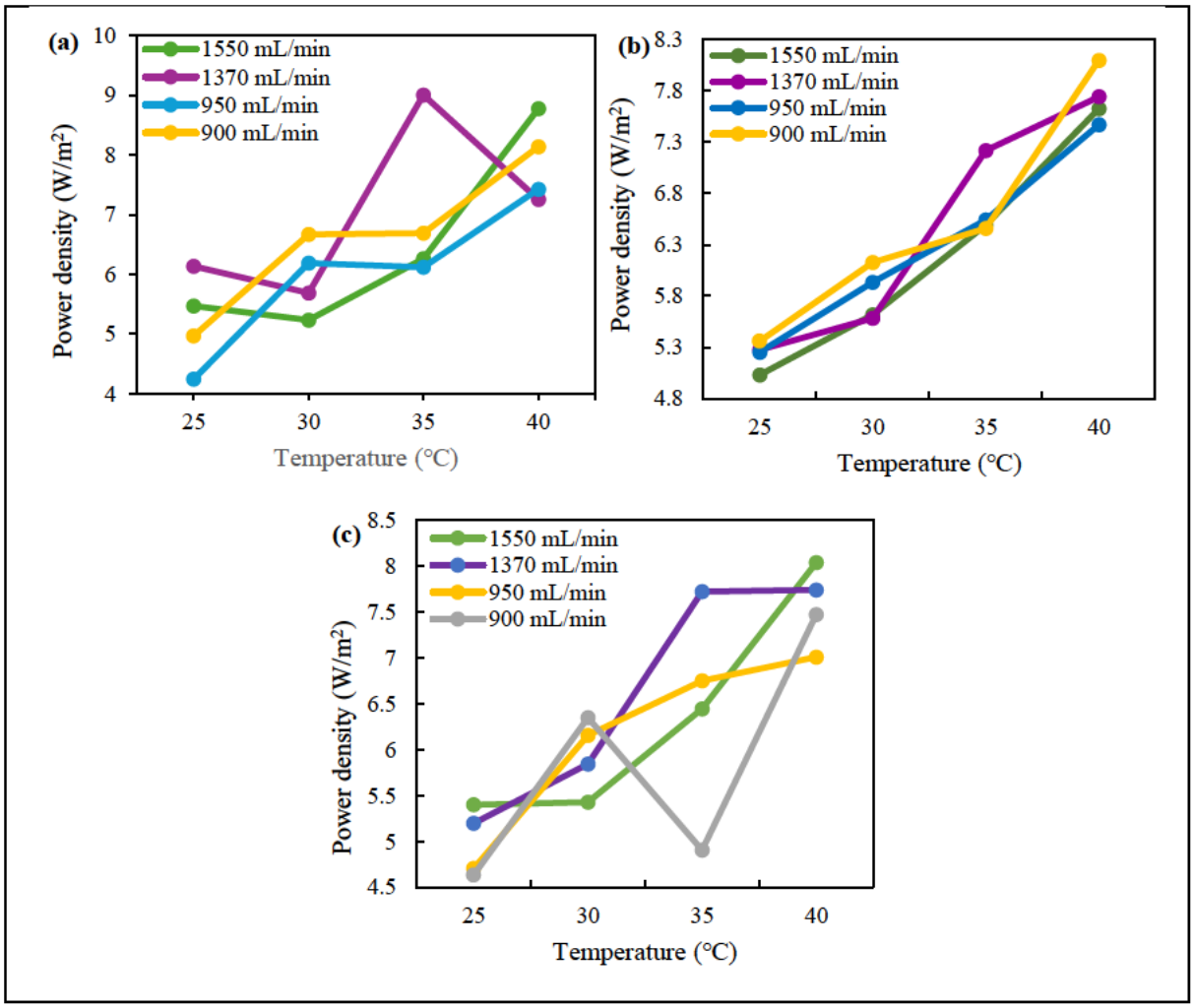

Figure 4-8: The effect of temperature on power density. Symbols (a, b and c) denote uMgeni, uMzimkhulu and uMkomaas river, respectively.

The most significant percentage increase in power density observed was 60.3%, occurring between 25 and 40 °C at a flow rate of 1370 mL/min, as depicted in **Figure 4-8**(a). Within the 25–30 °C temperature range, the data does not indicate the relationship between temperature increase and power density or OCV increase. However, in the 35–40 °C range, power density and OCV consistently increase with temperature. This observed phenomenon may be attributed to the low ion mobility at 25–30 °C compared to 35–40 °C, and at higher temperatures, feed waters can effectively transfer heat to the adjacent electrode compartment. Additionally, the conductivity is higher in the 35–40 °C range compared to the 25–30 °C range. It is worth noting that a temperature limit exists for operating the RED stack. **Table B-** outlines the maximum temperature allowed for the membranes in the stack used in this study.

Heating the feed solution requires energy, and the associated costs highlight the need to integrate RED technology with other technologies to maximize efficiency. Numerous studies have explored the integration of RED to heat the feed solution (Luo *et al.*, 2012; Olkis *et al.*,

2018; Giacalone *et al.*, 2019; Ortega-Delgado *et al.*, 2019). This integration is crucial for optimizing energy utilization and improving the performance of the RED stack. By leveraging synergies with complementary technologies, such as waste heat recovery or solar energy, the aim is to mitigate the energy consumption associated with heating the feed solutions.

4.2.1.3. Internal resistance

Internal resistance in the RED stack represents the opposition to the flow of electrical current within the stack. This resistance is primarily due to factors such as the ion exchange membranes, the river water and seawater, and the resistance at the electrode compartment. Higher internal resistance results in more voltage drop and power loss within the stack.

Increasing the temperature of the feed led to a decrease in internal resistance, as shown by **Figure 4-9**(a to c).

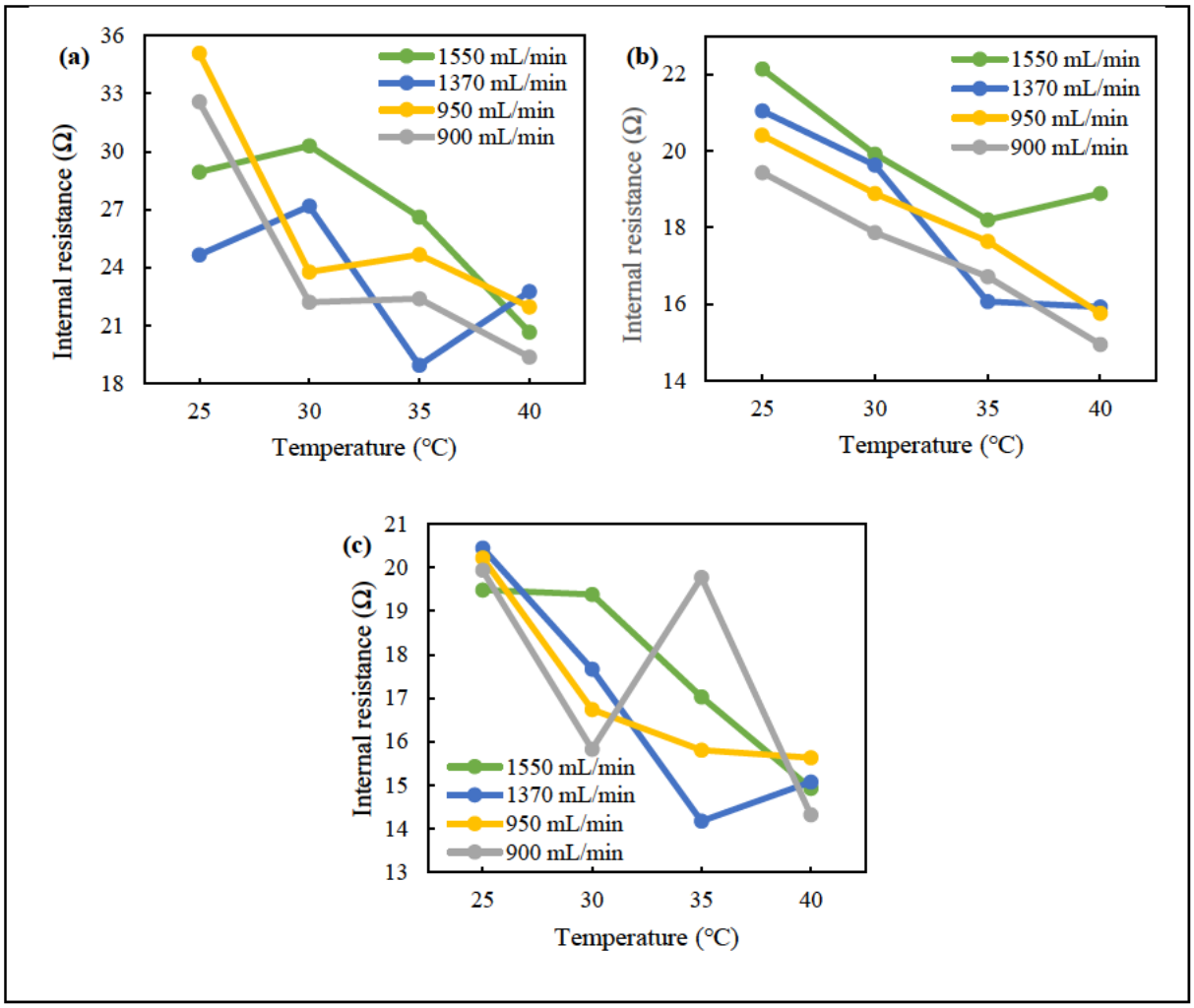

Figure 4-9: The effect of temperature on internal resistance. Symbols (a, b and c) denote uMgeni, uMzimkhulu and uMkomaas river, respectively.

This agrees with the existing literature (Tedesco *et al.*, 2015; Moya, 2016; Mehdizadeh *et al.*, 2019; Elmakki *et al.*, 2023). Guo *et al*., (2018) used different aqueous solutions as feed at 10, 25 and 40 °C. The study showed that the internal resistance decreased with the increase in the feed temperature. When the temperature was raised from 10 to 40 °C, the internal resistance was reduced from 6.11 to 4.42 Ω. Furthermore, Cui *et al*., (2022) observed that the internal resistance decreased from 9.23 to 6.06 Ω when the temperature was increased. Additionally, Michal *et al*. (2018) noticed a significant reduction in the internal resistance of up to 45% from 78.8 to 43.2 Ω of cm^2/cell when the feed temperature increased from 15 to 35 °C. Avci *et al*., (2018) reported a 13% and 44% reduction of internal resistance for natural and artificial solutions when the temperature was raised from 20 to 60 °C.

As the temperature increases, the kinetic energy of the ions in the solution also increases. This higher thermal energy enables ions to move more rapidly through the solutions and the ion-

exchange membranes. Faster ion mobility means ions can migrate more easily through the membranes, reducing the resistance encountered during their passage. This increased ionic mobility contributes to lower internal resistance.

Moreover, temperature directly affects the viscosity of the feed solutions. Higher temperatures result in lower viscosity. Reduced viscosity means that the solutions flow more smoothly and easily through the RED stack, creating less resistance to ion transport. Lower resistance within the solution itself leads to lower internal resistance overall. Another reason is that temperature influences the mass transfer rate at the membrane–solution interfaces. At higher temperatures, ions' diffusion rate toward and away from the membrane surfaces is typically faster. This improved mass transfer helps maintain higher ion concentration gradients near the membrane interfaces, reducing concentration polarization and the associated resistance.

Temperature significantly affects the thickness of the DBL. As temperature increases, the thickness of the DBL decreases (Zhang *et al.*, 2016). This is attributed to the stronger screening effect of electrical attractions between fixed charge groups and ions in the bulk solution, resulting from increased ion mobility. Furthermore, increasing temperatures inside the stack causes the ionic conductivity of the river and seawater and the conductivity of the membrane to increase, which in turn leads to a decrease in internal resistance.

The lowest internal resistances of 14.17 and 14.31 Ω were measured at the highest temperatures, as depicted in **Figure 4-9** (c), utilizing the uMkomaas River. This aligns with the reported relationships in previous studies by other researchers. When used as the feed for the stack, the uMkomaas River exhibited lower internal resistances compared to other rivers, as seen in **Figure 4-9**(c). This pattern was observed in 87% of the instances. This correlation could be attributed to the higher conductivity of uMkomaas water, signifying its enhanced ability to carry an electric charge. While higher conductivity is generally advantageous, it is crucial to note that extremely high concentrations of ions can pose challenges in ion transport through IEMs (Fan and Yin, 2019). Such high concentrations may lead to increased internal resistance, as extreme levels can decrease the permselectivity of the membranes, thereby affecting the OCV that can be generated.

4.2.2. The effect of flowrate on….

4.2.2.1. Internal resistance

This study had no conclusive relationship between flow rate and internal resistance. This might be because the flow rates were too high for the membranes. Higher flow rates can help reduce concentration polarization. However, excessively high flow rates might disrupt the balance of the membranes, leading to uneven ion distribution and local stagnant zones in channels when ions travel through the membranes (Pawlowski *et al.*, 2017). Excessive flow rate means that the rate at which the feed solutions flow through the RED stack exceeds what is optimal for the system. Excessively high flow rates can disrupt this balance by introducing challenges the membranes may struggle to handle. The disruption in membrane balance can result in uneven ion distribution across the membranes. Normally, ions should be evenly distributed for efficient ion transport. As ions travel through the membranes, any balance or uneven distribution disruption can affect how effectively the ions move. Some regions of the membrane may experience higher concentrations of ions, while others may have lower concentrations. Maintaining an optimal flow rate is crucial for efficiently operating a RED stack, ensuring uniform ion distribution and minimizing disruptions to the membrane balance.

Another potential factor contributing to the inconsistency in results could be variations in the tightness of closing the stack. Upon minimising fouling, the stack was opened multiple times for cleaning during the experiments. Opening the stack allows for maintenance activities but can introduce variability in how well the stack is sealed when it is closed again. These variations could contribute to the inconsistency observed in the experimental results. Internal resistance may be more sensitive to external influences on the stack, and any changes in these influences can significantly impact internal resistance more than OCV.

Temperature plays a crucial role in ion mobility; even a slight temperature variation can result in a noticeable change in internal resistance. For instance, if the water bath temperature is set at 30 ℃ but deviates to 31 ℃, this deviation might contribute to internal resistance not aligning consistently with the expected values.

Figure *4-10*(b) shows an increase in internal resistance when the flow rate was increased, which is opposite to what was expected.

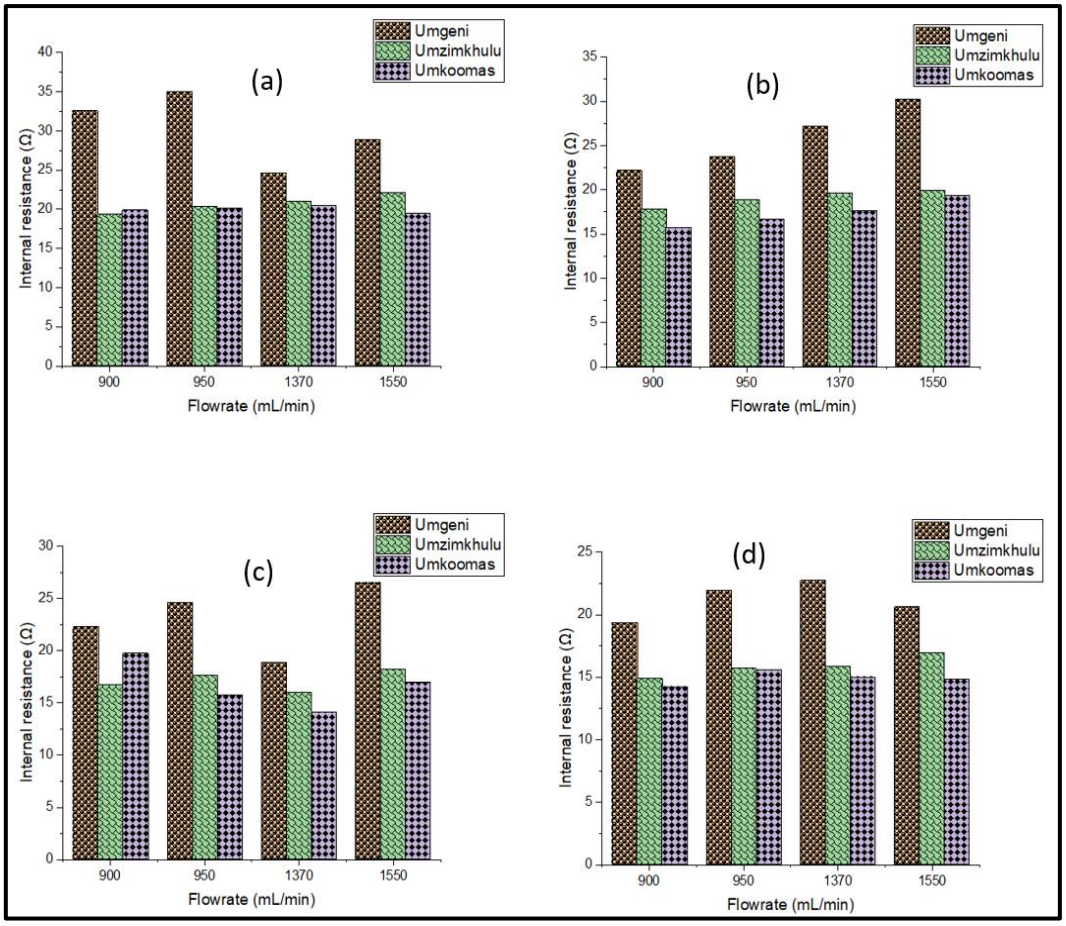

Figure 4-10: The effect of flow rate on internal resistance at varying temperatures. Symbols (a, b and c) denote 25, 30, 35 and 40 °C, respectively.

The reason for this might be that natural waters contain multivalent ions. Fouling occurs over time. Fouling occurs more easily when the feed solution has multivalent ions. The fouling of the membranes hinders ion transportation, causing an increase in internal resistance. Additionally, with membrane fouling, permselectivity decreases, allowing ions to pass through the membrane less freely.

Most researchers found that flowrate of the feed solutions has an inverse relationship with internal resistance (Długoł *et al.*, 2010; Avci *et al.*, 2018; Ortiz-imedio *et al.*, 2019; Membranes *et al.*, 2021; Elmakki *et al.*, 2023). It is evident that when the stack operated with uMgeni River water as the feed solution, it consistently exhibited higher internal resistance across all investigated cases. Conversely, uMkomaas River water generally demonstrated the lowest internal resistance in most instances. This is because, amongst the three river waters, uMgeni had the lowest conductivity while uMkomaas had the highest conductivity.

In **Figure *4-10***(a), when the flow rate was set to 950 mL/min, the internal resistance of uMgeni water was 42% higher than that of uMzimkhulu water. Water conductivity measures its ability to conduct electric current, and the presence of ions influences it. The presence of ions in water facilitates the flow of electric charge. The conductivity of water is directly influenced by the concentration of ions in the water. The more ions present, the higher the water conductivity, which, in turn, lowers the internal resistance. Water conductivity influences the rate at which concentration polarization develops. Higher water conductivity may mitigate the effects of concentration polarization, helping to maintain lower internal resistance.

Literature has shown that resistance is mainly determined by the lower concentration compartment (Galama *et al.*, 2014; Pawlowski *et al.*, 2017; Tristán *et al.*, 2020; Li *et al.*, 2022). This is because the salt concentration near the membrane surface is lower than in the bulk on the concentrated compartment side, and higher near the membrane than in the diluted bulk on the opposite side. Dlugolecki *et al*., (2008) highlighted that power density is predominantly determined by the resistance of the less concentrated solution compartment and remains independent of membrane properties. Furthermore, Rijnaarts *et al*., (2017) observed that resistances in the seawater compartment contribute relatively little, owing to a low AEM area resistance (1.0 $\Omega.cm^2$). Conversely, the river water compartment accounted for most cell resistance due to its lower conductivity.

In **Figure *4-10***, the highest internal resistances (35.08 and 32.57 Ω) were observed at the lowest flow rates (900 and 950 mL/min). On the other hand, the lowest internal resistances were generally observed at the highest flow rate. This agrees with what other researchers have found (Długoł *et al.*, 2010; Avci *et al.*, 2018; Ortiz-imedio *et al.*, 2019; Membranes *et al.*, 2021; Elmakki *et al.*, 2023). Avci *et al*. (2018) observed that increasing the flow rate from 20 to 40 L/h resulted in a 42 and 36% reduction in internal resistances for natural and artificial solutions. Vermaas *et al*., (2011a) noted that, at lower flow rates, significant resistance is induced by the diffusive boundary layer near the membranes.

Lower internal resistance coincided with higher power density; on the other hand, higher internal resistance generally leads to reduced power density. This agrees with what other researchers found (Tedesco *et al.*, 2015; Ortiz-imedio *et al.*, 2019; Elmakki *et al.*, 2023). Internal resistance is the opposition to the flow of ions through the components of the RED stack. As electric current flows through the stack, it encounters resistance. This resistance leads to ohmic losses, where some electrical energy is converted into heat. This resistance results in

the reduction of voltage. The voltage generated by the RED stack is a crucial factor in determining power density. If a significant portion of the voltage is lost across internal resistance, the voltage available for power generation decreases. As the voltage for power generation decreases due to higher internal resistance, the overall power density is reduced. Instead, the electrical energy that could have been converted into useful power is dissipated as heat within the stack.

4.2.2.2. OCV

Figure *4-11* shows a direct relationship between the flow rate of the feed solutions and OCV. This agrees with what other researchers found (Długołe et al., 2009; Ashu *et al.*, 2015). Tufa *et al*., (2015) noted an increase in OCV of up to 35% (from 1.7 to 2.3 V) and a corresponding increase in power density of up to 47% (from 0.75 W/m² to 1.1 W/m²) with the flow rate raised from 0.7 cm/s to 1.1 cm/s. Additionally, Fu *et al*., (20 20) observed an OCV increase from 1.25 V to 1.39 V by raising the velocity from 0.24 cm/s to 1.19 cm/s.

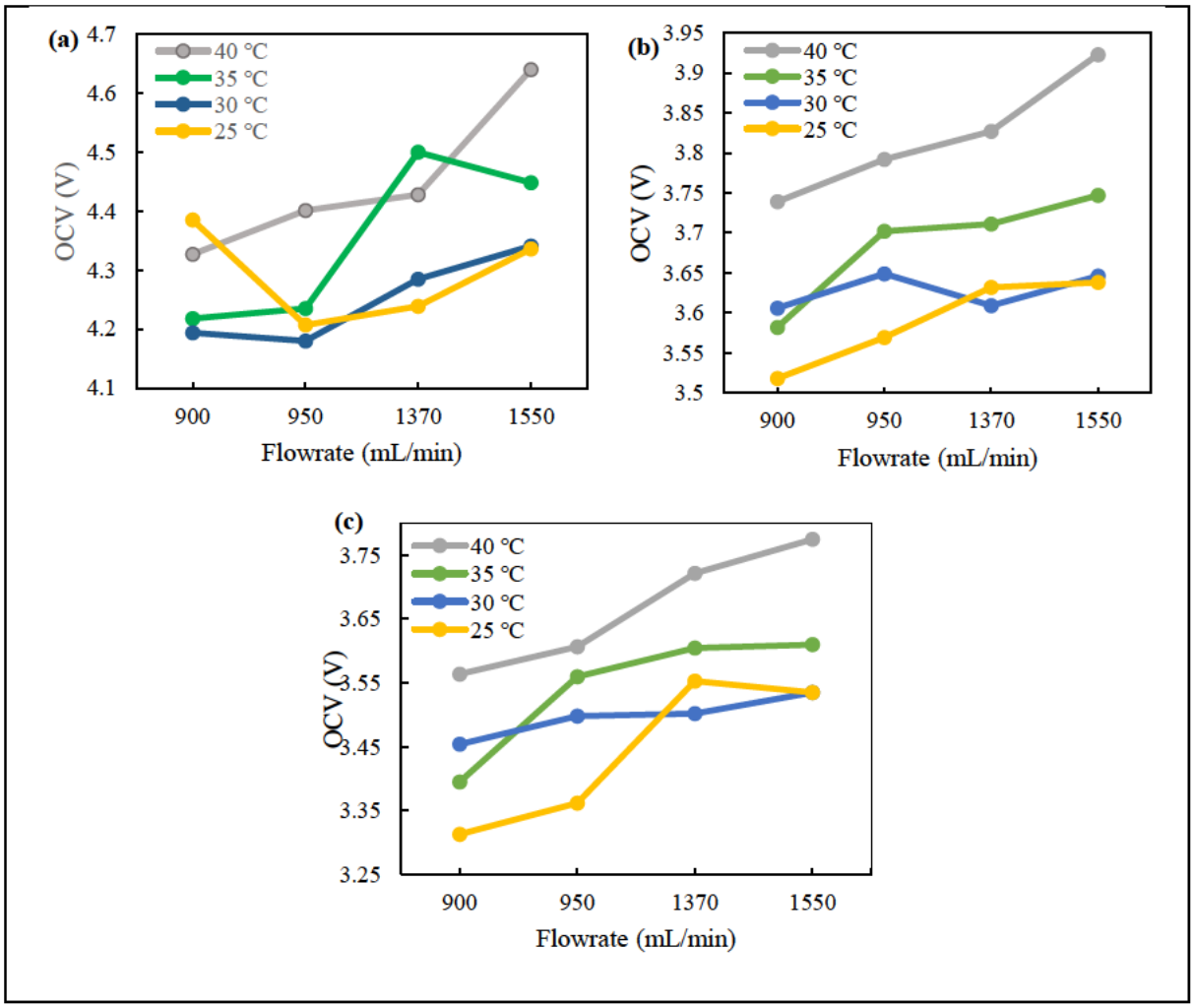

Figure 4-11: The effect of flow rate on OCV. Symbols (a, b and c) denote uMgeni, uMzimkhulu and uMkomaas river.

Increasing the flow rate enhances mass transfer rates and helps mitigate concentration polarization. The OCV increases because the ion exchange membrane maintains a large concentration gradient. Furthermore, increasing the flow rate promotes ions' movement within the feed solutions. With faster-moving ions, they can more readily cross the IEMs, leading to a higher OCV. Also, increasing feed flow rates in an RED system reduces the impact of ion diffusion on the salinity ratio, primarily due to the shorter residence time of the feed solutions within the RED stack. Increasing the feed flow rates makes the salinity ratio less affected by ion diffusion. This is because, with higher flow rates, there is less time for ions to diffuse across the membranes, and the concentration gradients are maintained more effectively.

Among the river water samples used, the highest measured values of OCV were consistently observed when using the uMgeni River sample, followed by the uMzimkhulu River and the uMkomaas River. This pattern was observed in all cases where OCV was measured. It should

be noted that uMgeni has the lowest conductivity among the three rivers. The OCV depends on a strong salinity gradient, which indicates a significant difference in ion concentration between the concentrated solution (seawater) and the low-concentration solution (river water) on either side of the ion exchange membranes. The highest salinity gradient observed between seawater and uMgeni River water explains why the uMgeni River consistently yielded the highest OCVs in all measured cases.

The highest observed OCV was 4.64 V, recorded with uMgeni water at a flow rate of 1550 mL/min, the highest flow rate during the experiments. Conversely, the lowest OCV measured was 3.313 V, observed with uMkomaas water at a 900 mL/min flow rate, corresponding to the lowest flow rate during the experiments. As anticipated, the trend aligns with previous discussions, indicating that higher flow rates of the feed solutions correlate with higher OCV, while lower flow rates exhibit the opposite effect. It is noteworthy that the uMkomaas River, characterized by the highest conductivity, yielded the lowest OCV, consistent with findings in the existing literature on the salinity gradient ratio effect on OCV (Vermaas et al., 2011b; Geise *et al.*, 2014; Ortiz-imedio *et al.*, 2019; Yasukawa *et al.*, 2020).

4.2.2.3. Power density

This study did not identify a clear relationship between flow rate and power density, as seen in **Figure 4-11**. This could be attributed to several contributing factors. Power density, being the product of OCV and internal resistance, is influenced by both. According to equation 3.1, the ideal condition for increasing power density involves increasing OCV while decreasing internal resistance. However, since internal resistance did not exhibit a linear relationship with flow rate in this study, a clearly defined relationship between power density and flow rate was not observed.

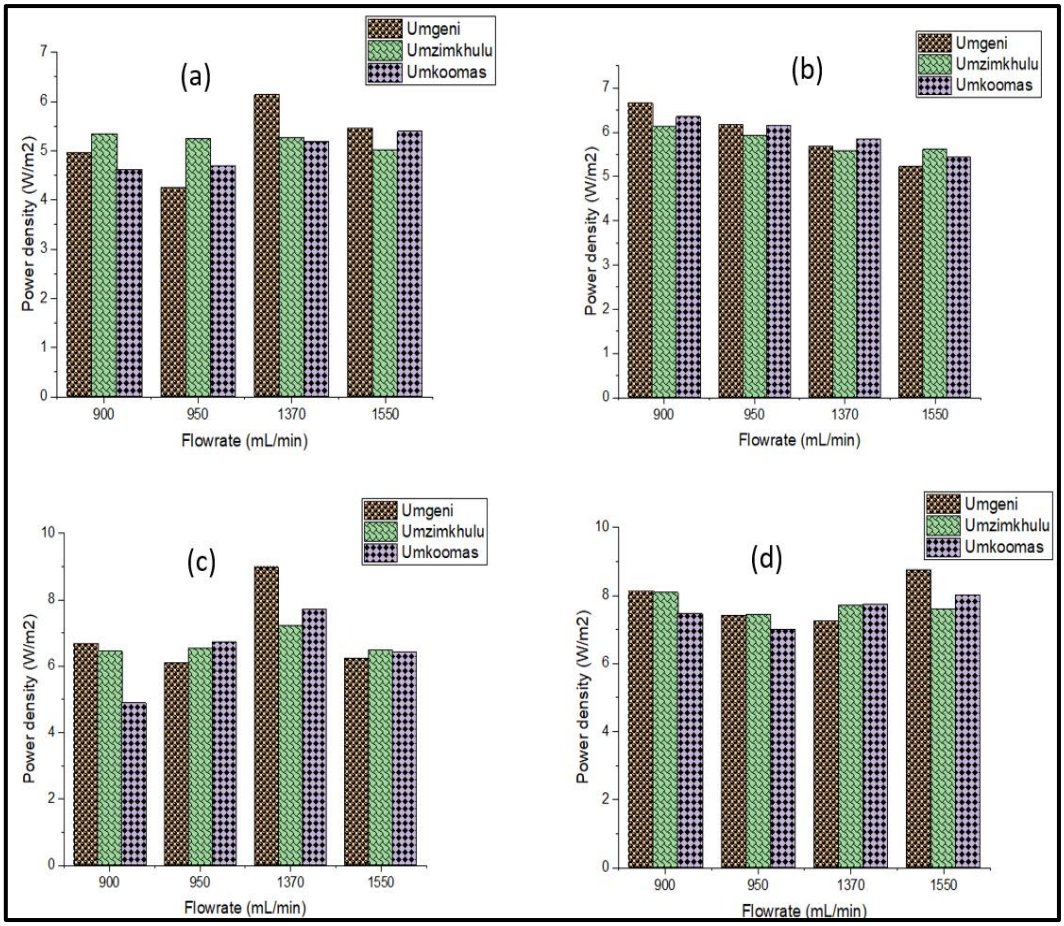

Figure 4-12: The effect of flow rate on power density at varying temperatures. Symbols (a, b, c and d) denote 25, 30, 35 and 40 ℃, respectively.

Among the three river samples, no distinct pattern in power density emerged due to variations in internal resistance. Although the uMgeni water sample exhibited superior results in OCV, a contributing factor to power density, the unpredictable relationship between internal resistance and river type prevented the establishment of a clear correlation between the type of river and power density.

Over time, fouling will occur at the electrodes. This fouling can cause variations in power output. Electrode fouling can significantly impact the reactions at the electrodes' surface. Fouling can physically cover a portion of the electrode surface, reducing the active surface area available for electrochemical reactions. This limits the sites where reactions occur, potentially decreasing the overall reaction rate. This fouling layer introduces additional resistance and hinders the transportation of reactants and products to and from the electrode surface, affecting the system's reaction rates, stability and efficiency.

Previous studies have reported a linear relationship between power density and flow rate (Turek *et al*., 2008; Długołe *et al*., 2009; Vermaas *et al.*, 2014; Hidayati *et al.*, 2022). Elmakki *et al*., (2023) investigated the effect of feed solution velocity on power density and found that when velocity was increased from 0.25 to 1.18 cm/s, the power density increased from 2.14 W/m^2 to 2.17 W/m^2, respectively. Furthermore, Tufa *et al*., (2018) explored the relationship between power generation in RED and flow velocity, showing a progressive increase in power density from 0.08 to 0.13 W/m^2 when the flow velocity was increased from 0.6 to 6.9 cm/s. Additionally, Tristán *et al*., (2020) observed an increase in gross power with the Reynolds number.

4.3. Performance evaluation between Natural and synthetic water

Table *4-5* presents measurements of synthetic and natural water samples under identical feed conditions with the same flow rate and temperature. The synthesized feed solution containing only NaCl had a comparable effect to natural solutions at the same flow rate and temperature. Surprisingly, the composition of the ERS played a more significant role than the type of feed solution. Whether using NaCl, KCl, Na_2SO_4, or the mixture as an ERS, the RED stack did not generate significantly more power output than using a mixture as an ERS with natural waters as the feed.

Table 4-5: Measured data from RED stack tests with temperature at ±25 ℃ and flow rate at 150 mL/min.

Feed type	ERS	Concentration	OCV (V)	Load voltage (V)	Power density (W/m^2)	Internal resistance (Ω)
NaCl	NaCl	5 g/L	4,156	0,431	3.579	40,620
		10 g/L	4,295	0,442	3.790	40,970
		20 g/L	2,09	0,333	1.483	24,798
		30 g/L	3,75	0,391	2.932	40,376
NaCl	Na_2SO_4	5 g/L	3,375	0,405	2.782	34,466
		10 g/L	3,036	0,389	2.426	31,981
		20 g/L	3,805	0,401	3.055	39,897
		30 g/L	2,922	0,38	2.286	31,440
NaCl	KCl	5 g/L	3,96	0,484	3.911	33,754
		10 g/L	2,97	0,432	2.689	27,612
		20 g/L	2,643	0,399	2.225	26,433
		30 g/L	3,4	0,54	3.909	24,892
NaCl	$K_3Fe(CN)_6$, $K_4Fe(CN)_6$, NaCl	0.05 M $K_3Fe(CN)_6$, 0.05 M $K_4Fe(CN)_6$, 2.5 M NaCl	4,354	0,715	3,662	23,920
		0.1 M $K_3Fe(CN)_6$, 0.1 M $K_4Fe(CN)_6$, 2.5 M NaCl	3,933	0.808	4,677	18,177
		0.2 M $K_3Fe(CN)_6$, 0.2 M $K_4Fe(CN)_6$, 2.5 M NaCl	3,672	0,81	4,700	16,606
		0.3 M $K_3Fe(CN)_6$, 0.3 M $K_4Fe(CN)_6$, 2.5 M NaCl	3,897	0,966	6,684	14,260
uMgeni		0.3 M $K_3Fe(CN)_6$, 0.3 M $K_4Fe(CN)_6$, 2.5 M NaCl	4,385	0,553	4.970	32,568
uMzimkhulu		0.3 M $K_3Fe(CN)_6$, 0.3 M $K_4Fe(CN)_6$, 2.5 M NaCl	3,518	0.685	5.360	19,438
uMkomaas		0.3 M $K_3Fe(CN)_6$, 0.3 M $K_4Fe(CN)_6$, 2.5 M NaCl	3,313	0,632	4.634	19,938

The highest power density recorded was 6.684 W/m^2, achieved with a synthetic feed solution and 0.3 M $K_3Fe(CN)_6$, 0.3 M $K_4Fe(CN)_6$, 2.5 M NaCl. This power density is 24.7% higher than

the best-performing river sample, specifically uMzimkhulu. Most researchers observed a reduction of more than 40% in power density when comparing synthesized solutions with natural solutions (Post *et al*., 2009; Tufa *et al.*, 2014; Vermaas et al., 2014; Avci *et al.*, 2016). Reducing internal resistance is crucial for increasing power output, and the highest power density is often associated with the lowest internal resistance. Avci *et al.,* (2018) observed that internal resistance was the dominant factor in power density.

The highest OCV recorded was 4.38 with the uMgeni River sample. However, in the overall analysis, when considering the electrode rinse solution with the mixture, OCV tended to be higher for synthesized solutions than for natural waters.

Natural waters contain multivalent ions, which can have a negative impact on power density. Their presence is known to contribute to an increase in internal resistance, which, in turn, negatively affects power density inside the stack. Additionally, due to their higher charge and stronger electrostatic interactions with other ions or molecules in the solution and on the membranes, multivalent ions are more prone to forming scale or precipitates in the feed solution, leading to fouling of the membranes. These ions carry a higher charge density than monovalent ions, making them more attractive to counterions and water molecules in the solution, further contributing to internal resistance. The literature reports evidence of the negative impact of multivalent ions on the RED stack. Divalent ions have a negative effect on the OCV, as Rijnaarts *et al.* (2017) demonstrated when investigating the effect of divalent cations ($Mg^{2+}$and Ca^{2+}) on RED. The study showed that when Mg^{2+} was present in the feed stream, the OCV decreased. This is caused by the uphill transport and decreased permselectivity when divalent ions exist (Moreno *et al.*, 2018). Tufa *et al.,* (2014) also observed a 63% (from 3.04 to 1.13 W/m^2) reduction in power density when Mg^{2+} was present. Additionally, Avci *et al*., (2018) investigated the energy that could be generated by mixing natural seawater and river water at different temperatures and flow rates. The study compared these results to those obtained using NaCl solutions with equivalent ionic strength. In their findings, total membrane resistances were higher when natural river water was used. This was because CEMs offered 5-6 times higher resistance than AEMs in seawater and river water. The explanation is that the affinity of fixed-charged groups of CEMs to Na^+ is lower than that of divalent ions, whereas, for AEMs, the affinity to Cl^- is higher than that of SO_4^{2-}. Additionally, non-Ohmic resistances on CEMs were higher than on AEMs because of the higher mobility of chlorine with sodium. This study revealed that using natural feeds significantly reduces the

performance of RED, because of the increased membrane resistance that leads to the reduction of OCV and the occurrence of uphill transport. Furthermore, the results indicated that a suitable pretreatment should be performed to soften the feed solution.

4.4. Potential sources of error and limitations

It is worth noting that this study does not encompass other renewable energy technologies, such as wind or solar power. Additionally, it does not extend its scope to the application of RED technology for purposes beyond electricity generation, keeping the research tightly focused. River water composition can fluctuate due to environmental factors such as weather, season, and upstream activity. Differences in ion concentration, organic content, and particulate matter can introduce variability into the results. Natural water sources often contain sediments or particulates that may clog the membranes, reducing system efficiency and altering results over time. Although filters help, they do not eliminate all the sediments or particulates. River water also contains various organic compounds and microorganisms, which contribute to membrane fouling. Scaling (mineral deposits) or fouling from river water samples could progressively impact performance and reduce ion exchange efficiency over time.

Regarding electrodes, changing the electrode rinse solution after a certain number of runs may result in cross-contamination between solutions, even with thorough rinsing. This can alter the conditions for subsequent runs. Moreover, different electrode rinse solutions can leave lingering effects on the electrodes, which may impact subsequent experiments, especially if rinsing procedures are not entirely consistent. Frequent solution changes may also accelerate electrode degradation, impacting performance and potentially skewing results.

Although a temperature control bath is used, small temperature variations could still occur, affecting ion transport across the membranes. Membranes may respond differently to slight temperature changes, which can further affect performance, particularly for ion exchange rates. Pumps may also introduce minor fluctuations in flow rates. Even small deviations from the set flow rate can influence ion transport rates and system efficiency.

Membrane degradation over multiple runs may alter the stack's efficiency, especially if membranes are not periodically replaced or cleaned. When reassembling the stack, any imperfections in the assembly or sealing could cause leaks or internal mixing of the feed

streams, leading to inaccurate power measurements. Lastly, the electricity consumed by the pumps was not factored into this study.

4.5. Summary

Four electrode rinse solutions were compared: NaCl, KCl, Na_2SO_4, and a mixture containing $K_3Fe(CN)_6$, $K_4Fe(CN)_6$ and NaCl. The comparison criteria included ERS concentration, flow rate, and composition. Among the three solutions excluding the redox mixture, NaCl exhibited the highest OCV measurements. However, overall performance, particularly regarding OCV and power density, was superior in the mixture. It was observed that both ERS composition and flow rate influenced the RED system's performance, but no linear relationship was identified between ERS concentration and system performance.

Regarding the three river samples used as feed solutions, uMgeni displayed the highest OCV measurements, which is attributed to a greater salinity difference between uMgeni and seawater unlike the other two rivers. However, uMgeni also exhibited the highest internal resistance among the three river samples, negatively impacting power density. The temperature had the most effect on OCV and power density. Increasing the temperature led to an increase in OCV and power density in all cases. However, it is important to note that while higher temperatures generally positively impact power output, there can be practical limits and trade-offs. Material stability, membrane durability, and the cost of maintaining elevated temperatures must be considered when operating the RED system.

The pH of the ERS remained within the range of 6.4 – 8.1 throughout the experimentation period. Similarly, the pH ranged from 6.1 to 9.5 for the feed solutions. These values align with the RED stack manufacturer's specifications (see **Table B-**), ensuring that they fall within the acceptable limits for the stack.

CHAPTER 5: Optimization

The main purpose of optimization was to establish the optimal operating conditions where the system can be operated with optimal power for a given flowrate and temperature. The OFAT technique was employed to determine the runs. Data gathered from those runs were than imported to the Design expert software under historical data. The software used that data as the basis for calculations. The optimization process employed a numerical method to improve two crucial operating parameters: the temperature and flow rate of the feed solution. By systematically exploring the entire design space using tailored models, this approach identified optimal conditions for each variable within the defined range (Almeida *et al.*, 2008; Mehmood *et al.*, 2018). The uMkomaas river sample was selected as the less concentrated feed solution due to consistent low internal resistances of the stack when it was used compared to the other two river samples.

The lack of correlation between the measured variables is depicted in **Figure *5-1***.

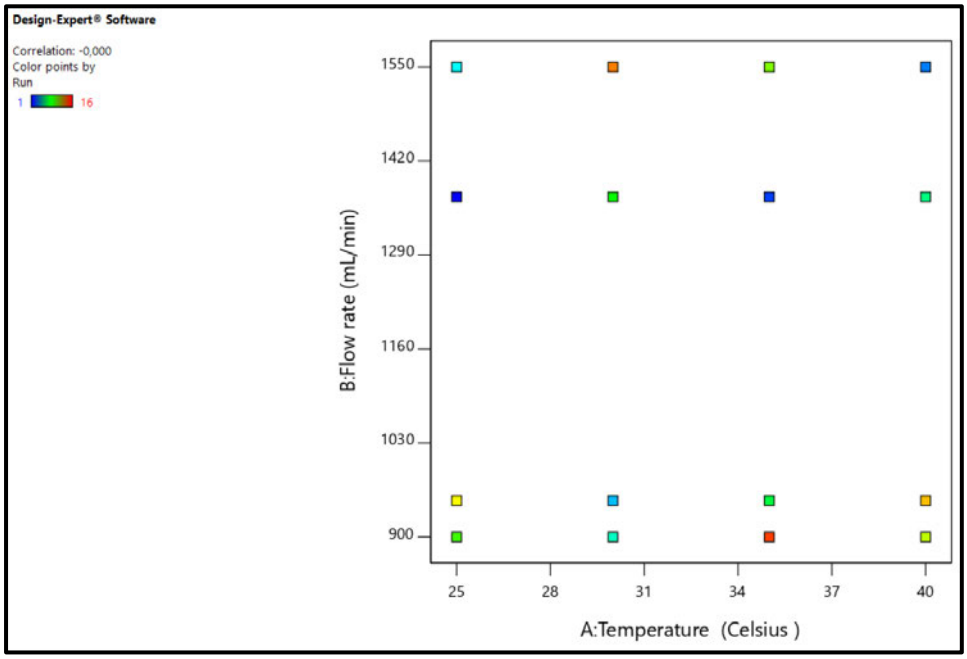

Figure 5-1: **Correlation plot illustrating relationships between variables and runs.**

This absence of correlation is particularly crucial when optimizing using software, especially in the realm of experimental design and statistical analysis (Hooda *et al.*, 2012). Uncorrelated variables are highly valued in this context because they simplify the interpretation of results. In the optimization process, correlated variables can introduce complexity, making it challenging to attribute changes in the response variable to specific factors. When variables are

entangled due to correlation, the effects of each variable become difficult to isolate. This complexity hinders the efficiency of experimentation and the precise understanding of variable impacts, especially in the design of experiments (DOE) (Akram and Garud, 2021).

The correlation of 0 between temperature and flowrate as observed in **Figure *5-1*** is desirable. In DOE, where various combinations of variable settings are tested, uncorrelated variables facilitate the isolation of individual variable effects, leading to a more accurate comprehension of their impact (Mehmood *et al.*, 2018). Moreover, correlated variables may introduce redundancy in the information they provide (Ba and Boyaci, 2007). Highly correlated variables often convey similar information, and including both in the optimization process may not yield additional insights. Models developed with correlated variables may struggle to generalize well to new data or conditions (Kumle *et al.*, 2021). On the other hand, uncorrelated variables contribute to the construction of a more reliable and robust model that can be applied to a broader range of scenarios. This is essential for ensuring that the model's applicability extends beyond the specific conditions under which it is developed (AKOSSOU, 2013; Karch, 2020).

Figure 5-2 and **Figure 5-3** shows that a ratio of maximum to minimum is 1.13945 for OCV and 1.43038 for VUL, respectively.

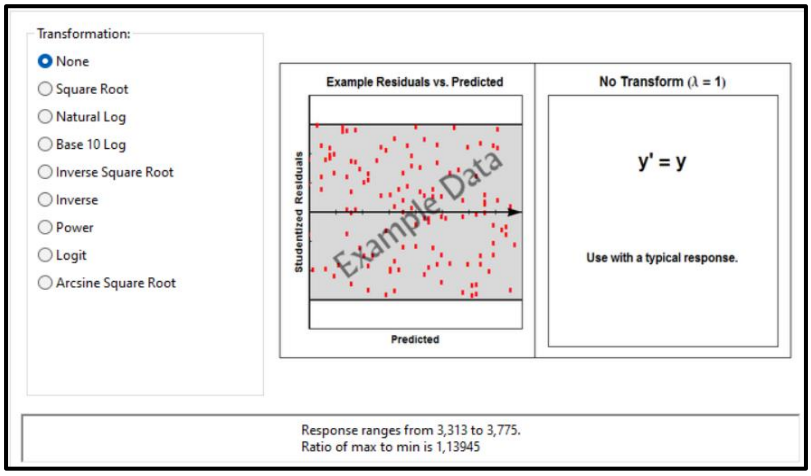

Figure 5-2: Level of transformation signal for OCV.

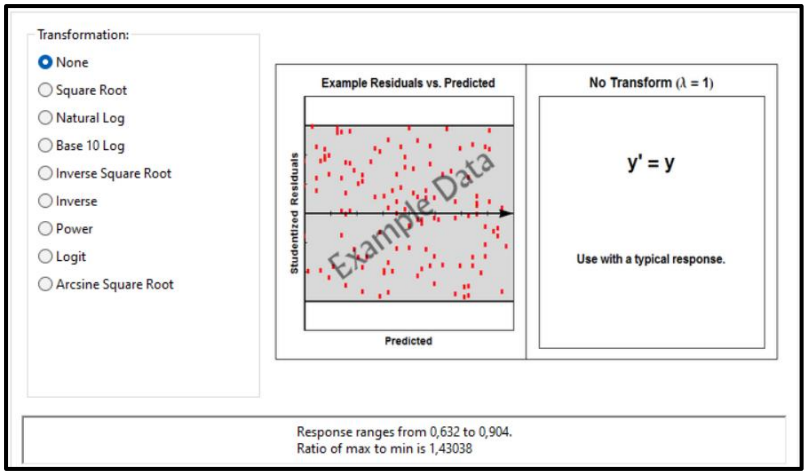

Figure 5-3: Level of transformation signal for VUL.

This implies that the data feed to the software is homoscedastic (Djalic and Terzic, 2021). A ratio greater than 10 usually indicates a transformation is required because the data is heteroscedastic. For ratios less than 3 the power transforms have little effect. The idea behind power transformations is to apply a mathematical function to the data that helps make the variance more constant across different levels (StatEase, 2023c).

5.1. Exploring ANOVA Techniques for Performance Analysis

In **Table *5-1*** and **Table 5-2**, the F-value of 13.37 and 10.22 implies the model is significant.

Table 5-1: **Response data for OCV**

Source	Sum of Squares	df	Mean Square	F-value	p-value
Model	**0.1895**	**5**	**0.0379**	**13.37**	**0.0004**
A-Temperature	0.1033	1	0.1033	36.43	0.0001
B-Flow rate	0.0663	1	0.0663	23.37	0.0007
AB	2.353E-06	1	2.353E-06	0.0008	0.9776
A^2	0.0046	1	0.0046	1.63	0.2304
B^2	0.0039	1	0.0039	1.38	0.2668
Residual	0.0369	10	0.0028		
Cor Total	0.2178	15			

Table 5-2: Response data for VUL

Source	Sum of Squares	df	Mean Square	F-value	p-value
Model	**0.1032**	**3**	**0.0344**	**10.22**	**0.0013**
A-Temperature	0.1006	1	0.1006	29.91	0.0001
B-Flow rate	0.0025	1	0.0025	0.7443	0.4052
AB	0.0010	1	0.0010	0.2863	0.6024
Residual	0.0404	12	0.0034		
Cor Total	0.1435	15			

This suggests that the model is providing useful information in explaining the variation in the response variable (Li *et al.*, 2016). For the optimized model in Design Expert, the p-value associated with each factor was calculated by the software. Factors with p-values below the 0.05 significance level were deemed statistically significant, providing evidence against the null hypothesis and highlighting their importance in influencing the response variable (Kumle *et al*., 2021).

In **Table 5-3** and **Table 5-4**, a standard deviation of 0.0533 and 0.564, respectively, is observed, which is highly favourable for the model.

Table 5-3: Fit statistics for OCV.

Standard deviation	0.0532	**R^2**	0.8699
Mean	3.54	**Adjusted R^2**	0.8048
C.V.%	1.51	**Predicted R^2**	0.6944
		Adequate Precision	11.4133

Table 5-4: Fit statistics for VUL.

Standard deviation	0.0580	**R^2**	0.7187
Mean	0.7657	**Adjusted R^2**	0.6484
C.V.%	7.57	**Predicted R^2**	0.5802
		Adequate Precision	8.4055

This value signifies a strong fit for the data and is indicative of the model's reliability and precision. Standard deviation refers to the standard deviation of the residuals in the context of regression analysis (Popoola, 2019). Residuals are the differences between the observed values and the values predicted by the regression model (Laanaya *et al*., 2017). They represent the

unexplained variation in the data. The standard deviation of the residuals is a measure of how spread out or dispersed the residuals are around the fitted values from the regression model. It provides an indication of the variability or randomness in the unexplained portion of the data.

A small standard deviation of residuals like in our case, suggests that the model's predictions are relatively consistent and close to the observed values. On the other hand, a larger standard deviation indicates greater variability in the residuals, implying that the model may not be capturing all the patterns in the data.

Adequate precision measures the signal to noise ratio (Hooda *et al.*, 2012). A ratio greater than 4 is desirable. A ratio of 11.4133 and 8.4055 as shown by **Table 5-3** and **Table 5-4** indicates an adequate signal which can be used to navigate the design space.

Coefficient of Variation as a Percentage (C.V.%) is a statistical measure that expresses the relative variability of a set of data points (Reed *et al*., 2002). It is often expressed as a percentage and is calculated as standard deviation divided by mean multiplied by 100. A C.V.% of 1.51 and 7.57 is very desirable. A small C.V.% indicates that the variability in the data is relatively low compared to the mean. This suggests that the data points are more tightly clustered around the mean, indicating greater consistency and stability (Reed *et al*., 2002).

In **Table 5-3**, the Predicted R^2 value of 0.6944 shows reasonable agreement with the Adjusted R^2 value of 0.8048, with a difference of less than 0.2. Similarly, in **Table 5-4**, the Predicted R^2 value of 0.5802 exhibits reasonable agreement with the Adjusted R^2 value of 0.6484, with a difference of less than 0.2. The software suggested the linear model since it’s maximized the Adjusted R^2 and the Predicted R^2 more than the other models. Adjusted R^2 and predicted R^2 are related but serve different purposes in the context of regression analysis. Adjusted R^2 is a modification of the regular R^2 that adjusts for the number of predictors in the model (Karch, 2020). It penalizes the use of additional predictors that do not significantly contribute to explaining the variance in the response variable. On the other hands, Predicted R^2 assesses the predictive performance of the model. It evaluates how well the model predicts new, unseen data. Higher predicted R^2 values suggest that the model is expected to perform well on new observations (AKOSSOU, 2013). It is particularly relevant when the goal is to assess the model's ability to make accurate predictions beyond the data used to train it. R is the correlation coefficient measuring the linear relationship between predictor and response variables (Karch, 2020).

In **Table 5-5** and **Table 5-6**, the coefficient estimate represents the expected change in response per unit change in factor value when all remaining factors are held constant (Grace and Bollen, 2005).

Table 5-5: Coefficients in terms of coded factors for OCV.

Factor	Coefficient Estimate	df	Standard Error	95% CI Low	95% CI High	VIF
Intercept	3.56	1	0.0368	3.48	3.64	
A-Temperature	0.1085	1	0.0180	0.0685	0.1486	1.01
B-Flow rate	0.0775	1	0.0160	0.0418	0.1132	1.04
AB	-0.0006	1	0.0211	-0.0475	0.0463	1.01
A^2	0.0382	1	0.0299	-0.0285	0.1050	1.0000
B^2	-0.0489	1	0.0416	-0.1415	0.0437	1.04

Table 5-6: Coefficients in terms of coded factors for VUL.

Factor	Coefficient Estimate	df	Standard Error	95% CI Low	95% CI High	VIF
Intercept	0.7672	1	0.0146	0.7354	0.7990	
A-Temperature	0.1071	1	0.0196	0.0644	0.1498	1.01
B-Flow rate	0.0148	1	0.0171	-0.0225	0.0520	1.0000
AB	0.0123	1	0.0229	-0.0377	0.0623	1.01

The intercept in an orthogonal design is the overall average response of all the runs. The coefficients are adjustments around that average based on the factor settings. When the factors orthogonal the VIFs are 1: VIFs greater than 1 indicate multi-collinearity, the higher the VIF the severe the correlation of the factors. VIFs less than 10 are preferred.

Figure 5-4 Shows that the residuals are approximately normally distributed, and the model is capturing the underlying patterns in the data well.

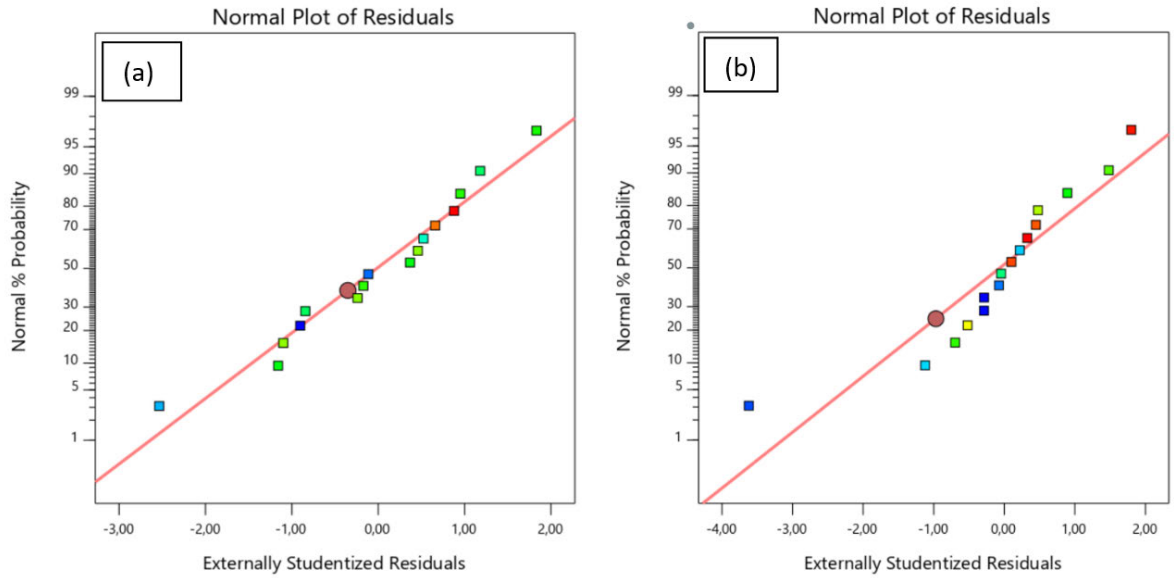

Figure 5-4: The Normal % Probability Residual plots for the responses (a) OCV (b) VUL

The Normal % Probability Residual plot assesses whether the residuals follow a normal distribution (Shepherd, 2020). If the points closely follow the 45-degree line, it indicates that the residuals are behaving in a manner consistent with a normal distribution and are well fitted (Tetteh, 2018). This implies that the model is effectively capturing the variance in the data, and the residuals exhibit a pattern that is expected under the assumptions of a linear regression model.

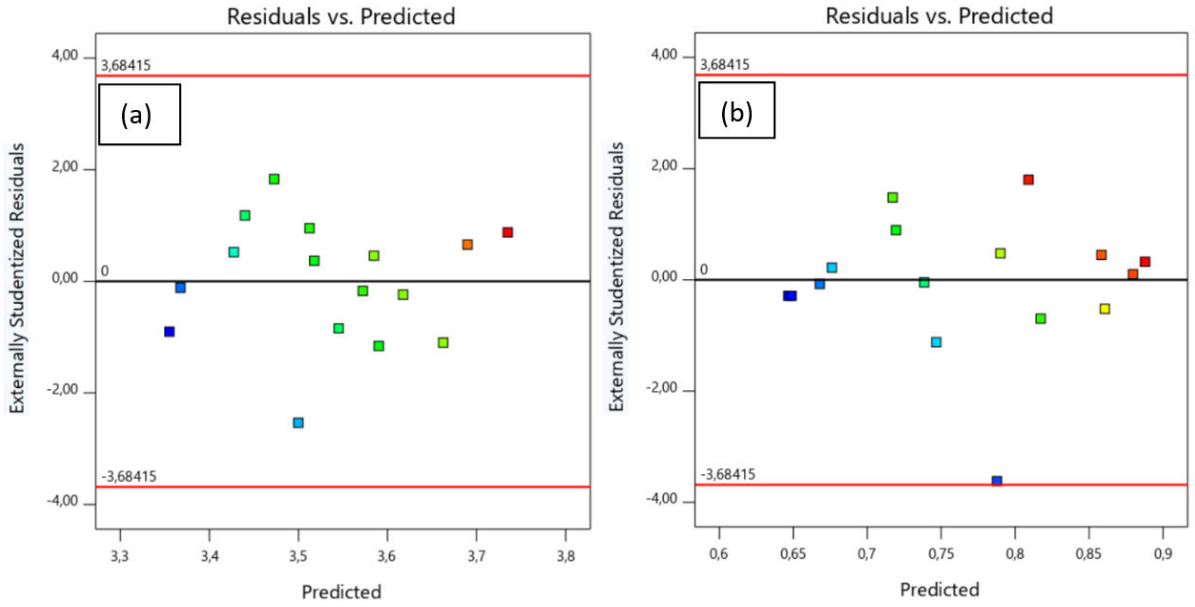

Figure 5-5: Residual plots for the responses (a) OCV (b) VUL

Residual plots represent the differences between the observed (inputted) values and the values predicted by the model. These differences, or residuals, are calculated by subtracting the predicted values from the actual observed values (Tetteh, 2018). This plot is useful for checking the homoscedasticity, which means that the variance of the residuals is constant across all levels of the predicted values. **Figure 5-5** shows that the point are scatters with no discernible pattern. This is a great sign that the model is homoscedastic.

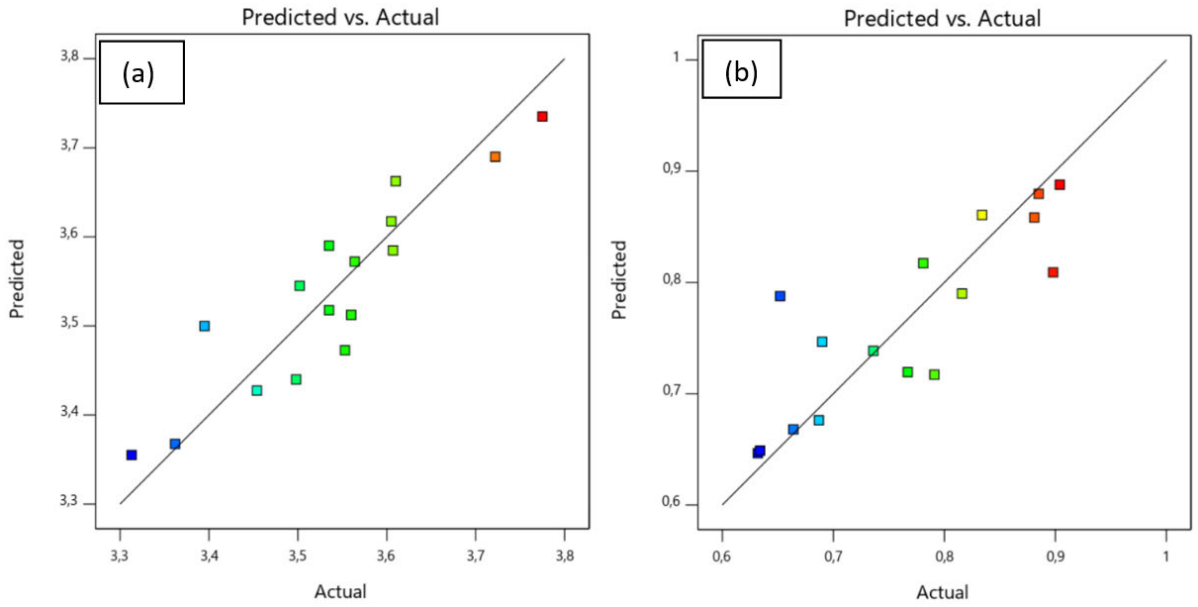

Figure 5-6: Predicted vs. Actual plot for the responses (a) OCV (b) VUL

Predicted vs. Actual plot assess how well a model's predictions align with the actual observed values (Ghafari *et al.*, 2009; Tetteh, 2018). **Figure 5-6** shows that most data points closely align with the 45-degree line in the Predicted vs. Actual plot, indicating a strong agreement between predicted and actual values. However, some deviation from the ideal line is observed. This discrepancy can be attributed to the use of historical data obtained through an OFAT method (StatEase, 2023b). The ideal scenario is a perfect 45-degree line where predicted values equal actual values. This line represents a perfect prediction. The closer the points are to the 45-degree line, the better the model's predictions align with the actual values. Deviations from the line indicate discrepancies between predicted and actual values.

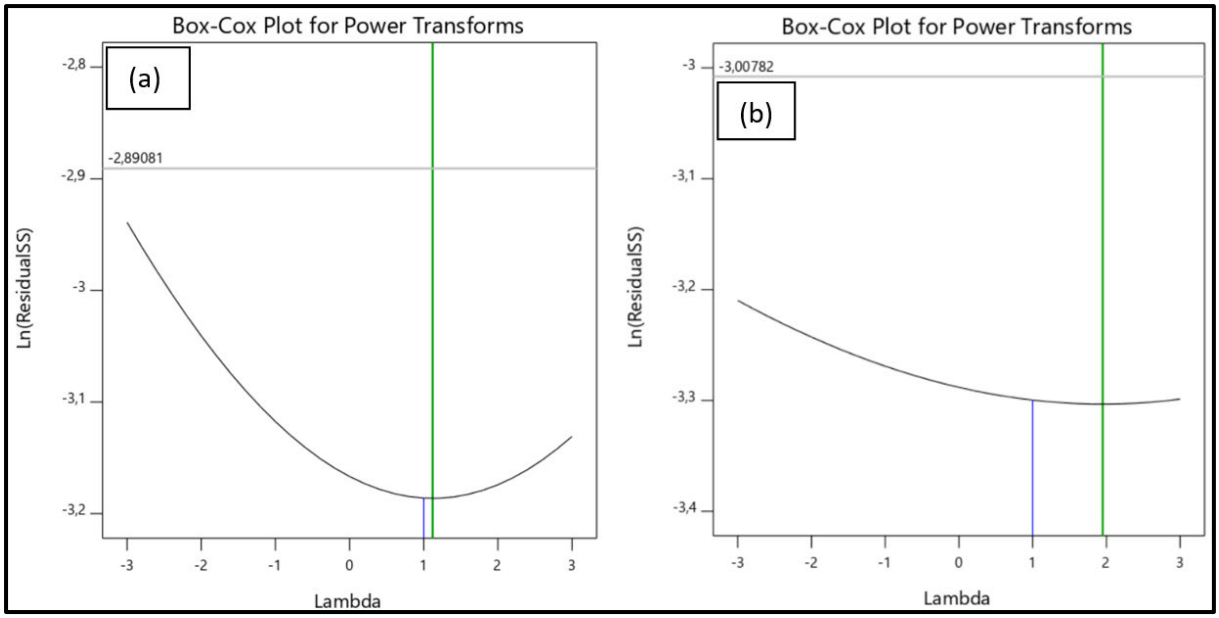

Figure 5-7: Box-Cox Plots for the responses (a) OCV (b) VUL

The Box-Cox transformation is a statistical technique used to stabilize the variance and make a dataset more closely approximate a normal distribution (Vélez, Correa and Marmolejo-ramos, 2015). In **Figure 5-7**, The blue line represents the current lambda, which was (1), and the green line represents the best lambda, which was (1.12). Ideally, the current lambda, which is the lambda that is applied to the data, should be as close to the best lambda as possible. Best lambda is the optimal value determined through statistical optimization. When the current lambda is close to the best lambda, it indicates that the chosen transformation is effective in achieving the goals of the Box-Cox transformation, such as stabilizing variance and making the data more approximately normal (StatEase, 2023a).

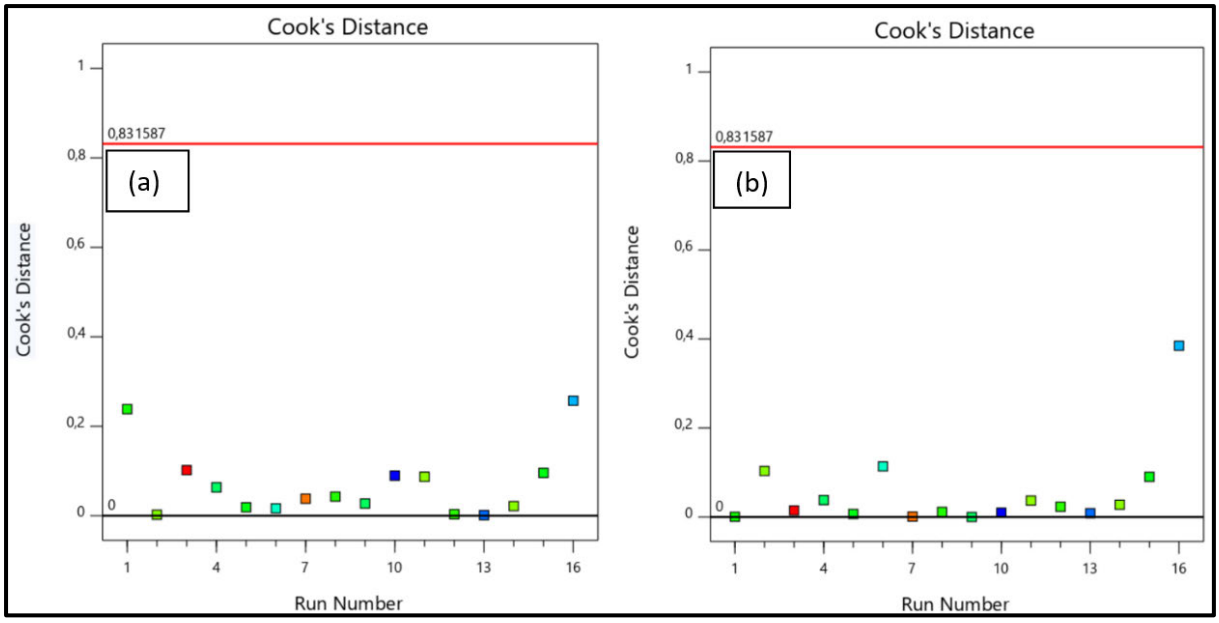

Figure 5-8: Cook's distance plot for the responses (a) OCV (b) VUL

Cook's distance is a measure of the influence of each individual observation on the fitted values of a regression model (Gonz, 2004). It is used to identify influential data points that may have a substantial impact on the model's coefficients or predictions (MathWorks, 2023). In **Figure 5-8**, the red line is a Cook's distance line, and points that fall above the red line are flagged as points outside the model's predictability. The points for our model fall within the predictability range.

5.2. 3D surface graphs and contour plots

The impact of factors on individual responses is visually depicted through 3D and contour plots, as shown in **Figure 5-9** and **Figure 5-10**. These graphical representations provide insights into the relationships between the factors and each response, as captured by the respective regression models. The graphical depiction of response surfaces enables a thorough grasp of interactions and trends among variables, facilitating the optimization of the investigated process (Tetteh and Rathilal, 2018).

Warmer colors (red and orange) indicate the regions of maximum response, while cooler colors (blue and green) signal the opposite. Yellow represents the median, signifying responses in the middle range. The shape of the response surface is determined by the equations that model the relationship between the factors and the response. In **Figure 5-9**(a) and **Figure 5-10**(b), moving from left to right on a contour plot reveals that OCV and VUL increase with flow rate. The red/orange color at the top right denotes the region where the response is maximized. Notably,

in **Figure 5-9**(b), it becomes evident that temperature has a more significant effect on the responses compared to flow rate because the elevation in the top right corner.

In **Figure 5-9**(a), the quadratic model was selected to depict the relationship between the variables. The curves and hills in the plot represent the variation in the response variables as the input variables change. Each curve or hill corresponds to a contour line or surface of constant response. The curvature and steepness of these curves or hills indicate the sensitivity of the response to changes in the input variables. For the VUL plot in **Figure 5-10**(b), the 2FI model was chosen to represent the variables.

In **Figure 5-9**(b), the incline slope from 25 to 40 ℃ reveals that an increase in temperature corresponds to a rise in OCV. The highest OCV is achieved at the maximum temperatures and flow rates. **Figure 5-9**(b) further illustrates that elevating both temperature and flow rate from 25 ℃ and 900 mL/min to 40 ℃ and 1550 mL/min results in a 14% increase in response. A parallel trend is mirrored in VUL, as depicted in **Figure 5-10**(b). The orange colour gradient in **Figure 5-10**(a), spanning from bottom to top, signifies that the interaction between flow rate and temperature leads to higher VUL earlier than observed in the OCV plot in **Figure 5-9**(a).

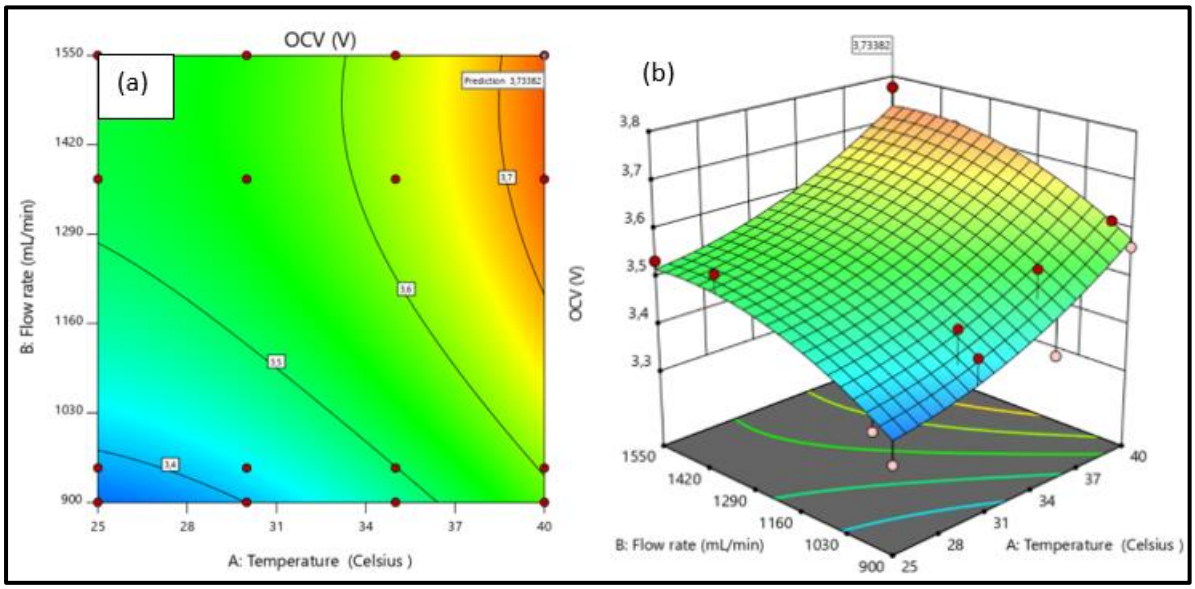

Figure 5-9: Response surface plot showing the effects of temperature and flowrate on OCV as the response (a) contour (b) 3D plot

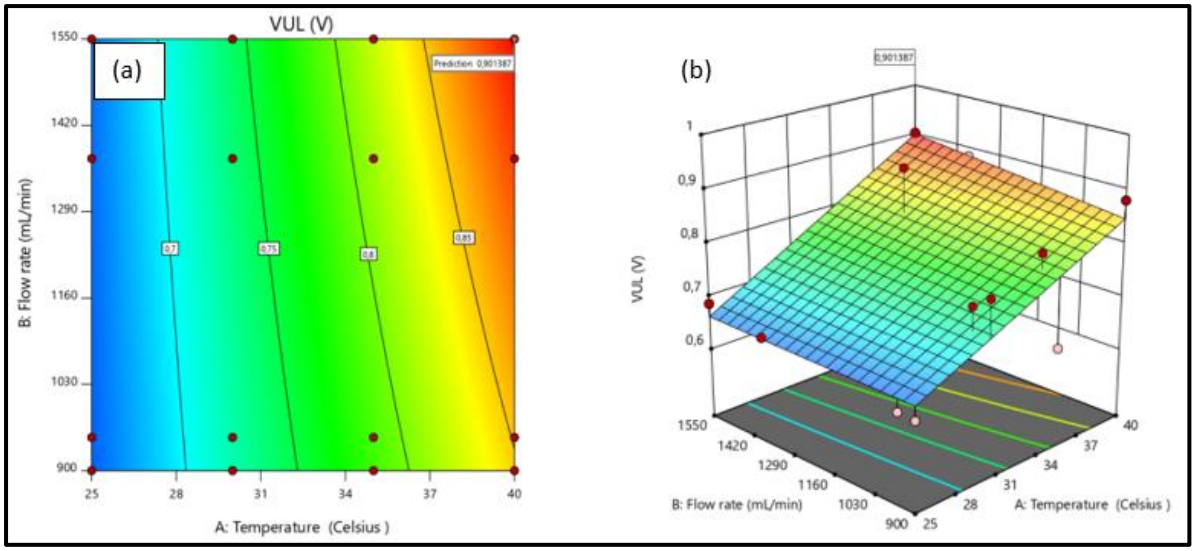

Figure 5-10: Response surface plot showing the effects of temperature and flowrate on VUL as the response (a) contour (b) 3D plot

5.3. RED system variable optimization

The numerical optimization tool, incorporated within the RSM, was employed to optimize the values of the two operating variables within the RED system. This approach facilitated the systematic exploration of the design space, allowing for the identification of optimal conditions for the specified variables.

The result of the optimization is shown in **Figure 5-11**.

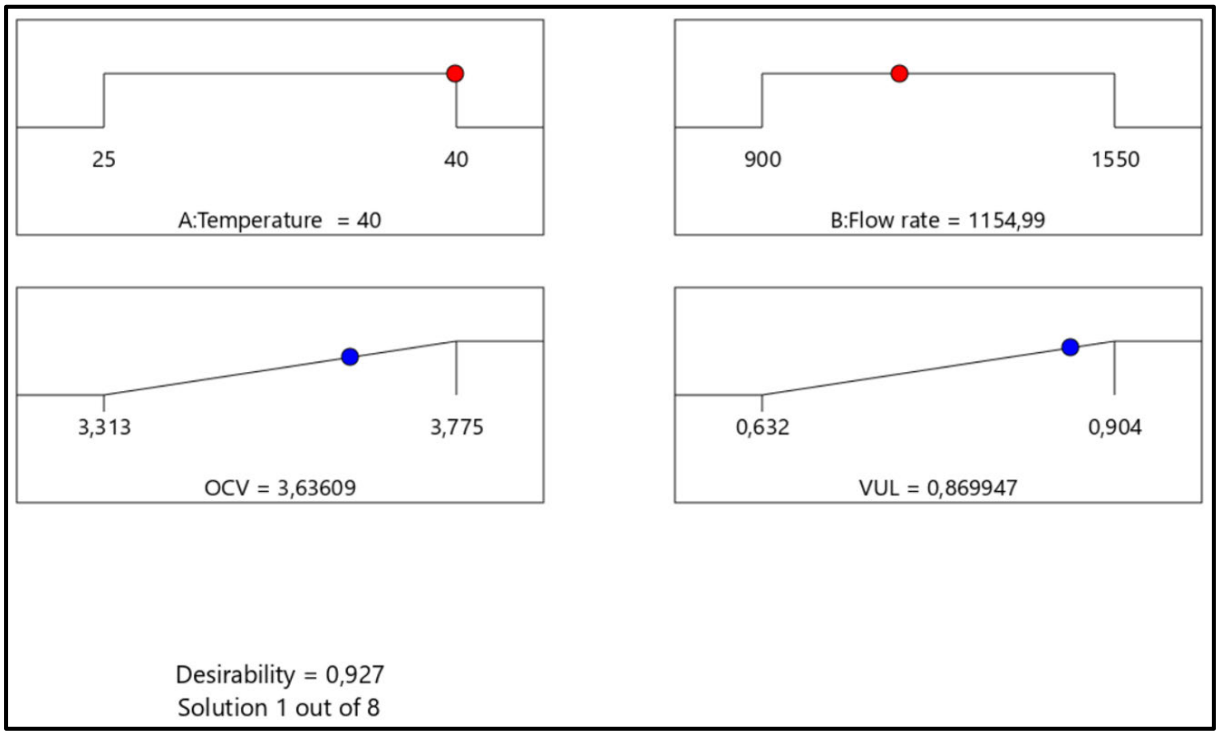

Figure 5-11: Ramp plot displaying the optimized conditions of RED system variables at desirability of 92.7%.

The ramp graphs illustrate the optimum operating conditions and the desirability obtained. For a desirability of 92.7% and operating temperature and flow rate of 40 ℃ and 1550 mL/min respectively, a OCV and VUL of 3.735 V and 0.888 V would be achieved. Among the 8 solutions, the one with the maximum desirability value was chosen as the optimized condition for the response. To validate these results, an additional set of 4 runs was conducted. **Table 5-7** provides details of the optimization conditions. All input variables were maintained within their specified ranges, leading to the maximization of the response variables.

Table 5-7: Conditions of optimization of RED system variables.

Variables	Lower limit	Higher limit	Goal
Flow rate (mL/min)	900	1550	In range
Temperature (℃)	25	40	In range
VUL (V)	0.632	0.904	Maximize
OCV (V)	3.313	3.775	Maximize

5.4. Confirmation of runs

The results of the confirmatory runs are presented in **Table 5-8**.

Table 5-8: Confirmation runs that were conducted. The percentage represents the difference between the expected value and the actual value.

Runs	OCV (V)	VUL (V)	OCV (%)	VUL (%)
1	3.964	0.931	+9	+7
2	3.236	0.704	-11	-19
3	3.091	0.731	-15	-16
4	4.363	0.826	+20	-5

However, the results were not as conclusive as anticipated. One possible explanation is that the model employed was linear, which does not capture all relationships as effectively as a quadratic model, for example. Additionally, a slight difference was observed in the conductivity of the water used for the historical data compared to that used for the confirmation runs. The seawater conductivity was recorded at 56.9 mS/cm, while the conductivity of the river water used in the confirmation runs measured 1791 µS/cm. The averages for the runs were 3.664 V for OCV and 0.798 V. According to **Table 5-9**, these values fall within the specified limits of 3.511 – 3.761 V for OCV and 0.738 – 1.002 V for VUL, respectively.

Table 5-9: Confirmation runs limits for responses.

Solution 1 of 8 response	95% PI low	Data Mean	95% PI high
OCV	3.511	*	3.761
VUL	0.738	*	1.002

CHAPTER 6: Conclusion and Recommendations

Chapter overview

This chapter provides a comprehensive summary of the key results and significant findings from the research. It also offers recommendations for future research endeavours and informed decision-making.

6.1. Major Findings of this Research

- The highest value of OCV was 4.64 V and was found when using the uMgeni River sample. This can be explained by the difference in conductivity between the seawater and UMgeni River samples, which was higher than the other two.
- The feed temperature had more effect on power generation than the flow rate. Higher OCV and power density values were constantly found at higher temperatures, but that was not the case at higher flow rates. This is because temperature increases the mobility of ions more than the flow rate.
- The highest power density value found was 9 W/m^2, recorded using a natural river sample (uMgeni). This was achieved at a temperature of 35 ℃ and a flow rate of 1370 mL/min. This power density value stands on the higher side when compared to values reported by other researchers.
- The concentration of the ERS did not show a linear relationship with the power generation of the RED stack.
- The mixture yielded superior outcomes than the other electrode rinse solutions which lacked redox properties. This is attributed to the redox species, which exhibit a low overpotential for electron transfer, resulting in reduced electrode resistance and maximizing electric power.
- The optimal conditions for power generation by the RED stack involve increasing the feed solutions' temperature and the ERS's flow rate.

6.2. Recommendations

Further research is suggested in this section. Research findings and observations informed the suggestions. As a result, the following recommendations have been made:

- The effect of electrode rinse solution temperature should be studied.

- More studies involving the use of natural solutions should be conducted. This approach would help in understanding how real-world water sources impact the membrane fouling process. By analyzing their specific contributions, it may be possible to find better ways to mitigate fouling or to design membranes that are more resistant to the types of fouling caused by these natural sources.
- The investigation must be conducted at the pilot scale level to feasibly benchmark the RED-stack technology with conventional and other renewable technologies.
- Compare the results from commonly used electrode rinse species with those obtained when using Redox pairs different from those used in this study.

REFERENCES

Achilli, A. and Childress, A.E. (2010a) 'Pressure retarded osmosis : From the vision of Sidney Loeb to the fi rst experimental installation — Review', *DES*, pp. 1–7. Available at: https://doi.org/10.1016/j.desal.2010.06.017.

Achilli, A. and Childress, A.E. (2010b) 'Pressure retarded osmosis: from the vision of Sidney Loeb to the first prototype installation', *Desalination*, 261(3), pp. 205–211.

Ahmad, A.L., Lau, K.K. and Abu Bakar, M.Z. (2005) 'Impact of different spacer filament geometries on concentration polarization control in narrow membrane channel', *Journal of Membrane Science*, 262(1–2), pp. 138–152. Available at: https://doi.org/10.1016/j.memsci.2005.06.056.

Akinbami, O.M., Oke, S.R. and Bodunrin, M.O. (2021) 'The state of renewable energy development in South Africa : An overview', *Alexandria Engineering Journal*, 60(6), pp. 5077–5093. Available at: https://doi.org/10.1016/j.aej.2021.03.065.

AKOSSOU, A.Y.J. (2013) 'Impact of data structure on the estimators R-square and adjusted R-square in linear regression.', *International Journal of Mathematics and Computation* [Preprint], (January).

Akram, W. and Garud, N. (2021) 'Design expert as a statistical tool for optimization of 5-ASA-loaded biopolymer-based nanoparticles using Box Behnken factorial design', *Future Journal of Pharmaceutical Sciences*, 7(1). Available at: https://doi.org/10.1186/s43094-021-00299-z.

Al-Sahali, M. and Ettouney, H. (2007) 'Developments in thermal desalination processes: Design, energy, and costing aspects', *Desalination*, 214(1–3), pp. 227–240. Available at: https://doi.org/10.1016/j.desal.2006.08.020.

Al, S., Diaz-elsayed, N., Benjamin, J. and Arias, M.E. (2022) 'An environmental and economic sustainability assessment of a pressure retarded osmosis system', *Desalination*, 537(June), p. 115869. Available at: https://doi.org/10.1016/j.desal.2022.115869.

Alanne, K. and Saari, A. (2006) 'Distributed energy generation and sustainable development', 10, pp. 539–558. Available at: https://doi.org/10.1016/j.rser.2004.11.004.

Almeida, M., Erthal, R., Padua, E., Silveira, L. and Am, L. (2008) 'Talanta Response surface methodology (RSM) as a tool for optimization in analytical chemistry', 76, pp. 965–977. Available at: https://doi.org/10.1016/j.talanta.2008.05.019.

Altıok, E., Kaya, Z., Güler, E., Kabay, N. and Bryjak, M. (2021) 'Performance of Reverse Electrodialysis System for Salinity Gradient Energy Generation by Using a Commercial Ion Exchange Membrane Pair with Homogeneous Bulk Structure'.

Anis, S.F., Hashaikeh, R. and Hilal, N. (2019) 'Reverse osmosis pretreatment technologies and future trends: A comprehensive review', *Desalination*, 452(October 2018), pp. 159–195. Available at: https://doi.org/10.1016/j.desal.2018.11.006.

Ashu, R., Curcio, E., Brauns, E., Baak, W. Van, Fontananova, E. and Di, G. (2015) 'Membrane Distillation and Reverse Electrodialysis for Near-Zero Liquid Discharge and low energy seawater desalination', 496, pp. 325–333. Available at: https://doi.org/10.1016/j.memsci.2015.09.008.

Ashu, R., Noviello, Y., Di, G., Macedonio, F., Ali, A., Drioli, E., Fontananova, E., Bouzek, K. and Curcio, E. (2019) 'Integrated membrane distillation-reverse electrodialysis system for energy- efficient seawater desalination', *Applied Energy*, 253(July), p. 113551. Available at: https://doi.org/10.1016/j.apenergy.2019.113551.

Ashu, R., Pawlowski, S., Veerman, J., Bouzek, K., Fontananova, E., Velizarov, S., Goulão, J., Nijmeijer, K. and Curcio, E. (2018) 'Progress and prospects in reverse electrodialysis for salinity gradient energy conversion and storage', 225(March), pp. 290–331. Available at: https://doi.org/10.1016/j.apenergy.2018.04.111.

Ashu, R., Piallat, T., Hnát, J., Fontananova, E., Paidar, M., Chanda, D., Curcio, E. and Bouzek, K. (2020) 'Salinity gradient power reverse electrodialysis : Cation exchange membrane design based on polypyrrole-chitosan composites for enhanced monovalent selectivity', 380(August 2019). Available at: https://doi.org/10.1016/j.cej.2019.122461.

Ashu, R., Rugiero, E., Chanda, D., Hnàt, J., Baak, W. Van, Veerman, J., Fontananova, E., Di, G., Drioli, E., Bouzek, K. and Curcio, E. (2016) 'Salinity gradient power-reverse electrodialysis and alkaline polymer electrolyte water electrolysis for hydrogen production', 514, pp. 155–164. Available at: https://doi.org/10.1016/j.memsci.2016.04.067.

Audinos, R. (1992) 'Electric power produced from two solutions of unequal salinity by reverse electrodialysis'.

Avci, A.H., Sarkar, P., Tufa, R.A., Messana, D., Argurio, P., Fontananova, E., Di, G. and Curcio, E. (2016) 'Effect of Mg2+ ions on energy generation by Reverse Electrodialysis', *Journal of Membrane Science*, 520, pp. 499–506. Available at: https://doi.org/10.1016/j.memsci.2016.08.007.

Avci, A.H., Tufa, R.A., Fontananova, E., Di, G. and Curcio, E. (2018) 'Reverse Electrodialysis for energy production from natural river water and seawater', 165, pp. 512–521. Available at: https://doi.org/10.1016/j.energy.2018.09.111.

Ba, D. and Boyaci, I.H. (2007) 'Modeling and optimization i: Usability of response surface methodology', *Journal of Food Engineering*, 78(3), pp. 836–845. Available at: https://doi.org/10.1016/j.jfoodeng.2005.11.024.

Babayomi, O.O., Dahoro, D.A. and Zhang, Z. (2022) 'Affordable clean energy transition in developing countries: Pathways and technologies', *Iscience*, 25(5).

Bai, W., Samineni, L., Chirontoni, P., Krupa, I., Kasak, P., Popelka, A., Saleh, N.B. and Kumar, M. (2023) 'Quantifying and reducing concentration polarization in reverse osmosis systems', *Desalination*, 554(November 2022), p. 116480. Available at: https://doi.org/10.1016/j.desal.2023.116480.

Bashyal, J. (2023) *Ionic Lattice and Ionic Compounds*. Available at: https://thechemistrynotes.com/ionic-lattice/ (Accessed: 16 November 2023).

Benjamin, M.M. (2014) *Water chemistry*. Waveland Press.

Benneker, A.M., Rijnaarts, T., Lammertink, R.G.H. and Wood, A. (2018) 'E ff ect of temperature gradients in (reverse) electrodialysis in the Ohmic regime', 548(September 2017), pp. 421–428. Available at: https://doi.org/10.1016/j.memsci.2017.11.029.

Besha, A.T., Tsehaye, M.T., Aili, D., Zhang, W. and Tufa, R.A. (2019) 'Design of monovalent ion selective membranes for reducing the impacts of multivalent ions in reverse electrodialysis', *Membranes*, 10(1), p. 7.

Bodner, E.J., Saakes, M., Sleutels, T. and Buisman, C.J.N. (2019) 'The RED Fouling Monitor : A novel tool for fouling analysis', *Journal of Membrane Science*, 570–571(July 2018), pp. 294–302. Available at: https://doi.org/10.1016/j.memsci.2018.10.059.

Brennan, S.T. and Lowenstein, T.K. (2002) 'The major-ion composition of Silurian seawater', *Geochimica et Cosmochimica Acta*, 66(15), pp. 2683–2700. Available at: https://doi.org/10.1016/S0016-7037(02)00870-0.

Buckingham, M.A., Hammoud, S., Li, H., Beale, C.J., Sengel, J.T. and Aldous, L. (2020) 'A fundamental study of the thermoelectrochemistry of ferricyanide/ferrocyanide: cation, concentration, ratio, and heterogeneous and homogeneous electrocatalysis effects in thermogalvanic cells', *Sustainable energy & fuels*, 4(7), pp. 3388–3399.

Burheim, O.S., Seland, F., Pharoah, J.G. and Kjelstrup, S. (2012) 'Improved electrode systems for reverse electro-dialysis and electro-dialysis', 285, pp. 147–152. Available at: https://doi.org/10.1016/j.desal.2011.09.048.

Cañedo-Argüelles, M., Kefford, B.J., Piscart, C., Prat, N., Schäfer, R.B. and Schulz, C.J. (2013) 'Salinisation of rivers: An urgent ecological issue', *Environmental Pollution*, 173, pp. 157–167. Available at: https://doi.org/10.1016/j.envpol.2012.10.011.

Chen, C. and Qin, H. (2019) 'A mathematical modeling of the reverse osmosis concentration process of a glucose solution', *Processes*, 7(5). Available at: https://doi.org/10.3390/pr7050271.

Choi, J., Kim, W., Kim, H.K., Yang, S.C., Han, J., Jeung, Y.C. and Jeong, N.J. (2022) 'Fouling behavior of wavy-patterned pore- fi lling membranes in reverse electrodialysis under natural seawater and sewage ef fl uents', pp. 1–12. Available at: https://doi.org/10.1038/s41545-022-00149-2.

Ciofalo, M., Cerva, M. La, Liberto, M. Di, Gurreri, L., Cipollina, A. and Micale, G. (2019) 'Optimization of net power density in Reverse Electrodialysis', *Energy*, 181, pp. 576–588. Available at: https://doi.org/10.1016/j.energy.2019.05.183.

Cohen, B. and Winkler, H. (2014) 'Greenhouse gas emissions from shale gas and coal for electricity generation in South Africa', *South African Journal of Science*, 110(3–4), pp. 2–6. Available at: https://doi.org/10.1590/sajs.2014/20130194.

Cui, W., Ji, Z., Tumba, K., Zhang, Z. and Wang, J. (2022) 'Response of salinity gradient power generation to inflow mode and temperature difference by reverse electrodialysis', *Journal of Environmental Management*, 303(8), p. 114124. Available at: https://doi.org/10.1016/j.jenvman.2021.114124.

Culcasi, A., Gurreri, L., Micale, G. and Tamburini, A. (2021) 'Bipolar membrane reverse electrodialysis for the sustainable recovery of energy from pH gradients of industrial wastewater : Performance prediction by a validated process model', *Journal of Environmental Management*, 287, p. 112319. Available at: https://doi.org/10.1016/j.jenvman.2021.112319.

Culcasi, A., Gurreri, L., Zaffora, A., Cosenza, A., Tamburini, A., Cipollina, A. and Micale, G. (2020) 'Ionic shortcut currents via manifolds in reverse electrodialysis stacks', *Desalination*, 485(March), p. 114450. Available at: https://doi.org/10.1016/j.desal.2020.114450.

Daniilidis, A., Vermaas, D.A., Herber, R. and Nijmeijer, K. (2014) 'Experimentally obtainable energy from mixing river water , seawater or brines with reverse electrodialysis', 64, pp. 123–131. Available at: https://doi.org/10.1016/j.renene.2013.11.001.

Deng, D., Dydek, E.V., Han, J.H., Schlumpberger, S., Mani, A., Zaltzman, B. and Bazant, M.Z. (2013) 'Overlimiting current and shock electrodialysis in porous media', *Langmuir*, 29(52), pp. 16167–16177. Available at: https://doi.org/10.1021/la4040547.

Department of Energy (2020) *The South African energy sector report 2019*. Pretoria.

Dincer, I. (2000) 'Renewable energy and sustainable development : a crucial review', 4, pp. 157–175.

Djalic, I. and Terzic, S. (2021) 'Violation of the assumption of homoscedasticity and detection of heteroscedasticity', *Decision Making: Applications in Management and Engineering*, 4(1), pp. 1–18. Available at: https://doi.org/10.31181/dmame2104001d.

Długoł, P., Joanna, D., Nijmeijer, K. and Wessling, M. (2010) 'Ion conductive spacers for increased power generation in reverse electrodialysis', 347, pp. 101–107. Available at: https://doi.org/10.1016/j.memsci.2009.10.011.

Długoł, P., Nymeijer, K., Metz, S. and Wessling, M. (2008) 'Current status of ion exchange membranes for power generation from salinity gradients', 319, pp. 214–222. Available at: https://doi.org/10.1016/j.memsci.2008.03.037.

Długoł, P., Ogonowski, P., Metz, S.J., Saakes, M., Nijmeijer, K. and Wessling, M. (2010) 'On the resistances of membrane , diffusion boundary layer and double layer in ion exchange membrane transport', 349, pp. 369–379. Available at: https://doi.org/10.1016/j.memsci.2009.11.069.

Długołe, P., Gambier, A. and Wessling, M. (2009) 'Practical Potential of Reverse Electrodialysis As Process for Sustainable Energy Generation', 43(17), pp. 6888–6894.

Dottoressa, L.A. (2016) *Reverse electrodialysis processes for the production of chemicals and the treatment of contaminated wastewater*. University of Palermo.

Elmakki, T., Zavahir, S., Gulied, M., Qiblawey, H., Hammadi, B., Khraisheh, M., Shon, H.K., Park, H. and Han, D.S. (2023) 'Potential application of hybrid reverse electrodialysis (RED)-forward osmosis (FO) system to fertilizer-producing industrial plant for efficient water reuse', *Desalination*, 550(July 2022), p. 116374. Available at: https://doi.org/10.1016/j.desal.2023.116374.

Emmanuel, A.O., Oladipo, F.A. and E., O.O. (2012) 'Investigation of Salinity Effect on Compressive Strength of Reinforced Concrete', *Journal of Sustainable Development*, 5(6). Available at: https://doi.org/10.5539/jsd.v5n6p74.

Emsley, J. (2010) 'The elements', *Education in Chemistry*, 47(6), p. 189. Available at: https://doi.org/10.1016/b978-0-12-059858-8.50053-4.

Fan, H. and Yin, N. (2019) 'Elucidating conductivity-permselectivity tradeoffs in electrodialysis and reverse electrodialysis by structure-property analysis of ion-exchange membranes', *Journal of Membrane Science*, 573(November 2018), pp. 668–681. Available at: https://doi.org/10.1016/j.memsci.2018.11.045.

Fernandez-gonzalez, C., Zhang, B., Dominguez-ramos, A., Ibañez, R., Irabien, A. and Chen, Y. (2017) 'Enhancing fouling resistance of polyethylene anion exchange membranes using carbon nanotubes and iron oxide nanoparticles', *Desalination*, 411, pp. 19–27. Available at: https://doi.org/10.1016/j.desal.2017.02.007.

Fontananova, E., Messana, D., Tufa, R.A., Nicotera, I., Kosma, V., Curcio, E., Baak, W. Van,

Drioli, E. and Pro, G. Di (2017) ‘Effect of solution concentration and composition on the electrochemical properties of ion exchange membranes for energy conversion’, 340, pp. 282–293. Available at: https://doi.org/10.1016/j.jpowsour.2016.11.075.

Fu, L. (2020) ‘Performance parameters analysis of reverse electrodialysis process : Sensitive to the repeating unit pairs , inflow velocity and feed concentration’, (January), pp. 7093–7102. Available at: https://doi.org/10.1002/er.5354.

Galama, A.H., Post, J.W., Stuart, M.A.C. and Biesheuvel, P.M. (2013) ‘Validity of the Boltzmann equation to describe Donnan equilibrium at the membrane – solution interface’, *Journal of Membrane Science*, 442, pp. 131–139. Available at: https://doi.org/10.1016/j.memsci.2013.04.022.

Galama, A.H., Vermaas, D.A., Veerman, J., Saakes, M., Rijnaarts, H.H.M., Post, J.W. and Nijmeijer, K. (2014) ‘Membrane resistance : The effect of salinity gradients over a cation exchange membrane’, *Journal of Membrane Science*, 467, pp. 279–291. Available at: https://doi.org/10.1016/j.memsci.2014.05.046.

Gaye, A. (2008) ‘Human Development Report 2007 / 2008 Access to Energy and Human Development’.

Geise, M., Curtis, A.J., Hatzell, M.C., Hickner, M.A. and Logan, B.E. (2014) ‘Salt Concentration Di ff erences Alter Membrane Resistance in Reverse Electrodialysis Stacks’, pp. 8–11.

Ghafari, S., Abdul, H., Hasnain, M. and Akbar, A. (2009) ‘Application of response surface methodology (RSM) to optimize coagulation – flocculation treatment of leachate using poly-aluminum chloride (PAC) and alum’, 163, pp. 650–656. Available at: https://doi.org/10.1016/j.jhazmat.2008.07.090.

Gi, J., Zhang, B., Glabman, S., Uzal, N., Dou, X., Zhang, H., Wei, X. and Chen, Y. (2015) ‘Potential ion exchange membranes and system performance in reverse electrodialysis for power generation : A review’, 486, pp. 71–88. Available at: https://doi.org/10.1016/j.memsci.2015.02.039.

Giacalone, F., Vassallo, F., Gri, L., Ferrari, M.C., Micale, G., Scargiali, F., Tamburini, A. and Cipollina, A. (2019) ‘Thermolytic reverse electrodialysis heat engine : model development , integration and performance analysis’, 189(March), pp. 1–13. Available at: https://doi.org/10.1016/j.enconman.2019.03.045.

Global Energy Review 2019 (2020) *Global Energy Review 2019*. Available at: https://doi.org/10.1787/90c8c125-en.

Gómez-coma, L., Ortiz-martínez, V.M., Carmona, J., Palacio, L., Prádanos, P., Fallanza, M., Ortiz, A., Ibañez, R. and Ortiz, I. (2019) ‘Modeling the influence of divalent ions on membrane resistance and electric power in reverse electrodialysis’, *Journal of Membrane Science*, 592(August), p. 117385. Available at: https://doi.org/10.1016/j.memsci.2019.117385.

Gonz, G. (2004) ‘A note on the Cook ’ s distance’, 120, pp. 119–136. Available at: https://doi.org/10.1016/S0378-3758(02)00494-9.

Grace, J.B. and Bollen, K.A. (2005) ‘C ontributions Commentary’, 86(4), pp. 283–295.

Grigoriev, S.A., Fateev, V.N., Bessarabov, D.G. and Millet, P. (2020) ‘Current status, research trends, and challenges in water electrolysis science and technology’, *International Journal of Hydrogen Energy*, 45(49), pp. 26036–26058. Available at:

https://doi.org/10.1016/j.ijhydene.2020.03.109.

Gross, R., Leach, M. and Bauen, A. (2003) ‘Progress in renewable energy’, 29, pp. 105–122.

Güler, E. (2014a) *Anion exchange membrane design for reverse electrodialysis*. University of Twente Amsterdam, The Netherlands.

Güler, E. (2014b) *Anion exchange membrane design for reverse electrodialysis*. University of Twente. Available at: https://doi.org/10.3990/9789036535700.

Güler, E., Baak, W. Van, Saakes, M. and Nijmeijer, K. (2014) ‘Monovalent-ion-selective membranes for reverse electrodialysis’, 455, pp. 254–270. Available at: https://doi.org/10.1016/j.memsci.2013.12.054.

Güler, E., Elizen, R., Saakes, M. and Nijmeijer, K. (2014) ‘Micro-structured membranes for electricity generation by reverse electrodialysis’, 458, pp. 136–148. Available at: https://doi.org/10.1016/j.memsci.2014.01.060.

Güler, E., Elizen, R., Vermaas, D.A., Saakes, M. and Nijmeijer, K. (2013) ‘Performance-determining membrane properties in reverse electrodialysis’, 446, pp. 266–276. Available at: https://doi.org/10.1016/j.memsci.2013.06.045.

Guler, E., Zhang, Y., Saakes, M. and Nijmeijer, K. (2012) ‘Tailor-Made Anion-Exchange Membranes for Salinity Gradient Power Generation Using Reverse Electrodialysis’, pp. 2262–2270. Available at: https://doi.org/10.1002/cssc.201200298.

Guo, W., Ngo, H. and Li, J. (2012) ‘Bioresource Technology A mini-review on membrane fouling’, 122, pp. 27–34. Available at: https://doi.org/10.1016/j.biortech.2012.04.089.

Guo, Z., Ji, Z., Zhang, Y. and Yang, F. (2018) ‘Electrochimica Acta Effect of ions (K þ , Mg 2 þ , Ca 2 þ and SO 2 4) and temperature on energy generation performance of reverse electrodialysis stack’, 290, pp. 282–290. Available at: https://doi.org/10.1016/j.electacta.2018.09.015.

Gurreri, L., Battaglia, G., Tamburini, A., Cipollina, A., Micale, G. and Ciofalo, M. (2017) ‘Multi-physical modelling of reverse electrodialysis’, *Desalination*, 423(May), pp. 52–64. Available at: https://doi.org/10.1016/j.desal.2017.09.006.

Gurreri, L., Tamburini, A., Cipollina, A., Micale, G. and Ciofalo, M. (2014) ‘CFD prediction of concentration polarization phenomena in spacer- fi lled channels for reverse electrodialysis’, *Journal of Membrane Science*, 468, pp. 133–148. Available at: https://doi.org/10.1016/j.memsci.2014.05.058.

Gurreri, L., Tamburini, A., Cipollina, A., Micale, G. and Ciofalo, M. (2016) ‘Flow and mass transfer in spacer- fi lled channels for reverse electrodialysis : a CFD parametrical study’, 497, pp. 300–317. Available at: https://doi.org/10.1016/j.memsci.2015.09.006.

Hailemariam, R.H., Woo, Y.C., Damtie, M.M., Kim, B.C., Park, K.D. and Choi, J.S. (2020) ‘Reverse osmosis membrane fabrication and modification technologies and future trends: A review’, *Advances in Colloid and Interface Science*, 276, p. 102100. Available at: https://doi.org/10.1016/j.cis.2019.102100.

Han, J., Kim, H., Hwang, K., Jeong, N. and Kim, C. (2019) ‘Hydrogen Production from Water Electrolysis Driven by High Membrane Voltage of Reverse Electrodialysis’, 10(3), pp. 302–312.

Harmsen, G.J.A.N. (2010) ‘Electrical Power from Sea and River Water by Reverse Electrodialysis : A First Step from the Laboratory to a Real Power Plant’, 44(23), pp. 9207–9212.

Helfer, F., Lemckert, C. and Anissimov, Y.G. (2014) ‘Osmotic power with Pressure Retarded Osmosis : Theory , performance and trends – A review’, *Journal of Membrane Science*, 453, pp. 337–358. Available at: https://doi.org/10.1016/j.memsci.2013.10.053.

Hepbasli, A. and Ozgener, O. (2004) ‘A review on the development of wind energy in Turkey’, 8, pp. 257–276. Available at: https://doi.org/10.1016/j.rser.2003.10.006.

Hertzberger, A.J., Cusick, R.D. and Margenot, A.J. (2020) ‘A review and meta-analysis of the agricultural potential of struvite as a phosphorus fertilizer’, *Soil Science Society of America Journal*, 84(3), pp. 653–671.

Herzog, A. V, Lipman, T.E. and Kammen, D.M. (2001) ‘Renewable energy sources’, *Encyclopedia of life support systems (EOLSS). Forerunner Volume-‘Perspectives and overview of life support systems and sustainable development*, 76, pp. 1–63.

Hidayati, N., Kınalı, O., Kitada, S., Güler, E. and Kabay, N. (2022) ‘Investigations on the effects of operational parameters in reverse electrodialysis system for salinity gradient power generation using central composite design (CCD)’, 525(December 2021).

Hong, J.G. and Chen, Y. (2014) ‘Nanocomposite reverse electrodialysis (RED) ion-exchange membranes for salinity gradient power generation’, 460, pp. 139–147. Available at: https://doi.org/10.1016/j.memsci.2014.02.027.

Hong, J.G. and Chen, Y. (2015) ‘Evaluation of electrochemical properties and reverse electrodialysis performance for porous cation exchange membranes with sulfate-functionalized iron oxide’, *Journal of Membrane Science*, 473, pp. 210–217. Available at: https://doi.org/10.1016/j.memsci.2014.09.012.

Hooda, A., Nanda, A., Jain, M., Kumar, V. and Rathee, P. (2012) ‘Optimization and evaluation of gastroretentive ranitidine HCl microspheres by using design expert software’, *International Journal of Biological Macromolecules*, 51(5), pp. 691–700. Available at: https://doi.org/10.1016/j.ijbiomac.2012.07.030.

Hsu, J., Lin, S., Lin, C. and Tseng, S. (2017) ‘Power generation by a pH-regulated conical nanopore through reverse electrodialysis’, *Journal of Power Sources*, 366, pp. 169–177. Available at: https://doi.org/10.1016/j.jpowsour.2017.09.022.

Hsu, J., Su, T., Lin, C. and Tseng, S. (2019) ‘Electrochimica Acta Power generation from a pH-regulated nanochannel through reverse electrodialysis : Effects of nanochannel shape and non-uniform H þ distribution’, *Electrochimica Acta*, 294, pp. 84–92. Available at: https://doi.org/10.1016/j.electacta.2018.10.074.

Hulme, A.M., Davey, C.J., Parker, A., Williams, L., Tyrrel, S., Jiang, Y., Pidou, M., Water, C. and Mk, B. (2020) ‘Managing power dissipation in closed-loop reverse electrodialysis to maximise energy recovery during thermal-to-electric conversion’, *Desalination*, 496(July), p. 114711. Available at: https://doi.org/10.1016/j.desal.2020.114711.

Hulme, A.M., Davey, C.J., Tyrrel, S., Pidou, M. and Mcadam, E.J. (2021) ‘Transitioning from electrodialysis to reverse electrodialysis stack design for energy generation from high concentration salinity gradients’, *Energy Conversion and Management*, 244(June), p. 114493. Available at: https://doi.org/10.1016/j.enconman.2021.114493.

Iqbal, M., Iqbal, N., Ahmad, I., Ahmad, N. and Zahid, M. (2016) 'Response surface methodology application in optimization of cadmium adsorption by shoe waste : A good option of waste mitigation by waste', *Ecological Engineering*, 88, pp. 265–275. Available at: https://doi.org/10.1016/j.ecoleng.2015.12.041.

Jafary, T., Ramli, W., Daud, W., Ghasemi, M., Hong, B., Jahim, J., Ismail, M. and Su, S. (2015) 'Biocathode in microbial electrolysis cell ; present status and future prospects', 47, pp. 23–33. Available at: https://doi.org/10.1016/j.rser.2015.03.003.

Jande, Y.A.C. and Kim, W.S. (2014) 'Integrating reverse electrodialysis with constant current operating capacitive deionization', *Journal of Environmental Management*, 146, pp. 463–469. Available at: https://doi.org/10.1016/j.jenvman.2014.07.039.

Jang, J., Kang, Y., Han, J., Jang, K., Kim, C. and Kim, I.S. (2020) 'Developments and future prospects of reverse electrodialysis for salinity gradient power generation : Influence of ion exchange membranes and electrodes', *Desalination*, 491(May), p. 114540. Available at: https://doi.org/10.1016/j.desal.2020.114540.

Jeremiasse, A.W., Hamelers, H.V.M. and Buisman, C.J.N. (2010) 'Bioelectrochemistry Microbial electrolysis cell with a microbial biocathode', *Bioelectrochemistry*, 78(1), pp. 39–43. Available at: https://doi.org/10.1016/j.bioelechem.2009.05.005.

Jiménez Garcia, J., Berghezan, S., Caramês, J.M.M., Dard, M.M. and Marques, D.N.S. (2017) 'Effect of cross-linked vs non-cross-linked collagen membranes on bone: A systematic review', *Journal of Periodontal Research*, 52(6), pp. 955–964. Available at: https://doi.org/10.1111/jre.12470.

Jin, D., Xi, R., Xu, S., Wang, P. and Wu, X. (2021) 'Numerical simulation of salinity gradient power generation using reverse electrodialysis', 512(May). Available at: https://doi.org/10.1016/j.desal.2021.115132.

Ju, J., Choi, Y., Lee, S., Kim, H. and Jung, N. (2020) 'Effect of design and operating parameters on power generation in reverse electrodialysis (RED): experimental analysis and modeling', 191(August 2019), pp. 29–39. Available at: https://doi.org/10.5004/dwt.2020.25265.

Jwa, E., Yun, Y., Kim, H., Jeong, N. and Sik, K. (2020) 'Energy-e ffi cient seawater softening and power generation using a microbial electrolysis cell-reverse electrodialysis hybrid system', *Chemical Engineering Journal*, 391(May 2019), p. 123480. Available at: https://doi.org/10.1016/j.cej.2019.123480.

Kang, H., Kim, E. and Jung, S.P. (2017) 'ScienceDirect Influence of flowrates to a reverse electro-dialysis (RED) stack on performance and electrochemistry of a microbial reverse electrodialysis cell (MRC)', *International Journal of Hydrogen Energy*, 42(45), pp. 27685–27692. Available at: https://doi.org/10.1016/j.ijhydene.2017.06.187.

Karch, J. (2020) 'Improving on adjusted R-squared', *Collabra: Psychology*, 6(1), pp. 1–11. Available at: https://doi.org/10.1525/collabra.343.

Khalla, S.A. and Suss, M.E. (2019) 'Desalination via chemical energy : An electrodialysis cell driven by spontaneous electrode reactions', *Desalination*, 467(February), pp. 257–262. Available at: https://doi.org/10.1016/j.desal.2019.04.031.

Kim, S. and Hoek, E.M. V (2005) 'Modeling concentration polarization in reverse osmosis processes', 186, pp. 111–128. Available at: https://doi.org/10.1016/j.desal.2005.05.017.

Kingsbury, R.S., Liu, F., Zhu, S., Boggs, C., Armstrong, M.D., Call, D.F. and Coronell, O.

(2017) ‘Impact of natural organic matter and inorganic solutes on energy recovery from fi ve real salinity gradients using reverse electrodialysis’, 541(July), pp. 621–632. Available at: https://doi.org/10.1016/j.memsci.2017.07.038.

Klaysom, C., Moon, S., Ladewig, B.P., Lu, G.Q.M. and Wang, L. (2011) ‘Preparation of porous ion-exchange membranes (IEMs) and their characterizations’, 371, pp. 37–44. Available at: https://doi.org/10.1016/j.memsci.2011.01.008.

Koter, S., Piotrowski, P. and Kerres, J. (1999) ‘Comparative investigations of ion-exchange membranes’, 153.

Kotoka, F. and Merino-garcia, I. (2020) ‘Surface Modifications of Anion Exchange Membranes for an Improved Reverse Electrodialysis Process Performance : A Review’, *Membranes* [Preprint], (Lc).

Kotoka, F., Merino-Garcia, I. and Velizarov, S. (2020) ‘Surface modifications of anion exchange membranes for an improved reverse electrodialysis process performance: A review’, *Membranes*, 10(8), p. 160.

Kowsari, E., Zare, A. and Ansari, V. (2015) ‘ScienceDirect Phosphoric acid-doped ionic liquid-functionalized graphene oxide / sulfonated polyimide composites as proton exchange membrane’, *International Journal of Hydrogen Energy*, 40(40), pp. 13964–13978. Available at: https://doi.org/10.1016/j.ijhydene.2015.08.064.

Kravchenko, M. V., Voloshkina, O.S. and Vasylenko, L.O. (2021) ‘Application of the reverse osmosis method for the purification of drinking water’, *Environmental safety and natural resources*, 40(4), pp. 32–45. Available at: https://doi.org/10.32347/2411-4049.2021.4.32-45.

Kumle, L., Võ, M.L.H. and Draschkow, D. (2021) ‘Estimating power in (generalized) linear mixed models: An open introduction and tutorial in R’, *Behavior Research Methods*, 53(6), pp. 2528–2543. Available at: https://doi.org/10.3758/s13428-021-01546-0.

Kwon, Kilsung; Park, Byung-Ho; Kim, Deok Han; Kim, D. (2017) ‘Comparison of spacer-less and spacer-filled reverse electrodialysis’, *Jornal of Renewables and Sustainable Energy*, 9(4), p. 044502. Available at: https://doi.org/https://doi.org/10.1063/1.4996579.

Kwon, K., Han, J., Ho, B., Shin, Y. and Kim, D. (2015) ‘Brine recovery using reverse electrodialysis in membrane-based desalination processes’, *DES*, 362, pp. 1–10. Available at: https://doi.org/10.1016/j.desal.2015.01.047.

Laanaya, F., St-Hilaire, A. and Gloaguen, E. (2017) ‘Water temperature modelling: comparison between the generalized additive model, logistic, residuals regression and linear regression models’, *Hydrological Sciences Journal*, 62(7), pp. 1078–1093. Available at: https://doi.org/10.1080/02626667.2016.1246799.

Lacey, R. ~E. (1980) ‘Energy by reverse electrodialysis’, *Ocean Engineering*, 7(1), pp. 1–47.

Lee, K.L., Baker, R.W. and Lonsdale, H.K. (1981) ‘Membranes for power generation by pressure-retarded osmosis’, *Journal of membrane science*, 8(2), pp. 141–171.

Lee, S., Jeong, Y., Chae, S., Yeon, K., Lee, Y., Kim, C., Jeong, N. and Park, J. (2016) ‘Journal of Physics and Chemistry of Solids Porous carbon-coated graphite electrodes for energy production from salinity gradient using reverse electrodialysis’, *Journal of Physical and Chemistry of Solids*, 91, pp. 34–40. Available at: https://doi.org/10.1016/j.jpcs.2015.12.006.

Li, J., Zhang, C., Wang, Z., Bai, Z. and Kong, X. (2022) ‘Salinity gradient energy harvested

from thermal desalination for power production by reverse electrodialysis', *Energy Conversion and Management*, 252(November 2021), p. 115043. Available at: https://doi.org/10.1016/j.enconman.2021.115043.

Li, N., Hu, Y., Lu, Y.Z., Zeng, R.J. and Sheng, G.P. (2016) 'Multiple response optimization of the coagulation process for upgrading the quality of effluent from municipal wastewater treatment plant', *Scientific Reports*, 6(April), pp. 1–13. Available at: https://doi.org/10.1038/srep26115.

Li, W., Krantz, W.B., Cornelissen, E.R., Post, J.W., Verliefde, A.R.D. and Tang, C.Y. (2013) 'A novel hybrid process of reverse electrodialysis and reverse osmosis for low energy seawater desalination and brine management', *Applied Energy*, 104, pp. 592–602. Available at: https://doi.org/10.1016/j.apenergy.2012.11.064.

Liu, F., Coronell, O. and Call, D.F. (2017) 'Electricity generation using continuously recirculated fl ow electrodes in reverse electrodialysis', *Journal of Power Sources*, 355, pp. 206–210. Available at: https://doi.org/10.1016/j.jpowsour.2017.04.061.

Loeb, S. (2001) 'One hundred and thirty benign and renewable megawatts from Great Salt Lake? The possibilities of hydroelectric power by pressure-retarded osmosis', *Desalination*, 141, pp. 85–91. Available at: https://doi.org/10.1016/S0011-9164(01)00392-7.

Loeb, S. and Norman, R.S. (1975) 'Osmotic power plants', *Science*, 189(4203), pp. 654–655.

Long, R., Li, B., Liu, Z. and Liu, W. (2018) 'Reverse electrodialysis : Modelling and performance analysis based on multi-objective optimization', *Energy*, 151, pp. 1–10. Available at: https://doi.org/10.1016/j.energy.2018.03.003.

Lowenstein, T.K., Timofeeff, M.N., Kovalevych, V.M. and Horita, J. (2005) 'The major-ion composition of Permian seawater', *Geochimica et Cosmochimica Acta*, 69(7), pp. 1701–1719. Available at: https://doi.org/10.1016/j.gca.2004.09.015.

Lund, H. (2007) 'Renewable energy strategies for sustainable development', *energy*, 32(6), pp. 912–919.

Luo, T., Abdu, S. and Wessling, M. (2018) 'Selectivity of ion exchange membranes : A review', 555(March), pp. 429–454. Available at: https://doi.org/10.1016/j.memsci.2018.03.051.

Luo, X., Cao, X., Mo, Y., Xiao, K., Zhang, X., Liang, P. and Huang, X. (2012) 'Electrochemistry Communications Power generation by coupling reverse electrodialysis and ammonium bicarbonate : Implication for recovery of waste heat', *Electrochemistry Communications*, 19, pp. 25–28. Available at: https://doi.org/10.1016/j.elecom.2012.03.004.

Luque, J., Salvo, D., Cosenza, A., Tamburini, A., Micale, G. and Cipollina, A. (2018) 'Long-run operation of a reverse electrodialysis system fed with wastewaters', *Journal of Environmental Management*, 217, pp. 871–887. Available at: https://doi.org/10.1016/j.jenvman.2018.03.110.

Marcus, Y. (2009) 'Effect of ions on the structure of water: structure making and breaking', *Chemical reviews*, 109(3), pp. 1346–1370.

MathWorks (2023) *Cook's Distance*, *Help Center*. Available at: https://www.mathworks.com/help/stats/cooks-distance.html.

Matthiasson, E. and Sivik, B. (1980) 'Concentration polarization and fouling', *Desalination*,

35, pp. 59–103.

Mehdizadeh, S., Kakihana, Y., Abo, T., Yuan, Q. and Higa, M. (2021) 'Power generation performance of a pilot-scale reverse electrodialysis using monovalent selective ion-exchange membranes', *Membranes*, 11(1), p. 27.

Mehdizadeh, S., Yasukawa, M., Abo, T. and Kakihana, Y. (2019) 'E ff ect of spacer geometry on membrane and solution compartment resistances in reverse electrodialysis', *Journal of Membrane Science*, 572(September 2018), pp. 271–280. Available at: https://doi.org/10.1016/j.memsci.2018.09.051.

Mehdizadeh, S., Yasukawa, M., Abo, T., Kuno, M. and Noguchi, Y. (2019) 'membranes The E ff ect of Feed Solution Temperature on the Power Output Performance of a Pilot-Scale Reverse Electrodialysis (RED) System with Di ff erent Intermediate Distance'.

Mehmood, T., Ahmed, A., Ahmad, A., Ahmad, M.S. and Sandhu, M.A. (2018) 'Optimization of mixed surfactants-based β-carotene nanoemulsions using response surface methodology: An ultrasonic homogenization approach', *Food Chemistry*, 253(January), pp. 179–184. Available at: https://doi.org/10.1016/j.foodchem.2018.01.136.

Mei, Y., Mei, Y. and Tang, C.Y. (2018) 'Recent developments and future perspectives of reverse electrodialysis technology : A review', (November). Available at: https://doi.org/10.1016/j.desal.2017.10.021.

Mei, Y. and Tang, C.Y. (2017) 'Co-locating reverse electrodialysis with reverse osmosis desalination : Synergies and implications', *Journal of Membrane Science*, 539(March), pp. 305–312. Available at: https://doi.org/10.1016/j.memsci.2017.06.014.

Mei, Y. and Tang, C.Y. (2018) 'Recent developments and future perspectives of reverse electrodialysis technology: A review', *Desalination*, 425, pp. 156–174.

Membranes, I., Mehdizadeh, S., Kakihana, Y., Abo, T., Yuan, Q. and Higa, M. (2021) 'Power Generation Performance of a Pilot-Scale Reverse Electrodialysis Using Monovalent Selective Ion-Exchange Membranes'. Available at: https://doi.org/10.3390/membranes11010027.

Mercer, E., Davey, C.J., Azzini, D., Eusebi, A.L., Tierney, R., Williams, L., Jiang, Y., Parker, A., Kolios, A., Tyrrel, S., Cartmell, E., Pidou, M. and McAdam, E.J. (2019) 'Hybrid membrane distillation reverse electrodialysis configuration for water and energy recovery from human urine: An opportunity for off-grid decentralised sanitation', *Journal of Membrane Science*, 584(March), pp. 343–352. Available at: https://doi.org/10.1016/j.memsci.2019.05.010.

Michal, N., Ashu, R., Hn, J., Kodým, R., Curcio, E. and Bouzek, K. (2018) 'Hydrogen production from industrial wastewaters: An integrated reverse electrodialysis - Water electrolysis energy system', *Journal of Cleaner Production*, 203, pp. 418–426. Available at: https://doi.org/10.1016/j.jclepro.2018.08.269.

Mohtasham, J. (2015) 'Review Article-Renewable Energies', 74, pp. 1289–1297. Available at: https://doi.org/10.1016/j.egypro.2015.07.774.

Moreno, J, Díez, V., Saakes, M. and Nijmeijer, K. (2018) 'Mitigation of the e ff ects of multivalent ion transport in reverse electrodialysis', *Journal of Membrane Science*, 550(October 2017), pp. 155–162. Available at: https://doi.org/10.1016/j.memsci.2017.12.069.

Moreno, Jordi, Grasman, S., Engelen, R. Van and Nijmeijer, K. (2018) 'Upscaling Reverse Electrodialysis'. Available at: https://doi.org/10.1021/acs.est.8b01886.

Moreno, J., Hart, N. De, Saakes, M. and Nijmeijer, K. (2017) ‘CO 2 saturated water as two-phase fl ow for fouling control in reverse electrodialysis’, *Water Research*, 125, pp. 23–31. Available at: https://doi.org/10.1016/j.watres.2017.08.015.

Moreno, J., Slouwerhof, E., Vermaas, D.A., Saakes, M. and Nijmeijer, K. (2016) ‘The Breathing Cell: Cyclic Intermembrane Distance Variation in Reverse Electrodialysis’. Available at: https://doi.org/10.1021/acs.est.6b02668.

Moshood, T.D., Nawanir, G., Mahmud, F., Sorooshian, S. and Adeleke, A.Q. (2021) ‘Green and low carbon matters: A systematic review of the past, today, and future on sustainability supply chain management practices among manufacturing industry’, *Cleaner Engineering and Technology*, 4, p. 100144.

Moya, A.A. (2016) ‘A numerical comparison of optimal load and internal resistances in ion-exchange membrane systems under reverse electrodialysis conditions’, *DES*, 392, pp. 25–33. Available at: https://doi.org/10.1016/j.desal.2016.04.016.

Moya, A.A. (2020) ‘Uphill transport in improved reverse electrodialysis by removal of divalent cations in the dilute solution : A Nernst-Planck based study’, *Journal of Membrane Science*, 598(December 2019), p. 117784. Available at: https://doi.org/10.1016/j.memsci.2019.117784.

Nadeem, M.A. and Idriss, H. (2020) ‘Effect of pH, temperature, and low light flux on the performance (16% STH) of coupled triple junction solar cell to water electrolysis’, *Journal of Power Sources*, 459(December 2019), p. 228074. Available at: https://doi.org/10.1016/j.jpowsour.2020.228074.

Nagarale, R.K., Gohil, G.S. and Shahi, V.K. (2006) ‘Recent developments on ion-exchange membranes and electro-membrane processes’, 119, pp. 97–130. Available at: https://doi.org/10.1016/j.cis.2005.09.005.

Nam, J.Y., Hwang, K.S., Kim, H.C., Jeong, H., Kim, H., Jwa, E., Yang, S.C., Choi, J., Kim, C.S., Han, J.H. and Jeong, N. (2019) ‘Assessing the behavior of the feed-water constituents of a pilot-scale 1000-cell-pair reverse electrodialysis with seawater and municipal wastewater effluent’, *Water Research*, pp. 261–271. Available at: https://doi.org/10.1016/j.watres.2018.10.054.

Nasir, M., Nakanishi, Y., Patmonoaji, A. and Suekane, T. (2020) ‘Effects of porous electrode pore size and operating fl ow rate on the energy production of capacitive energy extraction’, *Renewable Energy*, 155, pp. 278–285. Available at: https://doi.org/10.1016/j.renene.2020.03.163.

Nazif, A., Karkhanechi, H., Saljoughi, E. and Mahmoud, S. (2022) ‘Journal of Water Process Engineering Recent progress in membrane development , affecting parameters , and applications of reverse electrodialysis : A review’, *Journal of Water Process Engineering*, 47(March), p. 102706. Available at: https://doi.org/10.1016/j.jwpe.2022.102706.

Olkis, C., Santori, G. and Brandani, S. (2018) ‘An Adsorption Reverse Electrodialysis system for the generation of electricity from low-grade heat’, *Applied Energy*, 231(August), pp. 222–234. Available at: https://doi.org/10.1016/j.apenergy.2018.09.112.

Olume, V. and Renberth, K.E.E.T. (2002) ‘Estimates of Freshwater Discharge from Continents : Latitudinal and Seasonal Variations’, pp. 660–687.

Online, V.A., Tufa, R.A., Curcio, E., Baak, W. Van, Veerman, J., Grasman, S. and Fontananova, E. (2014) ‘RSC Advances generation by salinity gradient power-reverse’, pp.

42617–42623. Available at: https://doi.org/10.1039/C4RA05968A.

Ortega-delgado, B., Giacalone, F., Cipollina, A., Papapetrou, M. and Kosmadakis, G. (2019) 'Boosting the performance of a Reverse Electrodialysis – Multi-E ff ect Distillation Heat Engine by novel solutions and operating conditions', *Applied Energy*, 253(July), p. 113489. Available at: https://doi.org/10.1016/j.apenergy.2019.113489.

Ortiz-imedio, R., Gomez-coma, L., Fallanza, M., Ortiz, A., Ibañez, R. and Ortiz, I. (2019) 'Comparative performance of Salinity Gradient Power-Reverse Electrodialysis under different operating conditions', *Desalination*, 457(June 2018), pp. 8–21. Available at: https://doi.org/10.1016/j.desal.2019.01.005.

Pal, S., Mondal, R., Guha, S., Chatterjee, U. and Jewrajka, S.K. (2019) 'Homogeneous phase crosslinked poly (acrylonitrile- co -2-acrylamido-2- methyl-1-propanesulfonic acid) conetwork cation exchange membranes showing high electrochemical properties and electrodialysis performance', *Polymer*, 180(May), p. 121680. Available at: https://doi.org/10.1016/j.polymer.2019.121680.

Pattle, R.E. (1954) 'Production of electric power by mixing fresh and salt water in the hydroelectric pile', *Nature*, 174(4431), p. 660.

Pawlowski, S., Crespo, J.G. and Velizarov, S. (2014) 'Pressure drop in reverse electrodialysis : Experimental and modeling studies for stacks with variable number of cell pairs', 462, pp. 96–111. Available at: https://doi.org/10.1016/j.memsci.2014.03.020.

Pawlowski, S., Geraldes, V., Crespo, J.G. and Velizarov, S. (2016) 'Computational fl uid dynamics (CFD) assisted analysis of pro fi led membranes performance in reverse electrodialysis', 502, pp. 179–190. Available at: https://doi.org/10.1016/j.memsci.2015.11.031.

Pawlowski, S., Rijnaarts, T., Saakes, M., Nijmeijer, K. and Crespo, J.G. (2017) 'Improved fl uid mixing and power density in reverse electrodialysis stacks with chevron-pro fi led membranes', 531(February), pp. 111–121. Available at: https://doi.org/10.1016/j.memsci.2017.03.003.

Pawlowski, S., Sistat, P., Crespo, J.G. and Velizarov, S. (2014) 'Mass transfer in reverse electrodialysis : Flow entrance effects and diffusion boundary layer thickness', *Journal of Membrane Science*, 471, pp. 72–83. Available at: https://doi.org/10.1016/j.memsci.2014.07.075.

Popoola, L.T. (2019) 'Nano-magnetic walnut shell-rice husk for Cd(II) sorption: design and optimization using artificial intelligence and design expert', *Heliyon*, 5(8), p. e02381. Available at: https://doi.org/10.1016/j.heliyon.2019.e02381.

Post, J.W. (2009) *Blue Energy : electricity production from salinity gradients by reverse electrodialysis*. Wageningen University.

Post, J.W., Hamelers, H.V.M. and Buisman, C.J.N. (2009) 'Influence of multivalent ions on power production from mixing salt and fresh water with a reverse electrodialysis system', 330, pp. 65–72. Available at: https://doi.org/10.1016/j.memsci.2008.12.042.

Post, J.W., Veerman, J., Hamelers, H.V.M., Euverink, G.J.W., Metz, S.J., Nymeijer, K. and Buisman, C.J.N. (2007) 'Salinity-gradient power : Evaluation of pressure-retarded osmosis and reverse electrodialysis', 288, pp. 218–230. Available at: https://doi.org/10.1016/j.memsci.2006.11.018.

Principle, I.N. (2000) ‘Energy by reverse electrodialysis*’, 7, pp. 1–47.

Ranade, A., Singh, K., Tamburini, A., Micale, G. and Vermaas, D.A. (2022) ‘Feasibility of Producing Electricity, Hydrogen, and Chlorine via Reverse Electrodialysis’. Available at: https://doi.org/10.1021/acs.est.2c03407.

Reed, G.F., Lynn, F. and Meade, B.D. (2002) ‘Quantitative Assays’, 9(6), pp. 1235–1239. Available at: https://doi.org/10.1128/CDLI.9.6.1235.

Revenga, C., Le, C., Authors, L., Bos, R., Caudill, C., Chilton, J., Douglas, E.M., Meybeck, M., Prager, D., Authors, C., Balvanera, P., Barker, S., Maas, M., Nilsson, C., Oki, T., Editors, R., Rijsberman, F., Costanza, R. and Jacobi, P. (no date) ‘Fresh Water’.

Rijnaarts, T., Huerta, E., Baak, W. Van and Nijmeijer, K. (2017) ‘E ff ect of Divalent Cations on RED Performance and Cation Exchange Membrane Selection to Enhance Power Densities’, pp. 13028–13035. Available at: https://doi.org/10.1021/acs.est.7b03858.

Rijnaarts, T., Moreno, J., Saakes, M., Vos, W.M. De and Nijmeijer, K. (2019) ‘Role of anion exchange membrane fouling in reverse electrodialysis using natural feed waters’, *Colloids and Surfaces A*, 560(October 2018), pp. 198–204. Available at: https://doi.org/10.1016/j.colsurfa.2018.10.020.

Roman, M., Gutierrez, L., Dijk, L.H. Van, Vanoppen, M., Post, J.W., Wols, B.A., Cornelissen, E.R. and Verliefde, A.R.D. (2020) ‘Separation and Puri fi cation Technology E ff ect of pH on the transport and adsorption of organic micropollutants in ion-exchange membranes in electrodialysis-based desalination’, *Separation and Purification Technology*, 252(July), p. 117487. Available at: https://doi.org/10.1016/j.seppur.2020.117487.

Ryan, E., Turkmen, S. and Benson, S. (2020) ‘An Investigation into the application and practical use of (UV) ultraviolet light technology for marine antifouling’, *Ocean Engineering*, 216(June), p. 107690. Available at: https://doi.org/10.1016/j.oceaneng.2020.107690.

Sablani, S.S., Goosena, M.F.A. and Wilf, M. (2001) ‘Concentration polarization in ultrafiltration and reverse osmosis : a critical review’, 141, pp. 269–289.

Salters, B. and Piola, R. (2017) ‘UVC light for antifouling’, *Marine Technology Society Journal*, 51(2), pp. 59–70. Available at: https://doi.org/10.4031/MTSJ.51.2.10.

Santoro, S., Ashu, R., Halil, A., Fontananova, E., Di, G. and Curcio, E. (2021) ‘Fouling propensity in reverse electrodialysis operated with hypersaline brine’, 228. Available at: https://doi.org/10.1016/j.energy.2021.120563.

Scialdone, O., Albanese, A., Angelo, A.D., Galia, A. and Guarisco, C. (2013) ‘Investigation of electrode material – redox couple systems for reverse electrodialysis processes . Part II : Experiments in a stack with 10 – 50 cell pairs’, 704, pp. 1–9. Available at: https://doi.org/10.1016/j.jelechem.2013.06.001.

Scialdone, O., Guarisco, C., Grispo, S., Angelo, A.D. and Galia, A. (2012) ‘Investigation of electrode material – Redox couple systems for reverse electrodialysis processes . Part I : Iron redox couples’, 681, pp. 66–75. Available at: https://doi.org/10.1016/j.jelechem.2012.05.017.

Scientific, Q.E. and Company, P. (1980) ‘and Bjiirn 53’, pp. 59–103.

Severin, B.F. and Hayes, T.D. (2021) ‘Effect of electrode rinse solutions on the electrodialysis of concentrated salts’, *Separation and Purification Technology*, 274(March), p. 119048. Available at: https://doi.org/10.1016/j.seppur.2021.119048.

Sharma, M., Das, P.P., Chakraborty, A. and Purkait, M.K. (2022) 'Clean energy from salinity gradients using pressure retarded osmosis and reverse electrodialysis : A review', *Sustainable Energy Technologies and Assessments*, 49(November 2021), p. 101687. Available at: https://doi.org/10.1016/j.seta.2021.101687.

Shepherd, B. (2020) 'PResiduals : An R Package for Residual Analysis', 94(12). Available at: https://doi.org/10.18637/jss.v094.i12.

Simo, C., Saakes, M. and Brilman, D. (2023) 'Toward Redox-Free Reverse Electrodialysis with Carbon-Based Slurry Electrodes'.

Simões, C., Pintossi, D., Saakes, M., Borneman, Z. and Brilman, W. (2020) 'Electrode segmentation in reverse electrodialysis : Improved power and energy efficiency', 492(July). Available at: https://doi.org/10.1016/j.desal.2020.114604.

Skilhagen, S.E., Dugstad, J.E. and Aaberg, R.J. (2008) 'Osmotic power—power production based on the osmotic pressure difference between waters with varying salt gradients', *Desalination*, 220(1–3), pp. 476–482.

Song, Y., Hidayat, S., Jatnika, A. and Park, J. (2021) 'Journal of Industrial and Engineering Chemistry Simultaneous hydrogen production and struvite recovery within a microbial reverse-electrodialysis electrolysis cell', 94, pp. 302–308.

Sorensen, B. (1991) 'A history of renewable energy technology'.

StatEase (2023a) *Box-Cox Plot, Design-Expert v13*. Available at: https://www.statease.com/docs/v13/tutorials/.

StatEase (2023b) *Historical Data, Design-Expert v13*. Available at: https://www.statease.com/docs/v13/tutorials/historical-rsm/ (Accessed: 9 December 2023).

StatEase (2023c) *Response Transformations, Design-Expert v12*. Available at: https://www.statease.com/docs/v12/contents/analysis/model-limits/ (Accessed: 7 December 2023).

Strathmann, H. (2004) *ION-EXCHANGE MEMBRANE SEPARATION PROCESSES*. First edit. Amsterdam.

Strathmann, H. (2011) *Introduction to membrane science and technology*. John Wiley & Sons.

Sugimoto, Y., Ujike, R., Higa, Minato, Kakihana, Y. and Higa, Mitsuru (2022) 'Power Generation Performance of Reverse Electrodialysis (RED) Using Various Ion Exchange Membranes and Power Output Prediction for a Large RED Stack'.

Suhendra, S.A., Elma, M., Syauqiyah, I. and Lamandau, D.R. (2023) 'Energy from Salinity Gradient of Wetland Saline Water Using Reverse Electrodialysis Membrane', 2(2), pp. 46–59.

Szulejko, J.E., Kumar, P., Deep, A. and Kim, K.H. (2017) 'Global warming projections to 2100 using simple CO2 greenhouse gas modeling and comments on CO2 climate sensitivity factor', *Atmospheric Pollution Research*, 8(1), pp. 136–140. Available at: https://doi.org/10.1016/j.apr.2016.08.002.

Takagi, R., Vaselbehagh, M. and Matsuyama, H. (2014) 'Theoretical study of the permselectivity of an anion exchange membrane in electrodialysis', *Journal of Membrane Science*, 470, pp. 486–493. Available at: https://doi.org/10.1016/j.memsci.2014.07.053.

Tedesco, M., Brauns, E., Cipollina, A., Micale, G., Modica, P., Russo, G. and Helsen, J. (2015)

‘Reverse electrodialysis with saline waters and concentrated brines: A laboratory investigation towards technology scale-up’, *Journal of Membrane Science*, 492, pp. 9–20. Available at: https://doi.org/10.1016/j.memsci.2015.05.020.

Tedesco, M, Cipollina, A., Galia, A., Micale, G. and Scialdone, O. (2017) ‘Reverse electrodialysis performed at pilot plant scale : evaluation of redox processes and simultaneous generation of electric energy and treatment of wastewater $’, *Water Research*, 125, pp. 123–131.

Tedesco, Michele, Cipollina, A., Tamburini, A. and Micale, G. (2017) ‘Towards 1 kW power production in a reverse electrodialysis pilot plant with saline waters and concentrated brines’, *Journal of Membrane Science*, 522, pp. 226–236. Available at: https://doi.org/10.1016/j.memsci.2016.09.015.

Tedesco, M., Hamelers, H.V.M. and Biesheuvel, P.M. (2016a) ‘Nernst-Planck transport theory for (reverse) electrodialysis : I . Effect of co-ion transport through the membranes channel’, 510, pp. 370–381. Available at: https://doi.org/10.1016/j.memsci.2016.03.012.

Tedesco, M., Hamelers, H.V.M. and Biesheuvel, P.M. (2016b) ‘Nernst-Planck transport theory for (reverse) electrodialysis : I . Effect of co-ion transport through the membranes channel’, *Journal of Membrane Science*, 510, pp. 370–381. Available at: https://doi.org/10.1016/j.memsci.2016.03.012.

Tedesco, M., Hamelers, H.V.M. and Biesheuvel, P.M. (2017) ‘Nernst-Planck transport theory for (reverse) electrodialysis : II . E ff ect of water transport through ion-exchange membranes’, *Journal of Membrane Science*, 531(December 2016), pp. 172–182. Available at: https://doi.org/10.1016/j.memsci.2017.02.031.

Tedesco, M., Hamelers, H.V.M. and Biesheuvel, P.M. (2018) ‘Nernst-Planck transport theory for (reverse) electrodialysis : III . Optimal membrane thickness for enhanced process performance’, *Journal of Membrane Science*, 565(August), pp. 480–487. Available at: https://doi.org/10.1016/j.memsci.2018.07.090.

Tedesco, M., Scalici, C., Vaccari, D. and Cipollina, A. (2016) ‘Performance of the first Reverse Electrodialysis pilot plant for power production from saline waters and concentrated brines’, 500, pp. 33–45.

Tedesco, Michele, Scalici, C., Vaccari, D., Cipollina, A., Tamburini, A. and Micale, G. (2015) ‘Performance of the first reverse electrodialysis pilot plant for power production from saline waters and concentrated brines’. Available at: https://doi.org/10.1016/j.memsci.2015.10.057.

Tedesco, M., Scalici, C., Vaccari, D., Cipollina, A., Tamburini, A. and Micale, G. (2016) ‘Performance of the fi rst reverse electrodialysis pilot plant for power production from saline waters and concentrated brines’, *Journal of Membrane Science*, 500, pp. 33–45. Available at: https://doi.org/10.1016/j.memsci.2015.10.057.

Tetteh, E. and Rathilal, S. (2018) ‘Evaluation of the coagulation floatation process for industrial mineral oil wastewater treatment using response surface methodology (RSM)’, *International Journal of Environmental Impacts*, 1(4), pp. 491–502. Available at: https://doi.org/10.2495/EI-V1-N4-491-502.

Tetteh, E.K. (2018) ‘Optimisation of dissolved air flotation (DAF) for separating industrial mineral oil from water’, (January).

Tetteh, E.K. and Rathilal, S. (2021) ‘Materials Today : Proceedings Application of magnetized

nanomaterial for textile effluent remediation using response surface methodology', *Materials Today: Proceedings*, 38, pp. 700–711. Available at: https://doi.org/10.1016/j.matpr.2020.03.827.

Tetteh, E.K., Rathilal, S. and Chollom, M.N. (2017) 'Pre-treatment of industrial mineral oil wastewater using response surface methodology', *Water and Society IV*, 216, pp. 181–191. Available at: https://doi.org/10.2495/WS170171.

Tong, X., Wang, X., Liu, S., Gao, H., Xu, C., Crittenden, J. and Chen, Y. (2018) 'A freestanding graphene oxide membrane for ef fi ciently harvesting salinity gradient power', *Carbon*, 138, pp. 410–418. Available at: https://doi.org/10.1016/j.carbon.2018.07.064.

Trist, C., Fallanza, M., Ib, R. and Ortiz, I. (2020a) 'applied sciences Reverse Electrodialysis : Potential Reduction in Energy and Emissions of Desalination'.

Trist, C., Fallanza, M., Ib, R. and Ortiz, I. (2020b) 'Reverse Electrodialysis : Potential Reduction in Energy and Emissions of Desalination', *Applied Sciences*, 10, pp. 1–21.

Tristán, C., Fallanza, M., Ibáñez, R. and Ortiz, I. (2020) 'Recovery of salinity gradient energy in desalination plants by reverse electrodialysis', *Desalination*, 496(September), p. 114699. Available at: https://doi.org/10.1016/j.desal.2020.114699.

Tristán, C., Pérez, G., Fallanza, M., Ortiz, A., Ibañez, R. and Ortiz, I. (2020) 'A comprehensive study on the effects of operation variables on reverse electrodialysis performance', *Desalination*, 482(November 2019), p. 114389. Available at: https://doi.org/10.1016/j.desal.2020.114389.

Tufa, R., Curcio, E., Van Baak, W., Grasman, S., Fontananova, E. and Di Profio, G. (2014) 'Energy Generation by Salinity Gradient Power–Reverse Electrodialysis (SGP-RE)', in *Atti del IX Convegno Nazionale dell'Associazione di Chimica per l'Ingegneria*. © 2014 Università del Salento–Coordinamento SIBA, p. 119.

Tufa, R.A., Curcio, E., van Baak, W., Veerman, J., Grasman, S., Fontananova, E. and Di Profio, G. (2014) 'Potential of brackish water and brine for energy generation by salinity gradient power-reverse electrodialysis (SGP-RE)', *RSC Advances*, 4(80), pp. 42617–42623.

Turek, M. and Bandura, B. (2007) 'Renewable energy by reverse electrodialysis', 205(May 2006), pp. 67–74. Available at: https://doi.org/10.1016/j.desal.2006.04.041.

Turek, M., Bandura, B. and Dydo, P. (2008) 'Power production from coal-mine brine utilizing reversed electrodialysis', 221, pp. 462–466. Available at: https://doi.org/10.1016/j.desal.2007.01.106.

Vanherck, K., Koeckelberghs, G. and Vankelecom, I.F.J. (2013) 'Progress in Polymer Science Crosslinking polyimides for membrane applications : A review', *Progress in Polymer Science*, 38(6), pp. 874–896. Available at: https://doi.org/10.1016/j.progpolymsci.2012.11.001.

Veerman, J. (2010) *Reverse electrodialysis: design and optimization by modeling and experimentation*. University of Groningen.

Veerman, J., Jong, R.M. De, Saakes, M., Metz, S.J. and Harmsen, G.J. (2009) 'Reverse electrodialysis : Comparison of six commercial membrane pairs on the thermodynamic efficiency and power density', 343, pp. 7–15. Available at: https://doi.org/10.1016/j.memsci.2009.05.047.

Veerman, J., Post, J.W., Saakes, M., Metz, S.J. and Harmsen, G.J. (2008) 'Reducing power

losses caused by ionic shortcut currents in reverse electrodialysis stacks by a validated model', 310, pp. 418–430. Available at: https://doi.org/10.1016/j.memsci.2007.11.032.

Veerman, J., Saakes, M., Metz, S.J. and Harmsen, G.J. (2009) 'Reverse electrodialysis : Performance of a stack with 50 cells on the mixing of sea and river water', 327, pp. 136–144. Available at: https://doi.org/10.1016/j.memsci.2008.11.015.

Veerman, J., Saakes, M., Metz, S.J. and Harmsen, G.J. (2010) 'Reverse electrodialysis : evaluation of suitable electrode systems', pp. 1461–1474. Available at: https://doi.org/10.1007/s10800-010-0124-8.

Vélez, J.I., Correa, J.C. and Marmolejo-ramos, F. (2015) 'A new approach to the Box – Cox transformation', 1(October), pp. 1–10. Available at: https://doi.org/10.3389/fams.2015.00012.

Vermaas, D.A., Guler, E., Saakes, M. and Nijmeijer, K. (2012) 'Theoretical power density from salinity gradients using reverse electrodialysis', 20, pp. 170–184. Available at: https://doi.org/10.1016/j.egypro.2012.03.018.

Vermaas, D.A., Kunteng, D., Saakes, M. and Nijmeijer, K. (2012) 'Fouling in reverse electrodialysis under natural conditions', 7. Available at: https://doi.org/10.1016/j.watres.2012.11.053.

Vermaas, D.A., Kunteng, D., Veerman, J. and Saakes, M. (no date) 'Periodic feed water reversal and air sparging as anti fouling strategies in reverse electrodialysis', pp. 1–6.

Vermaas, D.A., Kunteng, D., Veerman, J., Saakes, M. and Nijmeijer, K. (2014) 'Periodic feedwater reversal and air sparging as antifouling strategies in reverse electrodialysis', *Environmental science & technology*, 48(5), pp. 3065–3073.

Vermaas, D.A., Saakes, M. and Nijmeijer, K. (2011a) 'Doubled power density from salinity gradients at reduced intermembrane distance', *Environmental science & technology*, 45(16), pp. 7089–7095.

Vermaas, D.A., Saakes, M. and Nijmeijer, K. (2011b) 'Power generation using profiled membranes in reverse electrodialysis', 386, pp. 234–242. Available at: https://doi.org/10.1016/j.memsci.2011.09.043.

Vermaas, D.A., Saakes, M. and Nijmeijer, K. (2014) 'Enhanced mixing in the diffusive boundary layer for energy generation in reverse electrodialysis', 453, pp. 312–319. Available at: https://doi.org/10.1016/j.memsci.2013.11.005.

Vermaas, D.A., Veerman, J. and Nijmeijer, K. (2014) 'Environmental Science In fl uence of multivalent ions on renewable energy generation in reverse electrodialysis †', pp. 1434–1445. Available at: https://doi.org/10.1039/c3ee43501f.

Vörösmarty, C.J., Léveque, C., Revenga, C., Bos, R., Caudill, C., Chilton, J., Douglas, E.M., Meybeck, M., Prager, D. and Balvanera, P. (2005) 'Fresh water', *Millennium ecosystem assessment*, 1, pp. 165–207.

Vyazovkin, S. (2020) 'Activation energies and temperature dependencies of the rates of crystallization and melting of polymers', *Polymers*, 12(5). Available at: https://doi.org/10.3390/POLYM12051070.

Wagholikar, V. V, Zhuang, H., Jiao, Y., Moe, N.E., Ramanan, H., Goh, L.M., Barber, J., Lee, K.S., Lee, H.P. and Fuh, J.Y.H. (2017) 'Modeling cell pair resistance and spacer shadow factors in electro-separation processes', *Journal of Membrane Science*, 543(August), pp. 151–

162. Available at: https://doi.org/10.1016/j.memsci.2017.08.054.

Wang, X., Chen, G.Q., Zhang, W. and Deng, H. (2019) 'Journal of the Taiwan Institute of Chemical Engineers Surface-modified anion exchange membranes with self-cleaning ability and enhanced antifouling properties', *Journal of the Taiwan Institute of Chemical Engineers*, 105, pp. 8–16. Available at: https://doi.org/10.1016/j.jtice.2019.09.026.

Weiner, A.M., Mcgovern, R.K. and V, J.H.L. (2015) 'A new reverse electrodialysis design strategy which signi fi cantly reduces the levelized cost of electricity', *Journal of Membrane Science*, 493, pp. 605–614. Available at: https://doi.org/10.1016/j.memsci.2015.05.058.

Weinstein, J.N. (1976) 'Electric Power from Differences in salinity: The Dialytic Battery', *Science*, 191(4227), pp. 557–559. Available at: https://doi.org/DOI: 10.1126/science.191.4227.557.

Wenten, I.G. (2016) 'Reverse osmosis applications : Prospect and challenges', *DES*, 391, pp. 112–125. Available at: https://doi.org/10.1016/j.desal.2015.12.011.

Wick, G.L. (1977) 'Power from salinity gradients', 3(1), pp. 95–100.

Wu, X., Lv, Y., Sun, D., Zhang, Y. and Xu, S. (2023) 'Effects of electrode rinse solution on performance of hydrogen and electricity cogeneration system by reverse electrodialysis', 287(April). Available at: https://doi.org/10.1016/j.enconman.2023.117122.

Wu, X., Ren, Y., Zhang, Y., Xu, S. and Yang, S. (2022) 'Hydrogen production from water electrolysis driven by the membrane voltage of a closed-loop reverse electrodialysis system integrating air-gap diffusion distillation technology', 268(June). Available at: https://doi.org/10.1016/j.enconman.2022.115974.

Yasukawa, M., Mehdizadeh, S., Sakurada, T. and Abo, T. (2020) 'Power generation performance of a bench-scale reverse electrodialysis stack using wastewater discharged from sewage treatment and seawater reverse osmosis', 491(November 2019). Available at: https://doi.org/10.1016/j.desal.2020.114449.

Yu, L., Wang, L.P., Liao, H., Wang, J., Feng, Z., Lev, O., Loo, J.S.C., Sougrati, M.T. and Xu, Z.J. (2018) 'Understanding Fundamentals and Reaction Mechanisms of Electrode Materials for Na-Ion Batteries', *Small*, 14(16), pp. 1–22. Available at: https://doi.org/10.1002/smll.201703338.

Zhang, H., Jiang, D., Zhang, B., Gi, J. and Chen, Y. (2017) 'Electrochimica Acta A Novel Hybrid Poly (vinyl alcohol) (PVA)/ Poly (2 , 6-dimethyl-1 , 4- phenylene oxide) (PPO) Membranes for Reverse Electrodialysis Power System', *Electrochimica Acta*, 239, pp. 65–73. Available at: https://doi.org/10.1016/j.electacta.2017.04.008.

Zhang, W., Cheng, W., Tufa, R.A., Liu, C., Aili, D., Chanda, D., Chang, J., Wang, S., Zhang, Y. and Ma, J. (2021) 'Studies on Anion Exchange Membrane and Interface Properties by Electrochemical Impedance Spectroscopy: The Role of pH', *Membranes*, 11(10), p. 771.

Zhang, W., Ma, J., Wang, P., Wang, Z., Shi, F. and Liu, H. (2016) 'Investigations on the interfacial capacitance and the diffusion boundary layer thickness of ion exchange membrane using electrochemical impedance spectroscopy', *Journal of Membrane Science*, 502, pp. 37–47. Available at: https://doi.org/10.1016/j.memsci.2015.12.007.

Zhao, Y., Tang, K., Liu, H., Bruggen, B. Van Der, Sotto, A., Shen, J. and Gao, C. (2016) 'An anion exchange membrane modi fi ed by alternate electro- deposition layers with enhanced monovalent selectivity', *Journal of Membrane Science*, 520, pp. 262–271. Available at:

https://doi.org/10.1016/j.memsci.2016.07.026.

Zhou, X., Zhang, W., Li, J., Bao, X., Han, X. and Myintzu, M. (2022) ‘An electrochemical system for salinity gradient energy harvesting’, 255(January).

Zhu, S., Kingsbury, R.S., Call, D.F. and Coronell, O. (2018) ‘Impact of solution composition on the resistance of ion exchange membranes’, *Journal of Membrane Science*, 554(February), pp. 39–47. Available at: https://doi.org/10.1016/j.memsci.2018.02.050.

Zhu, X., Hatzell, M.C., Cusick, R.D. and Logan, B.E. (2013) ‘Electrochemistry Communications Microbial reverse-electrodialysis chemical-production cell for acid and alkali production’, *Electrochemistry Communications*, 31, pp. 52–55. Available at: https://doi.org/10.1016/j.elecom.2013.03.010.

Zhu, X., He, W. and Logan, B.E. (2015a) ‘In fl uence of solution concentration and salt types on the performance of reverse electrodialysis cells’, *Journal of Membrane Science*, 494, pp. 154–160. Available at: https://doi.org/10.1016/j.memsci.2015.07.053.

Zhu, X., He, W. and Logan, B.E. (2015b) ‘Reducing pumping energy by using different fl ow rates of high and low concentration solutions in reverse electrodialysis cells’, 486, pp. 215–221. Available at: https://doi.org/10.1016/j.memsci.2015.03.035.

Appendix A: Materials

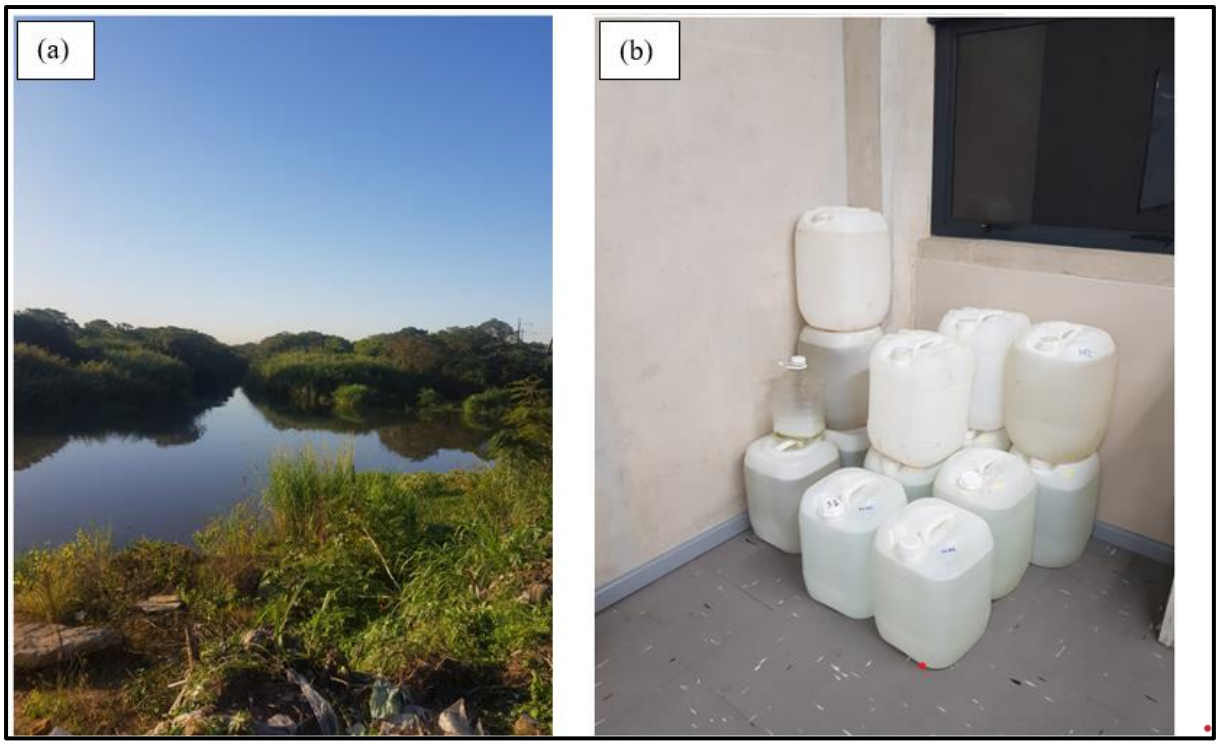

Figure A-1: (a) uMkomaas River water sampling spot (b) Unfiltered River water sample

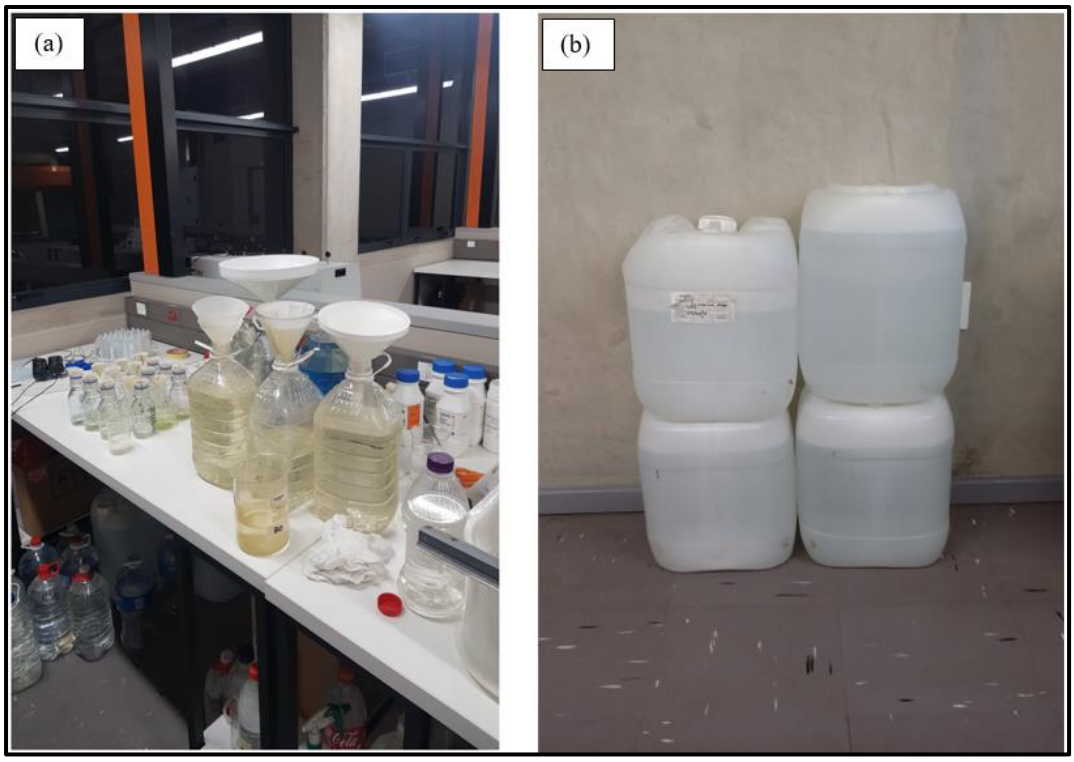

Figure A-2: (a) Natural water filtration process (b) filter Natural water sample

Figure A-3: Prepared electrode rinse solution of $K_3Fe(CN)_6$, $K_4Fe(CN)_6$, and NaCl

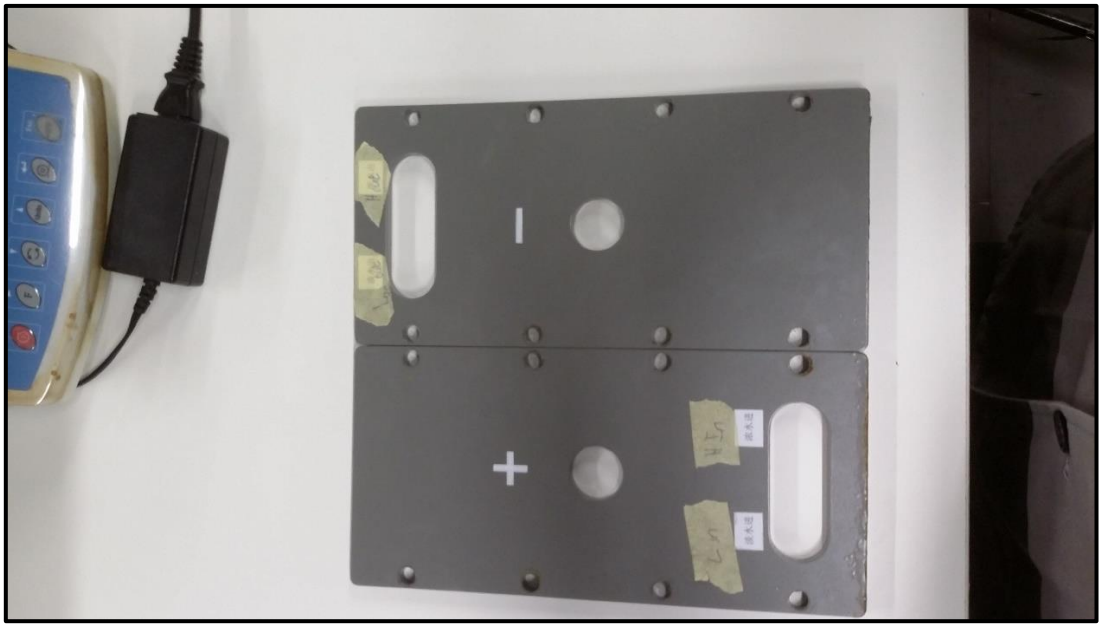

Figure A-4: End plates of the RED stack

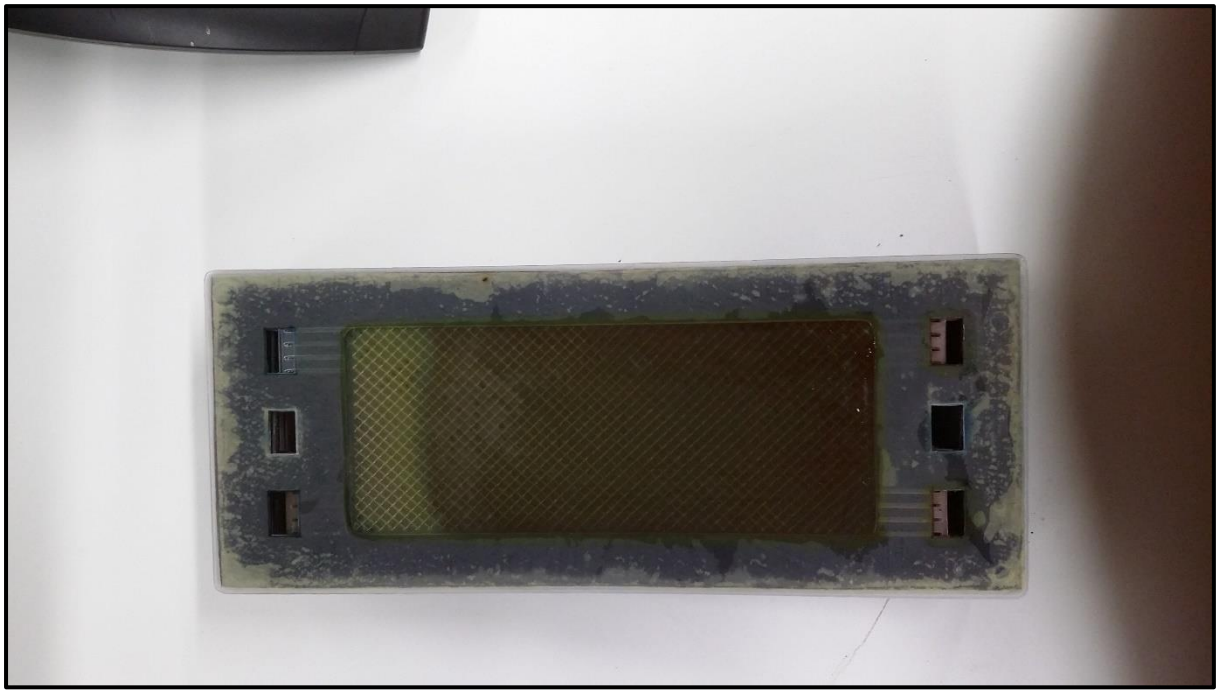

Figure A-5: Anion Exchange Membrane (AEM)

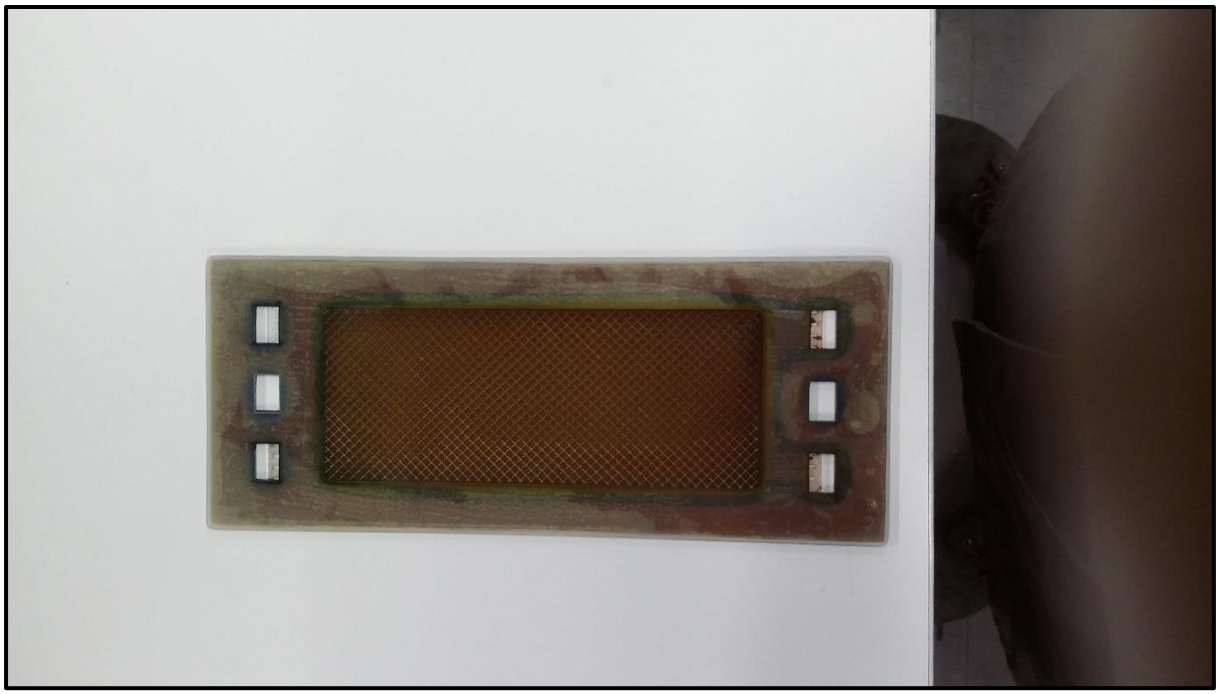

Figure A-6: Cation Exchange Membrane (CEM)

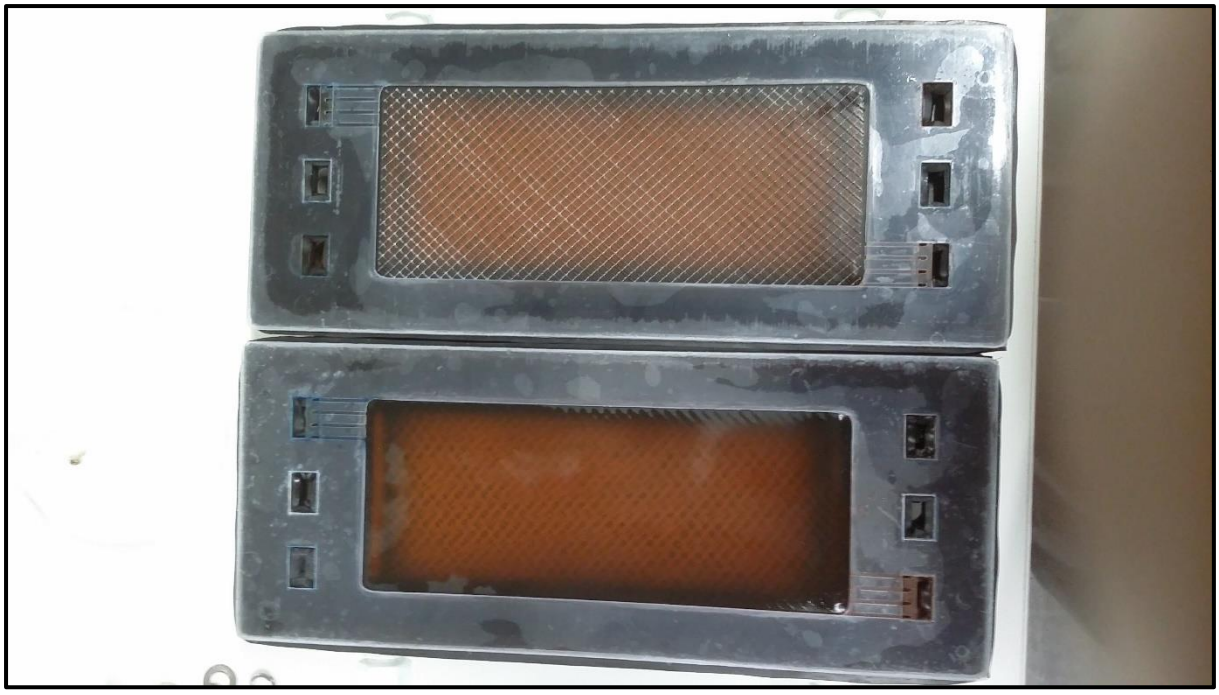

Figure A-7: Electrode rinse compartments

Appendix B: Raw data and specification

Table B-1: General properties and specifications of the RED stack used in the analysis.

Specification	Value
Effective membrane area (m^2)	0.0297
Membrane size (cm)	11×27
Spacer thickness (mm)	0.5
Processing length (mm)	80
Compartment width (mm)	160
Membrane spacing	Ca.1
Overcell (mm)	0.5
Spacer thickness (µm)	450
Mesh orientation to flow direction	45º
Porosity (%)	91
Material	Silicon/polypropylene
Cell frame and tube material	Polypropylene
Pressure drop over cell	Max, 0.5 bar

Table B-2: Properties of the ion-exchange membranes.

Membrane	AEM	CEM	End membrane
Thickness (µm)	100-110	100-120	220
Ion exchange capacity (meq/g)	1.2	3	1.8
Resistance (Ω cm^2)	~ 1.8	~ 2.5	~ 4.5
Burst strength (kg cm^2)	4-5	4-5	15
Water content (wt%)	~ 14	~ 9	-
pH stability	0-9	0-11	1-13
Maximum temperature (°C)	60	50	50
Membrane type	Strong alkaline (ammonium)	Strongly acidic (sulfonic acid)	Strongly acidic (sulfonic acid)
Reinforcement	Polyester	Polyester	polyethylene

Note: All parameters were provided by the manufacturer.

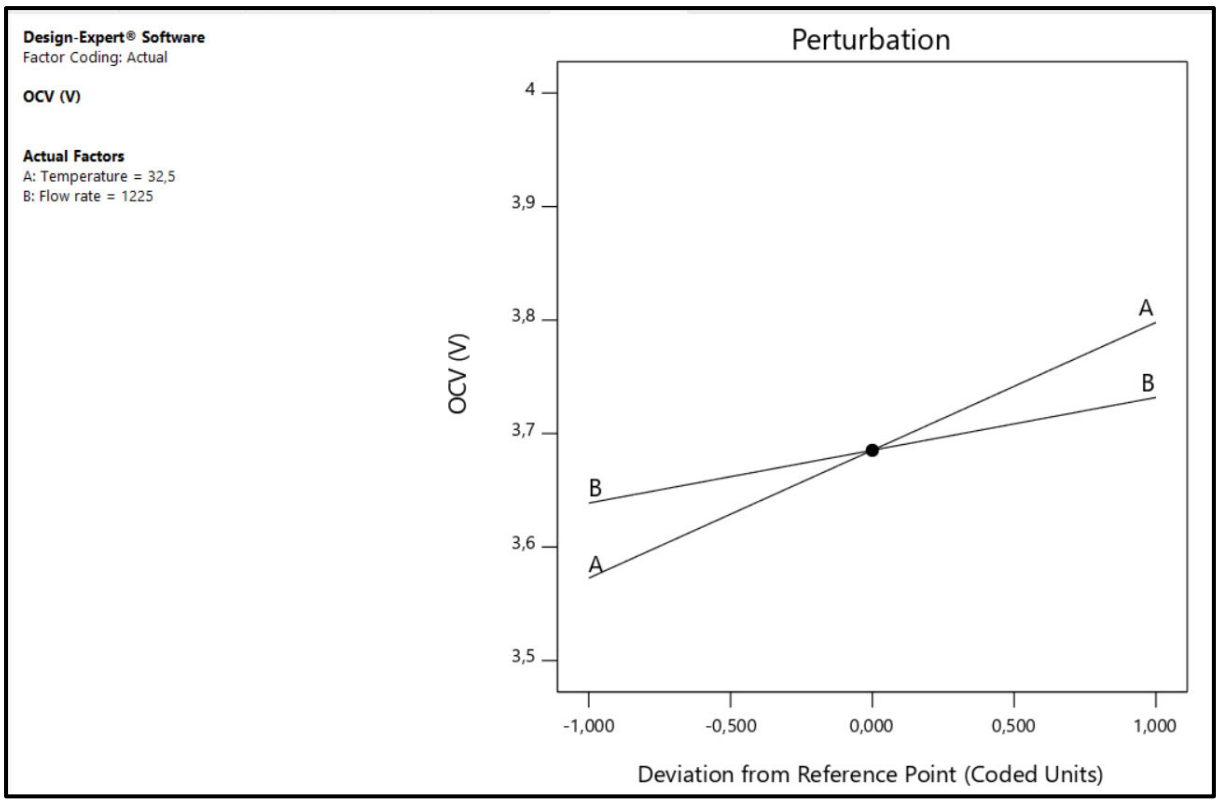

Figure B-1: Perturbation plot for OCV

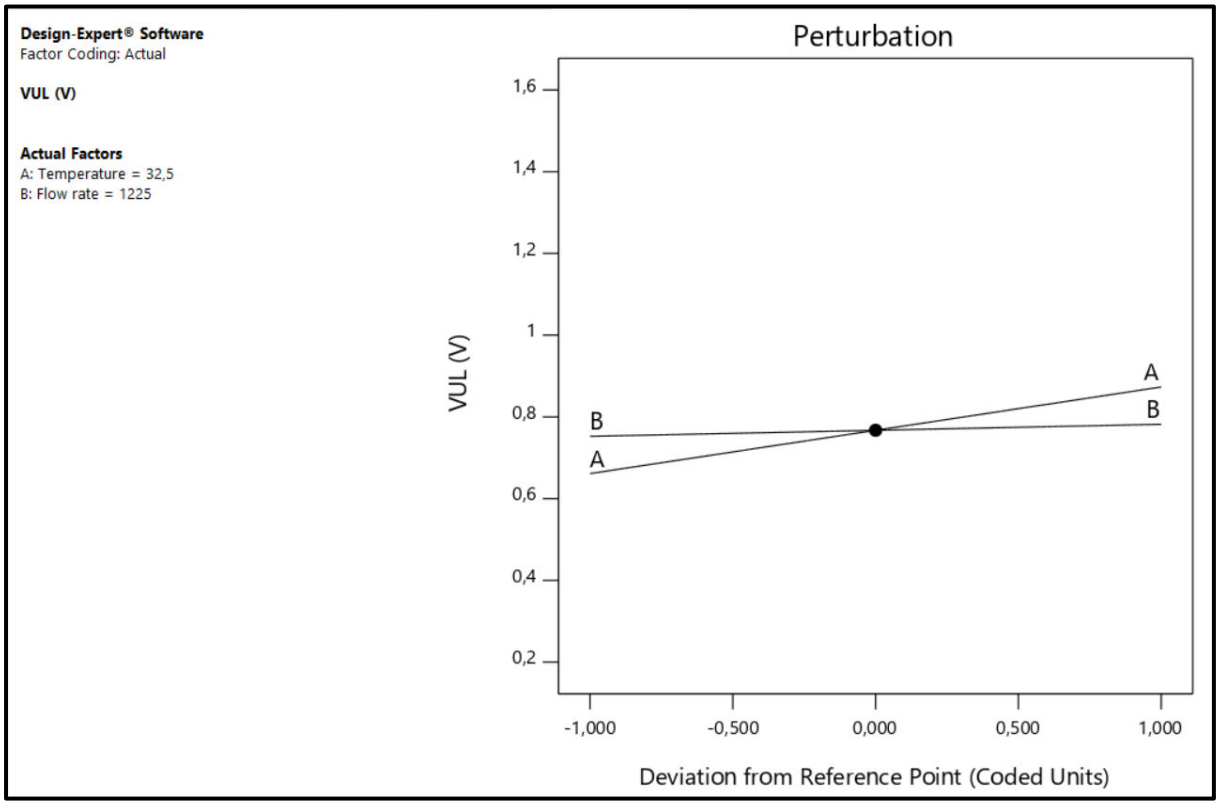

Figure B-2: Perturbation plot for VUL

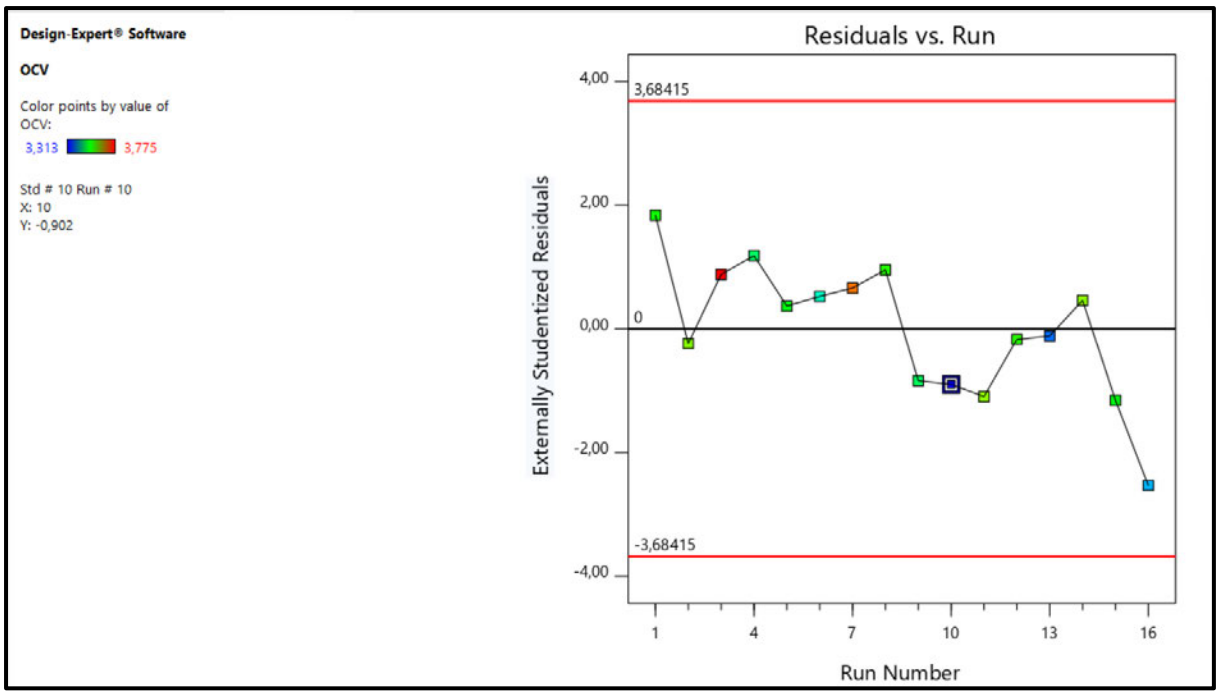

Figure B-3: Residuals v Runs plot for OCV.

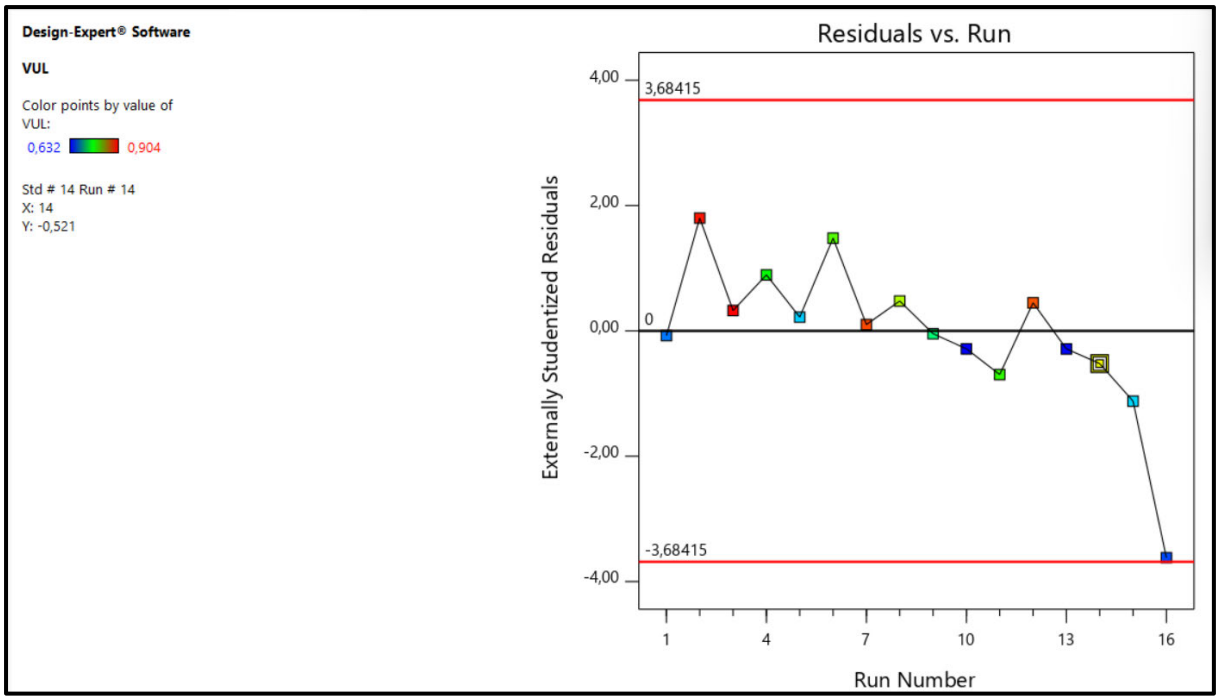

Figure B-4: Residuals v Runs plot for VUL.

Appendix C: Publications

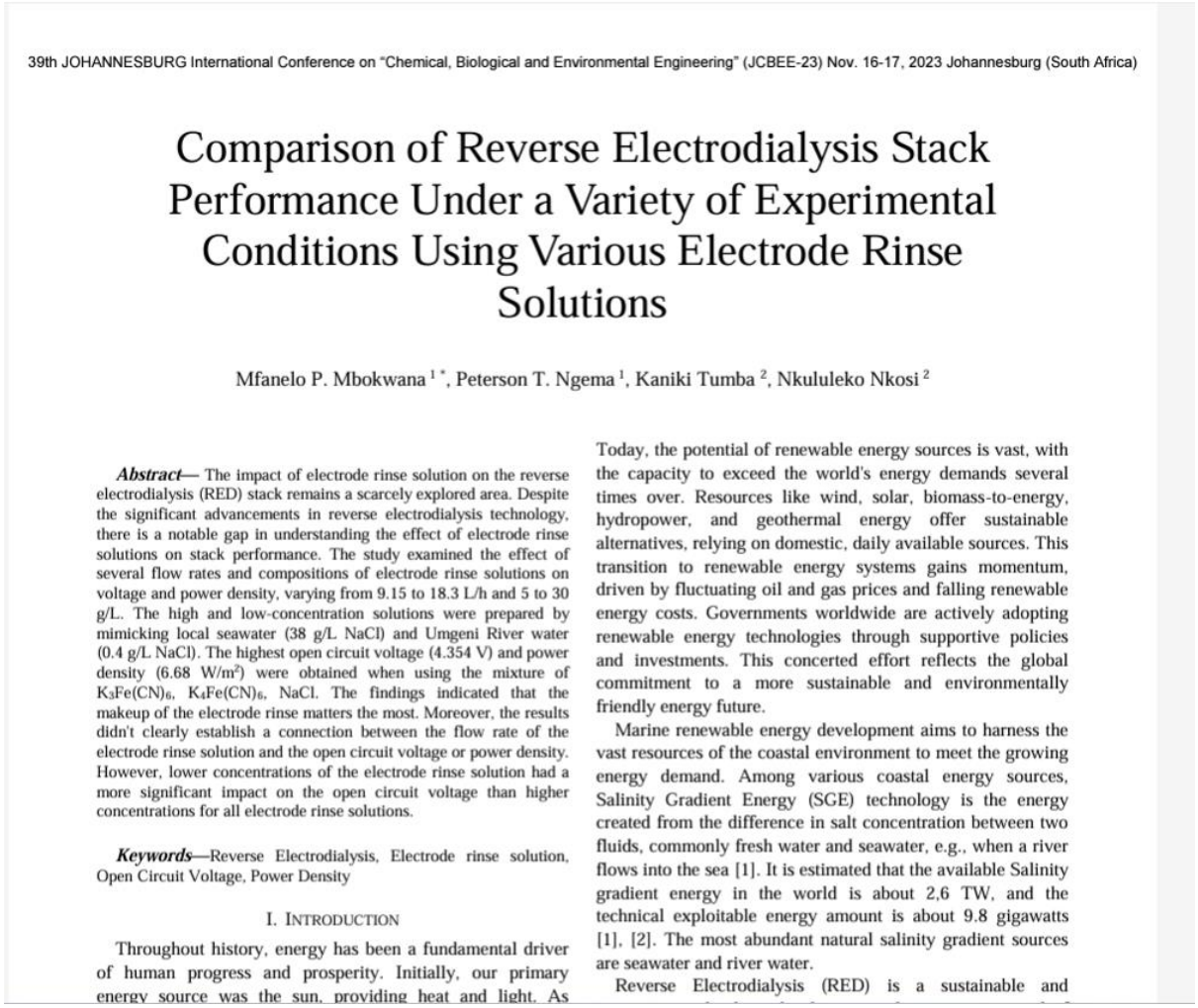

39th JOHANNESBURG International Conference on "Chemical, Biological and Environmental Engineering" (JCBEE-23) Nov. 16-17, 2023 Johannesburg (South Africa)

Comparison of Reverse Electrodialysis Stack Performance Under a Variety of Experimental Conditions Using Various Electrode Rinse Solutions

Mfanelo P. Mbokwana [1 *], Peterson T. Ngema [1], Kaniki Tumba [2], Nkululeko Nkosi [2]

***Abstract*—** The impact of electrode rinse solution on the reverse electrodialysis (RED) stack remains a scarcely explored area. Despite the significant advancements in reverse electrodialysis technology, there is a notable gap in understanding the effect of electrode rinse solutions on stack performance. The study examined the effect of several flow rates and compositions of electrode rinse solutions on voltage and power density, varying from 9.15 to 18.3 L/h and 5 to 30 g/L. The high and low-concentration solutions were prepared by mimicking local seawater (38 g/L NaCl) and Umgeni River water (0.4 g/L NaCl). The highest open circuit voltage (4.354 V) and power density (6.68 W/m^2) were obtained when using the mixture of $K_3Fe(CN)_6$, $K_4Fe(CN)_6$, NaCl. The findings indicated that the makeup of the electrode rinse matters the most. Moreover, the results didn't clearly establish a connection between the flow rate of the electrode rinse solution and the open circuit voltage or power density. However, lower concentrations of the electrode rinse solution had a more significant impact on the open circuit voltage than higher concentrations for all electrode rinse solutions.

***Keywords*—**Reverse Electrodialysis, Electrode rinse solution, Open Circuit Voltage, Power Density

I. Introduction

Throughout history, energy has been a fundamental driver of human progress and prosperity. Initially, our primary energy source was the sun, providing heat and light. As Today, the potential of renewable energy sources is vast, with the capacity to exceed the world's energy demands several times over. Resources like wind, solar, biomass-to-energy, hydropower, and geothermal energy offer sustainable alternatives, relying on domestic, daily available sources. This transition to renewable energy systems gains momentum, driven by fluctuating oil and gas prices and falling renewable energy costs. Governments worldwide are actively adopting renewable energy technologies through supportive policies and investments. This concerted effort reflects the global commitment to a more sustainable and environmentally friendly energy future.

Marine renewable energy development aims to harness the vast resources of the coastal environment to meet the growing energy demand. Among various coastal energy sources, Salinity Gradient Energy (SGE) technology is the energy created from the difference in salt concentration between two fluids, commonly fresh water and seawater, e.g., when a river flows into the sea [1]. It is estimated that the available Salinity gradient energy in the world is about 2,6 TW, and the technical exploitable energy amount is about 9.8 gigawatts [1], [2]. The most abundant natural salinity gradient sources are seawater and river water.

Reverse Electrodialysis (RED) is a sustainable and

Figure C-1: Published paper.